




Review

C-,N- and S-Doped TiO₂ Photocatalysts: A Review

Aleksandra Piątkowska ¹, Magdalena Janus ^{2,*}, Kacper Szymański ¹ and Sylwia Mozia ^{1,*}

- ¹ Department of Inorganic Chemical Technology and Environment Engineering, Faculty of Chemical Technology and Engineering, West Pomeranian University of Technology in Szczecin, ul. Pułaskiego 10, 70-322 Szczecin, Poland; aleksandra.piatkowska@zut.edu.pl (A.P.); kacper.szymanski@zut.edu.pl (K.S.)
- ² Department of Environmental Engineering, Faculty of Civil and Environmental Engineering, West Pomeranian University of Technology in Szczecin, al. Piastów 50, 70-311 Szczecin, Poland
- * Correspondence: magdalena.janus@zut.edu.pl (M.J.); sylwia.mozia@zut.edu.pl (S.M.); Tel.: +48-91-449-4083 (M.J.); +48-91-449-4730 (S.M.)

Abstract: This article presents an overview of the reports on the doping of TiO₂ with carbon, nitrogen, and sulfur, including single, co-, and tri-doping. A comparison of the properties of the photocatalysts synthesized from various precursors of TiO₂ and C, N, or S dopants is summarized. Selected methods of synthesis of the non-metal doped TiO₂ are also described. Furthermore, the influence of the preparation conditions on the doping mode (interstitial or substitutional) with reference to various types of the modified TiO₂ is summarized. The mechanisms of photocatalysis for the different modes of the non-metal doping are also discussed. Moreover, selected applications of the non-metal doped TiO₂ photocatalysts are shown, including the removal of organic compounds from water/wastewater, air purification, production of hydrogen, lithium storage, inactivation of bacteria, or carbon dioxide reduction.

Keywords: TiO₂; photocatalyst; photocatalysis; carbon; nitrogen; sulfur; doped; co-doped; tri-doped



Citation: Piątkowska, A.; Janus, M.; Szymański, K.; Mozia, S. C-,N- and S-Doped TiO₂ Photocatalysts: A Review. *Catalysts* **2021**, *11*, 144. <https://doi.org/10.3390/catal11010144>

Received: 30 November 2020
Accepted: 14 January 2021
Published: 19 January 2021

Publisher's Note: MDPI stays neutral with regard to jurisdictional claims in published maps and institutional affiliations.



Copyright: © 2021 by the authors. Licensee MDPI, Basel, Switzerland. This article is an open access article distributed under the terms and conditions of the Creative Commons Attribution (CC BY) license (<https://creativecommons.org/licenses/by/4.0/>).

1. Introduction

More than ever before, environmental problems have become a major concern. Urbanization and rapid growth of industries generate abundant amounts of pollutants which are released into the environment. Among them, there are highly hazardous materials such as pharmaceuticals [1,2], dioxins [3], pesticides [4], herbicides [1], phenols [4,5], and textile dyes [1,4–6]. This increasing occurrence of organic pollutants in the environment is a serious danger for health and the lives of humans and other living beings. Conventional treatment methods very often fail in the removal of these kinds of residues entirely, because of their high (bio)chemical stability. Moreover, a conventional approach is associated with the operational problems and high costs. Hence, the development of new and efficient methods of the removal of organic contaminants is a matter of growing interest [1,2,4].

In recent decades, semiconductor photocatalysis has been proved to be an efficient approach for organic compounds decomposition and degradation. TiO₂ has been widely and successfully used as a photocatalyst in many different areas (Figure 1) due to its advantages, such as low cost and good chemical stability. However, it requires employing relatively high photon energy to be activated. For this reason, many methods of narrowing of the band gap of TiO₂ have been proposed, aimed at the direct usage of sunlight [7,8]. Amongst them, doping of TiO₂ with non-metals such as carbon, nitrogen and sulfur is often reported as one of the most effective ways of increasing its photocatalytic activity under visible light [1,9,10]. Non-metal doping of TiO₂ leads to changes in the electronic band structure, resulting in a smaller band gap energy value, and thus an improved response in the visible light [7,8,11].

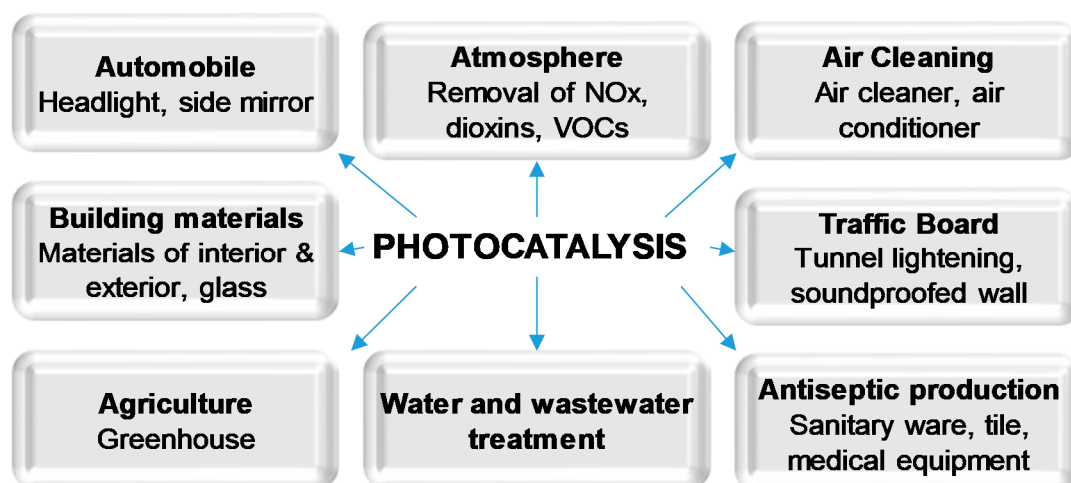


Figure 1. Applications of photocatalysis.

The idea of non-metal doping of TiO_2 has been discussed in numerous reviews through the years [1,9,10,12–23]. Most of the recent reviews referred to nitrogen only, which is one of the most frequently used non-metal dopants [17,24–34]. On the other hand, the reviews devoted exclusively to S-doped TiO_2 are very limited [35]. In some papers, the modifications of TiO_2 with carbon are also summarized [1,10,36,37]. Shi et al. [36] presented various carbon-based (nano)composites, including C-doped TiO_2 . Moreover, diverse, more complex configurations, e.g., with multi-walled carbon nanotubes (MWCNT) in $\text{TiO}_2\text{-SiO}_2/\text{MWCNT}$ [37], with carbon dots (CDs) in CDs-N-TiO_2 [38], and Ag-modified $g\text{-C}_3\text{N}_4/\text{N-doped TiO}_2$ [24] have been reported. There is only one review referring to the beneficial effects and challenges of tri-doping of TiO_2 with carbon, nitrogen, and sulfur, which was published in 2017 [39]. Moreover, recently, a review on single doping of TiO_2 with various non-metals, including C, N, and S was published [1].

In contrast with the above papers, this review focuses on a complex comparison of various types and configurations of TiO_2 doping with non-metals such as carbon, nitrogen, and sulfur, including single-, co-, and tri-doping. The aim of this work was to systematize the knowledge with reference to the abovementioned doping types, especially in terms of the doping mode (i.e., the way the dopant interacts with the unit cell of crystal structure or the surface of a semiconductor), the effect of the single-, co-, and tri-doping on the mechanism of photocatalysis, as well as the possible applications of the doped TiO_2 . The overview of the single C, N, and S doping creates a base for a better understanding of the co- and tri-doping. The first part of the review presents a brief introduction to the TiO_2 photocatalysis. The influence of various non-metal dopants (C, N, and S) on the photocatalysts' properties is reported in the subsequent sections. A discussion on the type of the doping source, TiO_2 precursor, and the photocatalyst preparation method is presented for all modes of doping of TiO_2 with C, N, or S. The morphological and structural characteristics of the photocatalysts as well as the photocatalytic activity are also summarized. The literature reports selected for this review are distributed appropriately among Sections 3–9 according to the description of the doping type proposed by the authors of the cited papers.

2. TiO_2 Photocatalysis

The discovery of the photocatalytic splitting of water on TiO_2 electrodes in 1972 heralded a new era of heterogeneous photocatalysis [40]. Despite several decades having passed since then, the most popular photocatalyst is still TiO_2 . Amongst the different structures of titania, anatase and rutile are commonly used in photocatalysis, with anatase displaying a higher photocatalytic activity.

In heterogeneous photocatalysis, a reaction takes place on the surface of a photocatalyst. The general mechanism of photocatalytic decomposition of organic compounds is summarized in Figure 2.

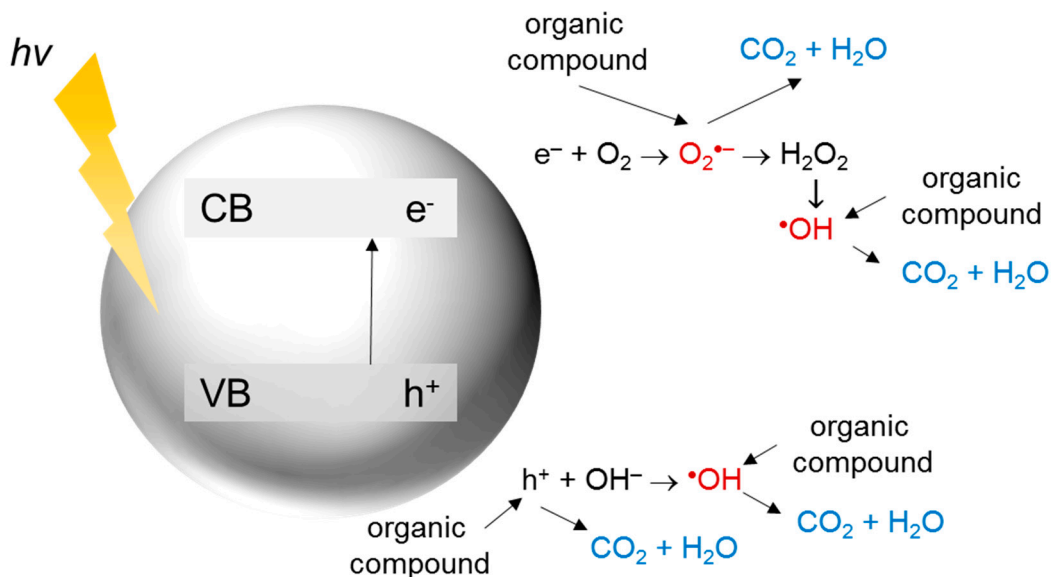
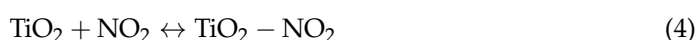
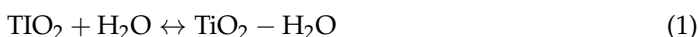


Figure 2. The mechanism of photocatalytic decomposition of organic compounds.

First, the energy higher than the band gap energy of the semiconductor is required for photon absorption and excitation of an electron (e^-) from the valence band (VB) to the conduction band (CB), resulting in hole (h^+) generation. The holes in the VB can react with the surface adsorbed water or hydroxyl ions to form hydroxyl radicals, which are extremely strong oxidants (oxidation potential around +2.7 V). The photoexcited electrons in the CB can generate superoxide radicals due to the reaction with oxygen, being the main electron acceptor in the system. Further reactions lead to the formation of other reactive oxygen species (ROS) such as hydrogen peroxide, hydroperoxyl radicals, or hydroxyl radicals. These species participate in the degradation of organic contaminants [41–44].

The effectiveness of the photodegradation of pollutants on the semiconductor surface is influenced by: (i) the chemical composition, structure and concentration of pollutants, (ii) the radiation intensity, (iii) the exposure time, (iv) the amount of photocatalyst used, (v) the oxygen content in the reaction medium, (vi) the pH value of the solution, (vii) the properties of a photocatalyst (specific surface area, crystallographic structure, number of surface defects, presence of additives and dopants, etc.) [45,46].

Photocatalysis can be also applied for the oxidation of inorganic compounds, such as nitrogen oxides. The mechanism of photocatalytic NO_x oxidation under UV illumination is represented by Equations (1)–(7) [47]. The reactants are adsorbed on the photocatalyst surface:



and subsequently the NO_x species undergo oxidation by the $\bullet OH$ radicals as follows:





Photocatalysis is also used for water splitting. In this process, the electrons excited to the CB participate in the H^+ reduction to generate H_2 , while the holes oxidize H_2O to form O_2 . To realize the water splitting, the bottom of the CB must be more negative than the reduction potential of H^+/H_2 (0 V vs. NHE (normal hydrogen electrode) at pH = 0), and the top of the VB must be more positive than the oxidation potential of $\text{H}_2\text{O}/\text{O}_2$ (1.23 V vs. NHE at pH = 0). Furthermore, the band gap of the semiconductor must exceed the free energy (1.23 eV) of water splitting [48].

In another approach, photocatalysis is applied for photoreduction of CO_2 [49–61], resulting in the production of CO , CH_4 , CH_3OH , HCOOH , or HCHO . The process can be realized either in the gaseous or liquid phase. In most systems, H_2O is used as a reductant and the first step of the process is the formation of $\bullet\text{H}$ and H_2 . The reaction mechanism of the subsequent steps is still under debate, and the pathways depend on the process conditions and the photocatalyst properties [58].

TiO_2 photocatalysis can be also applied for the selective photocatalytic oxidation of a broad range of organic compounds, including hydrocarbons, aromatic compounds, and alcohols. The hydroxylation of aromatics is one of the examples of the photocatalytic synthesis of industrially important chemicals. Phenol (Ph), hydroquinone, and catechol are the chemicals which are widely used as precursors of resins and pharmaceutical products. Alcohols, in principle, can be photocatalytically oxidized to the corresponding carbonyl compounds [62].

Another approach is the inactivation of bacteria by the photocatalytic process. Qiu et al. [63] confirmed that the cell damage occurred and the destruction of the cytoplasmic components such as DNA and enzymes was the primary reason responsible for the bacterial inactivation.

More details on the photocatalysis subject can be found elsewhere [40–44,63–66].

3. C-Doped TiO_2

The introduction of C atoms into TiO_2 structure can lead to band gap narrowing and thus improvement in visible light absorption. The C-doped TiO_2 photocatalysts were employed for the removal of organic compounds, e.g., dyes and pharmaceuticals, from aqueous matrices [67–70], the production of hydrogen, or utilized as the bactericidal agents [71–73]. The development of photocatalysts containing various carbon species has recently been presented by Shi et al. [36]. The authors paid special attention to the strategies of synthesis of C-doped TiO_2 , N,C-doped TiO_2 , metal-C-doped TiO_2 , and other co-doped C/ TiO_2 composites. In the present review, the C-doping of TiO_2 using different types of carbon precursors is discussed.

In general, it is hard to distinguish the most frequently used carbon precursors, because the researchers apply very different compounds to prepare C-doped TiO_2 photocatalysts. Some examples are summarized in Table 1. Among the applied compounds, there are several substances which simultaneously acted as the TiO_2 and carbon precursors, e.g., titanium carbide (TiC) [68,69,72], titanium(IV) oxyacetylacetonate [74], and titanium(IV) butoxide (TBOT) [73,75–77].

Table 1. Selected examples of methods and precursors applied during preparation of C-doped TiO_2 photocatalysts.

Method	TiO_2 Precursor	Carbon Source	References
Biomimetic template approach	TBOT	Banana stem fibers	[78]
Calcination	Aeroxide [®] TiO_2 P25 from Evonik, Germany (TiO_2 P25)	Polyethylene glycol	[79]
Chemical bath deposition (CBD)	Titanium isopropoxide (TTIP)	Melamine borate	[80]

Table 1. Cont.

Method	TiO ₂ Precursor	Carbon Source	References
Direct solution-phase carbonization	TiCl ₄	Diethanolamine (DEA)	[81]
Electrochemical anodization	Ti foils	Ascorbic acid	[82]
Electrospinning combining sol-gel	TBOT	Polyvinyl-pyrrolidone (PVP)	[83]
Electrospinning followed by heat treatment	TTIP	Acetic acid	[84]
Hydrolysis	TBOT	Glucose	[85]
Hydrothermal	TiC	TiC	[69]
Hydrothermal treatment and calcination	Ti(SO ₄) ₂	Glucose	[86]
Incipient wetness impregnation	TiO ₂ P25	Glucose	[87]
Oxidative annealing	TiC	TiC	[88]
Sol impregnation and carbonization	TBOT	Acetic acid	[84]
Sol-gel	TTIP, TBOT, TiCl ₄ , TiCl ₃	Ethanolamine (ETA), Glycine, Polyacrylonitrile (PAN), Polystyrene (PS), Starch, TBOT	[76,77,82,89–92]
Sol-gel and calcination	TBOT	Butterfly wings	[93]
Sol-gel bio-templating	TBOT	Cellulose	[94]
Sol-microwave	TBOT	Cellulose	[94]
Solution combustion synthesis	TTIP	Citric acid	[95]
Solvothermal	TTIP	Acetone	[71]
Solvothermal treatment and calcination	TiCl ₄	Alcohols (benzyl alcohol and anhydrous ethanol)	[75]
Thermal decomposition	TTIP	Oleylamine	[96]

Selection of the carbon precursor affects the properties of the photocatalyst. Mani et al. [95] prepared two series of C-doped TiO₂ via solution combustion synthesis using titanium nitrate (TiO(NO₃)₂) as TiO₂ precursor, and citric (Cit-TiO₂) and ascorbic (Asc-TiO₂) acids as carbon sources. The authors compared the properties and the photocatalytic activity of the photocatalysts in the Ph and Cr(VI) removal process. X-ray diffraction (XRD) studies confirmed the anatase phase with the crystallite size of 4–6 nm in both types of the photocatalysts. The band gap energy calculated from the diffuse reflectance UV–vis (UV-vis/DR) spectra was found to be 0.2 eV lower for Cit-TiO₂ compared to Asc-TiO₂ and equaled 2.8 eV. The observed specific surface area (S_{BET}) was found to be 290 and 230 m² g^{−1} for TiO₂ modified with citric and ascorbic acid, respectively. Due to the lower band gap energy and a higher S_{BET}, Cit-TiO₂ revealed higher photocatalytic activity under the simulated solar light irradiation than Asc-TiO₂. Moreover, both photocatalysts were more active than the commercial TiO₂ P25.

Numerous researchers have reported the C-doped TiO₂ fabrication by commonly used methods, such as sol-gel [73,77,90,91,93,97], sol-microwave [98], and solvothermal [67, 71,75,99]. However, there are also works, in which other approaches have been applied, including electrospinning [100], CBD [80], or hydrothermal treatment of TiC powder [69].

Qian et al. [101] presented the preparation procedure of TiO₂-based photocatalysts with a honeycombed structure (Figure 3). A facile template method of synthesis involves the use of PS microspheres as a template. The TiO₂ layer is formed on the surface of the template as a result of the hydrolysis process. Subsequently, calcination is applied in order to remove the template and obtain a honeycombed morphology. During the calcination, an

incomplete combustion of the PS results in the formation of carbon-doped TiO₂. There is a possibility of further processing of the as-received photocatalyst, for instance by depositing of Au onto C-doped TiO₂ layer.

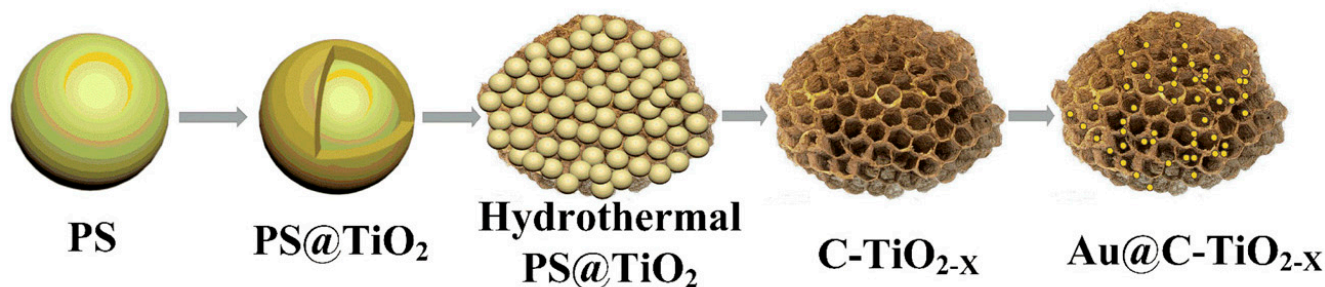


Figure 3. Schematic illustration of the preparation procedure of the honeycombed C-doped TiO₂ and Au@C-doped TiO₂. Reproduced from [101] with permission from Elsevier.

The successful incorporation of carbon atoms into the TiO₂ lattice can be confirmed on the basis of X-ray photoelectron spectroscopy (XPS) analysis [76,102–104]. Exemplary XPS spectra of the C-doped TiO₂ are shown in Figure 4 [103]. The two strong peaks occurring usually in the range of 527–531 and 456–465 eV correspond to O 1s and Ti 2p binding energies (BE), respectively, indicating the presence of oxygen and titanium [76,102–104]. The peaks centered near 530 eV are attributed either to lattice (O_{lat}) or surface adsorbed (O_{sur}) oxygen. The C-doping may result in a decrease in O 1s BE, thus enhancing the generation of oxygen vacancies (O_v). Qian et al. [101] reported an increase in the O_{lat}/O_{sur} ratio upon doping with carbon from 2.7 to 3.3. Furthermore, the introduction of carbon into the TiO₂ lattice results in a simultaneous increase in Ti³⁺ and Ti⁴⁺ binding energy, observed as a shift of the Ti 2p_{3/2} position, which is associated with a change in the coordination environment of O and Ti atoms. The C 1s peak is observed typically at about 284–285 eV. In the example shown in Figure 4b, this peak can be further deconvoluted into two peaks corresponding to BE of 284.7 and 288.4 eV, and representing residual carbon (C-C) with sp² hybridization and C atoms substituting Ti in the TiO₂ lattice (C-O) [76,102–104]. Other peaks related to carbon species can be also present in the case of C-modified TiO₂. For example, the peak assigned to the residual C=O species was observed at BE of 288.6 eV [101], while the Ti-C peak was reported at 282.3 eV [105].

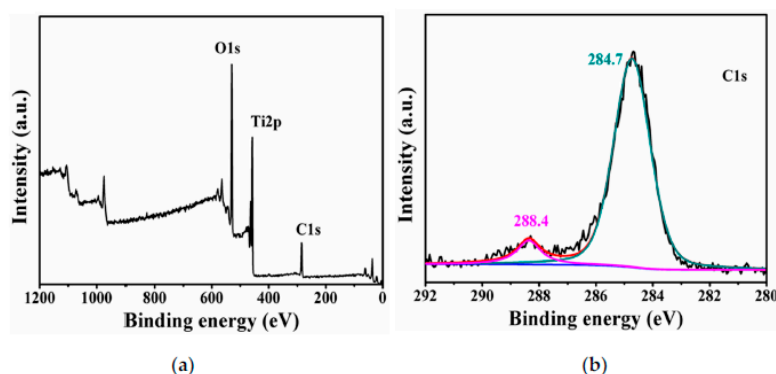


Figure 4. XPS spectra of C-doped TiO₂: (a) full scan; (b) focus scan of C 1s. Reproduced from [103] with permission.

The above data reveal that carbon doping into TiO₂ can occur according to 3 various pathways: (i) substitution of O_{lat} with C leading to a replacement of Ti-O by Ti-C bonds, (ii) replacement of Ti by C due to the rupture of Ti-O and creation of C-O bonds, or (iii) stabilization of C at the interstitial position [106,107].

C-doped TiO₂ photocatalysts exhibit enhanced photocatalytic activity associated with changes in the crystalline structure, narrowing of the band gap, and lowering of the point of zero charge value [1]. The crystalline structure is affected by the preparation conditions of the photocatalysts, such as calcination temperature and atmosphere. In general, the presence of carbon retards the phase transformation from anatase to rutile [1]. Moreover, it was found that the crystallinity of C-doped TiO₂ nanotubes can be enhanced by annealing in argon atmosphere instead of oxygen or nitrogen [108]. Furthermore, application of Ar or N₂ was found to be advantageous in terms of improvement in photocatalytic activity. That was ascribed to the formation of O_v due to C-doping, which could trap the electrons and reduce the recombination of e⁻/h⁺ pairs [108].

Figure 5 presents a comparison of the pathways of electron transfer in the C-doped TiO₂ annealed under inert (Ar, N₂) and oxidizing (O₂) atmosphere. In both cases, the formation of a new state above the VB can be observed, which was attributed to the C 2p state of the interstitial carbon. Moreover, in the case of the photocatalysts annealed in the inert environment, a formation of an additional state below the CB was postulated, which was ascribed to the antibonding C-O state resulting from the creation of O_v. The C-O state was not observed in the case of calcination in oxygen flow because such conditions diminished the O_v [108].

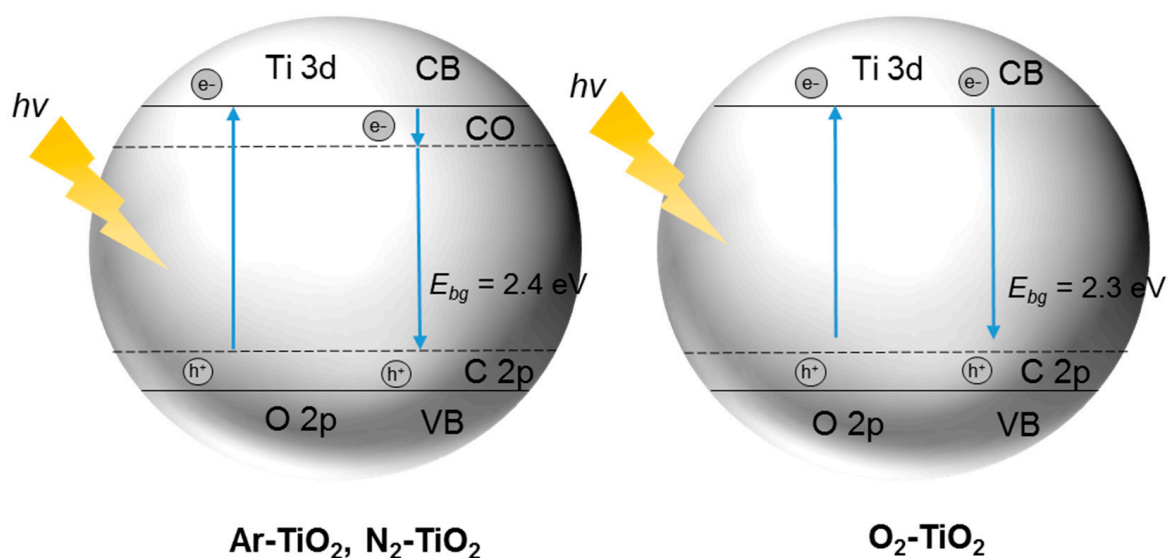


Figure 5. Pathways of electron transfer in the presence of radiation in C-doped TiO₂ annealed under inert (Ar-TiO₂, N₂-TiO₂) and oxidizing (O₂-TiO₂) atmosphere (adapted from [108]).

Shao et al. [109] proposed a possible mechanism of the enhanced photocatalytic activity of C-doped TiO₂ nanorods (Figure 6). The appearance of a new impurity energy level above the VB, caused by C-doping of TiO₂, results in narrowing of the band gap, and the photocatalyst can absorb the visible light. Direct promotion of electrons from the impurity level to the CB leads to the production of photogenerated electron–hole pairs. Electrons participate in the reduction of O₂ molecules to form O₂^{•-}, while holes oxidize hydroxyl ions and water molecules to [•]OH radicals.

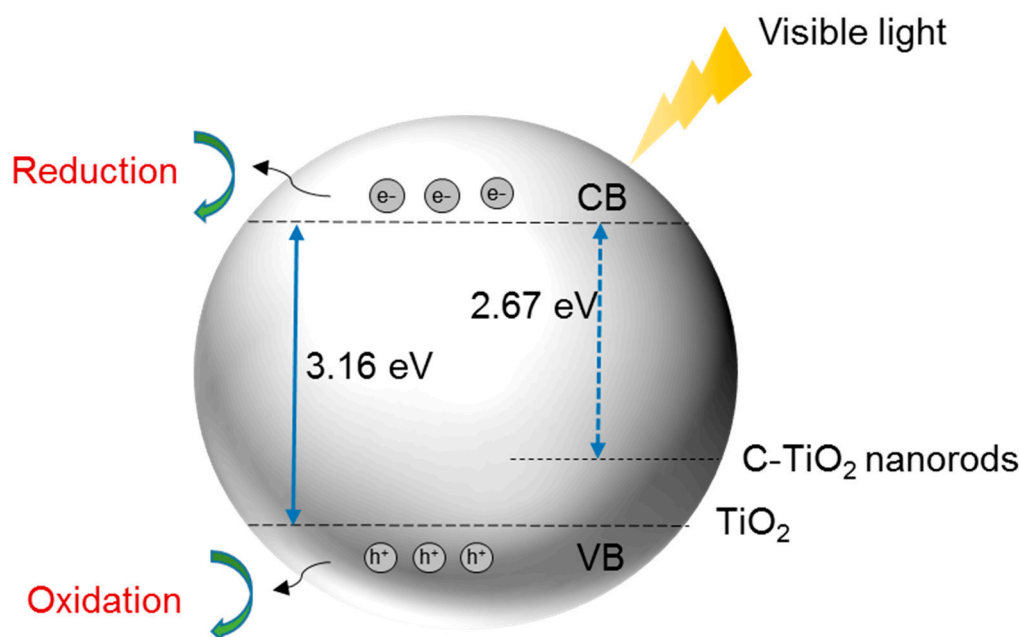


Figure 6. Schematic illustration of the mechanism of photocatalysis over C-doped TiO₂ nanorods under visible light (adapted from [109]).

The photocatalytic activity of the nonmetal-doped photocatalysts under visible light irradiation is commonly evaluated with the application of various dyes as model compounds, although such an approach was already discussed in the literature as the inappropriate method [110]. This is because dyes absorb visible light and as a result the photocatalytic reaction might be induced not only by the absorption of the visible light by the photocatalyst, but also by the photoabsorption of the radiation by the dye (i.e., dye sensitization). Nonetheless, since, in most literature reports on the visible light-active photocatalysts, the dyes are routinely applied, in this review some examples are also presented and discussed. For instance, Song et al. [100] applied the C-doped TiO₂/carbon nanofibrous films (CTCNF) for photocatalytic decomposition of rhodamine B (Rh B) under visible light irradiation. After 150 min of the experiment the decolorization rate reached 66.4%–94.2%, being the lowest for the film carbonized at 900 °C and the highest for the film carbonized at 800 °C (CTCNF-800). The photocatalytic stability of the CTCNF-800 was kept constant during six cycles of recycle and reuse, with the decolorization efficiency exceeding 92%. Moreover, the authors reported good durability of the film stored for 1 year in air without illumination (90% Rh B decolorization efficiency).

The C-doped TiO₂ photocatalysts were also applied for the removal of other organic compounds, such as pharmaceuticals, personal care products and even bacteria, from water [67–70,72,73], as well as for hydrogen production [71]. For instance, Shi et al. [68] prepared the carbon self-doped TiO₂ flakes (CTF) with octahedral bipyramid skeleton structure and exposed {001} facet by hydrothermal treatment of TiC powder in a HF-HNO₃ aqueous solution. The photocatalyst was applied for the mineralization of antibiotic ciprofloxacin (CIP) under visible light irradiation. The researchers revealed that about 70% of CIP was mineralized in 6 h of experiment. For comparison, the CIP mineralization in the presence of TiO₂ P25 as a reference did not occur, while in the case of C-doped TiO₂ sheets (CTS), it was about half the value (35%). According to the authors, the enhanced photoactivity of CTF was mainly caused by the synergic effect of several factors: (i) the narrowing of the band gap due to the carbon doping, (ii) the higher percentage of the exposed {001} facets, (iii) the larger specific surface area of C-doped TiO₂, and (iv) its unique octahedral bipyramid skeleton structure.

The application of C-doped TiO₂ for the removal of various pollutants from air was also examined [81,111]. Huang et al. [81] applied mesoporous nanocrystalline C-doped

TiO₂ obtained through a direct solution-phase carbonization using TiCl₄ and DEA as precursors in order to oxidize NO_x in indoor air conditions under simulated solar light irradiation. The effectiveness of removal was significantly higher compared to the commercial TiO₂ P25 and amounted to 25% and 12% after 40 min of irradiation in the case of C-doped TiO₂ calcined at 500 and 600 °C, respectively.

Shim et al. [73], fabricated C-doped TiO₂ in order to inactivate *Listeria monocytogenes* bacteria. After 2.5 h of visible light irradiation with and without UV radiation, a 2.10 and 2.45 log reduction in bacteria was achieved, respectively. The authors stated that the photocatalytically produced ROS were responsible for the observed disinfection effect.

The C-doped TiO₂ materials were also applied for hydrogen production [71]. In the presence of the carbon-doped TiO₂ decorated with reduced graphene oxide (r-GO) and methanol as an electron donor, the H₂ production under visible light (400–690 nm) amounted to 1.50 ± 0.2 mmol g⁻¹ h⁻¹ [71].

In another approach, the C-doped TiO₂ was applied for photoreduction of CO₂ [59]. A series of photocatalysts were prepared by sol-gel method with the application of citric acid as a carbon source. The best performance exhibited the C-doped TiO₂ calcined at 300 °C and subsequently subjected to Al reduction treatment. The space-time yield of CH₄ and CO amounted to 4.1 and 2.5 μmol g⁻¹ h⁻¹ under solar light, and 0.53 and 0.63 μmol g⁻¹ h⁻¹ in the case of visible light irradiation, respectively.

The presented above overview shows that C-doping of TiO₂ is at the center of interest of numerous researchers. Various substrates and synthesis methods have been applied for production of C-doped TiO₂. Among them, the most common approaches include utilization of sugars, organic acids, and (bio)polymers as carbon sources and titanium alkoxides as TiO₂ precursors, and synthesis of the photocatalysts via sol-gel, sol-microwave, and solvothermal methods. There are only a few works on less common approaches, such as those based on utilization of banana stem fibers and butterfly wings as carbon sources, or application of electrospinning for the photocatalysts fabrication. The C-doped TiO₂ was reported to have a potential application in photocatalytic processes utilizing visible or solar light. They include removal of organic contaminants from water, bacterial inactivation and hydrogen production. Nonetheless, a majority of papers are still focused on the decolorization of dyes, while degradation and mineralization of other contaminants are less extensively investigated.

4. N-Doped TiO₂

Among all the non-metal dopants, nitrogen is the one most frequently used [1]. This is predominantly due to its small ionization energy and its atomic size comparable with that of oxygen [112]. Numerous precursors of nitrogen have been employed for the preparation of N-doped TiO₂, as can be seen in Table 2.

Table 2. Selected examples of methods and precursors applied during preparation of the N-doped TiO₂ photocatalysts.

Method	TiO ₂ Precursor	Nitrogen Source	References
Addition of N source to the TiO ₂ precursor solution	TBOT	Tetramethyl-ethylene-diamine	[113]
Bioprocess	TBOT	Extrapallial fluid of fresh blue mussels	[114]
Centrifugal spinning	Titanium diisopropoxide bis(acetyl-acetonate)	PVP	[115]
Colloidal crystal-templating	TBOT	Ethanediamine	[116]
CVD	TiCl ₄	<i>tert</i> -butylamine, benzylamine	[117,118]
Electrochemical	Titania nanotubes	Diethylenetriamine, ethylenediamine, hydrazine	[113,119–121]
Electrochemical anodization	Titanium foils	Ammonium fluoride	[122]

Table 2. Cont.

Method	TiO ₂ Precursor	Nitrogen Source	References
Hydrolysis	TTIP	NH ₄ Cl, pyridine	[123–125]
Hydrothermal	TBOT	KNO ₃	[126]
Hydrothermal treatment of TiN with H ₂ O ₂	TiN	TiN	[127]
Incomplete oxidation of titanium nitride	TiN	TiN	[128]
L-alanine acids assisted process	TTIP	L-alanine acids	[129]
Low temperature non-aqueous solvent-thermal method	TiCl ₄	NH ₄ Cl	[130,131]
One-pot hybridization	TTIP	Ethylenediaminetetraacetic acid disodium salt (EDTA-Na ₂)	[132]
Radio-frequency magnetron reactive sputtering	TiO _x film	N(NO _x)	[133]
Sol-gel	TTIP, TBOT, TiCl ₄ , Titanic acid	Urea, NH ₃ , nitromethane, <i>n</i> -butylamine, N ₂ , hydrazine, HNO ₃ , guanidinium chloride, ethylenediamine, diethanolamine, NH ₄ NO ₃ , NH ₄ Cl, (NH ₄) ₂ CO ₃	[119,134–151]
Solvent-based ambient condition sol process	TiCl ₄	<i>N,N</i> -dimethylformamide (DMF)	[152]
Solvothermal	TBOT, TiCl ₄	Trimethylamine (TEA), PVP, hydrazine, diethylamine	[102,153–158]
Sonication of aqueous solution	TiO ₂ P25	4-nitrophenol (4-NP)	[159]
Sonochemical	TiO ₂ P25, TBOT,TTiP	Sodium amide, hydroxylamine hydrochloride, urea	[160–162]
Surfactant-free solvothermal treatment	TBOT,TiCl ₄	Carbamide	[163]
Two cycle microwave-assisted hydrothermal	TTIP	Diaminohexane	[164]

A comparison of the properties of the N-doped TiO₂ photocatalysts prepared from TTIP as a TiO₂ precursor and three different nitrogen sources (urea, ethylenediamine (EDA) and trimethylamine (TEA)), at different N/Ti molar ratios, was presented by Mahy et al. [165]. They prepared photocatalysts with activity extended towards the visible region using an aqueous sol-gel synthesis. For urea and TEA-modified photocatalysts, the anatase-brookite TiO₂ nanoparticles (NPs) were formed, with a specific surface area of 200–275 m² g⁻¹. In the case of EDA-modified photocatalysts, the formation of a rutile phase was observed and the S_{BET} was 185–240 m² g⁻¹. The XPS measurements suggest the incorporation of nitrogen in the TiO₂ materials through Ti–O–N bonds, allowing light absorption in the visible region.

Makropoulou et al. [166] synthesized the N-doped TiO₂ photocatalysts using TTIP as a TiO₂ precursor and various nitrogen dopants: urea, TEA and NH₃. A comparison of their properties is presented in Table 3. The highest specific surface area was observed for the N-doped TiO₂ prepared with urea dopant, while the lowest band gap energy value was found in the case of the photocatalyst prepared with TEA.

Table 3. A comparison of the properties of the N-doped TiO₂ photocatalysts synthesized using TTIP as TiO₂ precursor and different nitrogen sources (concentration of 25 vol%) [166].

Photocatalyst	d _{TiO₂} ^a (nm)	S _{BET} ^b (m ² g ⁻¹)	E _{bg} ^c (eV)
N-TiO ₂ (urea)	10.8	79	3.03
N-TiO ₂ (TEA)	11.5	12	2.89
N-TiO ₂ (NH ₃)	18.0	29	3.01

^a Crystallite size estimated from XRD. ^b S_{BET} estimated with the Brunauer-Emmett-Teller (BET) method. ^c Band gap energy determined according to the Tauc method.

Huang et al. [164] prepared novel N-doped anatase mesoporous bead photocatalysts using a two-cycle microwave-assisted hydrothermal method with three various nitrogen precursors: 1,6-diaminohexane (HDA), TEA and urea. They used TTIP as a TiO₂ precursor. Different nitrogen sources gave different degrees of N doping: 6.16, 1.14, and 1.24 wt.% for HDA, TEA and urea, respectively.

Apart from different nitrogen precursors, various other approaches for N doping into TiO₂ have also been described (Table 2). Typically, wet chemical methods were applied, including hydrolysis [164,167–173], sol-gel [112,134,165,174–187], solvothermal [135,153,188] and plasma enhanced electrolysis [173,189]. There are also dry methods, such as magnetron sputtering [190,191] and other approaches, e.g., chemical vapor deposition (CVD) [136], pulsed laser deposition (PLD) [192], and arc melting [193].

The as-prepared N-doped TiO₂ is typically post-annealed to improve the photocatalytic activity. Zhang et al. [185] investigated the influence of the calcination temperature on the optical and photocatalytic properties of the photocatalysts. They found that the temperature should not be lower than 200 °C. Moreover, a very high calcination temperature was reported to have an adverse effect on the TiO₂ photocatalytic activity. The highest visible-light activity of N-TiO₂ at N/Ti molar ratio of 1 was observed for the calcination temperature of 350 °C.

Krivtsov et al. [194] demonstrated that thermal treatment at temperatures of 400–500 °C caused nitrogen species to occupy interstitial positions in TiO₂. However, the treatment under air at higher temperatures almost completely removed the N-dopants, reducing the photoactivity.

Mohamed et al. [183] examined photocatalytic activity of the N-doped TiO₂ calcined at different temperatures. They prepared the photocatalysts with the sol-gel method using HNO₃ and TBOT as N and TiO₂ precursors, respectively. The results of their research are presented in Table 4. The photocatalytic activity increased under both visible and UV irradiation as the calcination temperature increased, reaching its maximum at 400 °C. A further increase in the temperature led to a decrease in the photocatalytic activity both for visible and UV light. Moreover, the efficiency of Ph photodecomposition under visible light in the presence of the N-doped TiO₂ was visibly higher compared to that observed for commercial TiO₂ P25 and pure anatase TiO₂ (TAA). The incorporation of nitrogen resulted in a considerably narrower band gap, leading to an improved vis-light photoactivity of the modified photocatalysts compared to the undoped TiO₂.

Table 4. Properties and photocatalytic activity of the N-doped TiO₂ photocatalysts prepared at different calcination temperature, where T75 is the photocatalyst dried at 75 °C, and T200, T400, T600 and T800 are the photocatalysts calcined at 200, 400, 600, and 800 °C respectively, TAA is pure anatase TiO₂ purchased from Sigma Aldrich. Initial concentration of Ph was 50 mg L⁻¹ [183].

Photocatalyst	Calcination Temperature (°C)	Anatase (%)	Rutile (%)	E _{bg} (eV)	Decomposition of Ph after 540 min (%)	
					Visible Light	UV Light
T75	-	95.0	5.0	2.80	81.07	68.00
T200	200	52.8	47.2	2.54	86.92	84.00
T400	400	38.3	61.7	2.50	99.16	99.60

Table 4. Cont.

Photocatalyst	Calcination Temperature (°C)	Anatase (%)	Rutile (%)	E_{bg} (eV)	Decomposition of Ph after 540 min (%)	
					Visible Light	UV Light
T600	600	12.0	88.0	2.60	95.28	92.00
T800	800	0	100	3.06	53.99	44.88
TAA	-	100	0	3.85	5.21	57.86
TiO ₂ P25	-	72	28	3.24	5.21	80.64

There are two possible modes of nitrogen incorporation into the TiO₂ structure, interstitial (addition of nitrogen into the TiO₂ lattice) and substitutional (replacement of oxygen) [112,195]. To show the state of nitrogen, XPS analysis is performed. In the literature, the peak around 400 eV is widely assigned to the interstitial nitrogen species, directly bound to the lattice oxygen (Ti-O-N) [164,195]. According to Marques et al. [134] and Mahy et al. [165], the photoelectron lines associated with Ti-N bonds inherent to a successful substitutional doping appear in the 396–398 eV range, while lines above 400 eV are usually assigned to the interstitially doped nitrogen. Cao et al. [196] confirmed the presence of the peak at 399.4 eV, implying substitutional nitrogen doping (O-Ti-N) and the other peak at 400.8 eV, which can be assigned to the interstitial nitrogen doping (Ti-O-N) (Figure 7). It has been reported that the interstitial N atoms give rise to the higher energy states in the band gap and behave as stronger hole trapping sites, reducing the direct oxidation ability. They are also easily oxidized in air at high temperatures [193].

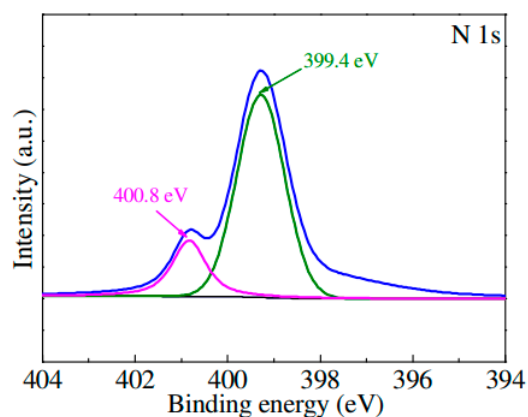


Figure 7. Photoelectron N 1s spectral region for the N-doped TiO₂ photocatalyst. Reproduced from [196] with permission from Elsevier.

The N 1s peak localized around 400 eV may also correspond to many other contributions, potentially due to impurities, usually indicating the presence of oxidized nitrogen species such as N₂O₂²⁻, NO_x, N₂, NH_x or NHOH [165,172,174]. Nitrogen within nitrites (NO₂⁻) and nitrates (NO₃⁻) is commonly characterized by the N 1s with BE higher than 403 eV, while nitrogen within nitrides (N₃⁻) occurs in a range of 396–398 eV [195].

Nitrogen incorporation into TiO₂ creates an N 2p intermediate band localized above the O 2p VB. That results in a decrease in the band gap of the photocatalyst and a shift of the optical absorption to the visible light region. It was reported [39,197,198] that substitutional N-doping of TiO₂ narrows the band gap to a lesser extent than the interstitial N-doping.

The mechanism of photocatalysis in the presence of N-doped TiO₂ is summarized in Figure 8. The substitutional nitrogen state (N_s) and the interstitial nitrogen state (N_i) are directly responsible for the origin of the visible light induced photocatalysis. Nitrogen doping allows the electron to be excited from the N impurity levels (N_s and N_i) to the CB of TiO₂ (paths B and C). Then the electron can be trapped by the oxygen vacancy, which is

an energetically favorable process. The electrons in the CB and O_v states may recombine with h^+ in the N impurity levels, which is an unfavorable phenomenon. Alternatively, the photoexcited e^- can reduce O_2 molecules to $O_2^{\bullet-}$, resulting further in the formation of $\bullet OH$. Hydroxyl radicals can be also generated upon reaction of the holes with H_2O or OH^- . Pathway A, representing direct excitation of electrons from VB to CB of TiO_2 , is not possible under visible light irradiation [17,199].

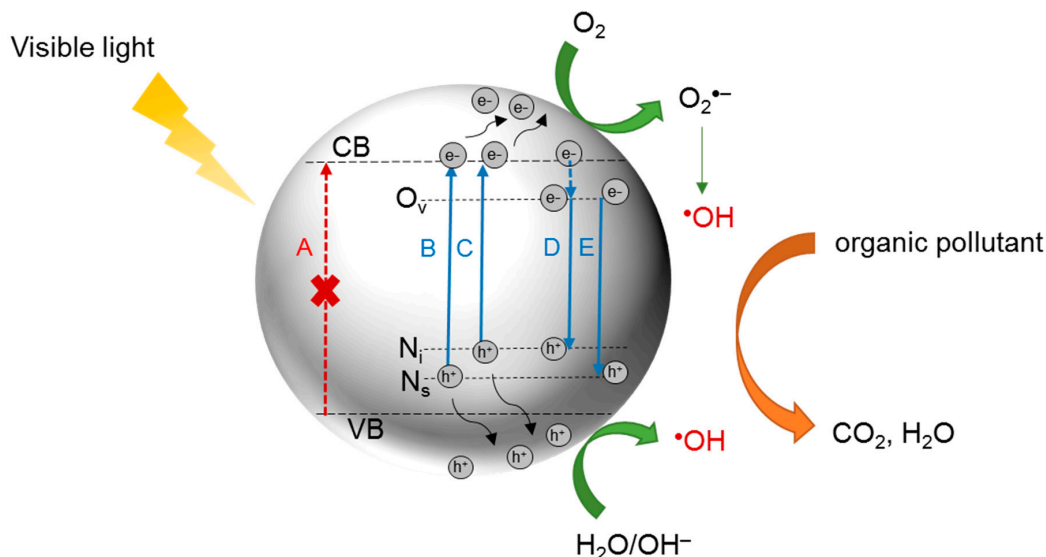


Figure 8. Effect of N-doping on TiO_2 photocatalysis. Proposed band structure of N-doped TiO_2 under visible light irradiation (adapted from [17,39,200]).

A modified mechanism was proposed by Cao et al. [196] in the case of the solar-driven photocatalysis over Ti^{3+} and N co-doped photocatalysts. The materials were obtained by $NaBH_4$ reduction of urea-modified mesoporous TiO_2 spheres under Ar atmosphere and elevated temperature ($350\text{ }^\circ C$). The mechanism is schematically illustrated in Figure 9. N-doping of TiO_2 resulted in emerging of a new impurity level above the VB, which was already discussed above. Additionally, below the CB, an intermediate energy level was generated by introduction of Ti^{3+} and O_v . That narrowed the band gap and consequently improved photocatalytic efficiency in a visible light.

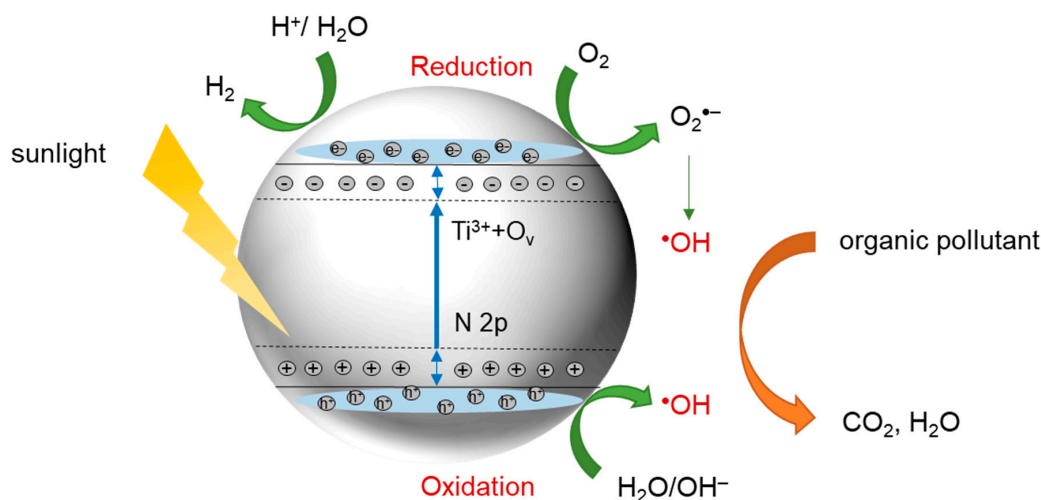


Figure 9. Schematic illustration for the solar-driven photocatalytic mechanism of N-doped TiO_2 (adapted from [196]).

The ratio of the substitutional to interstitial N can be changed, e.g., via the calcination procedure. Bjelajac et al. [201] reported that N-doping of TiO₂ nanotubes realized by annealing in an ammonia atmosphere resulted in both substitutional and interstitial incorporation of nitrogen. However, only interstitial N was observed when a post-treatment by calcination in air was realized. It was also reported [200] that in the case of the doping of a crystalline material (strong Ti-O bonds), the substitution of oxygen with N can be prevented, which results in a lower concentration of substitutional N. On the opposite, the amorphous structure of TiO₂ (weak Ti-O bonds) facilitates substitutional N-doping.

Nonetheless, the role of the interstitial and substitutional nitrogen in the improvement in the photocatalytic activity of N-doped TiO₂ is still unclear. Some authors reported that interstitial N exhibited better photoactivity under visible irradiation than substitutional N [202,203], while others reported that the substitutional N improves the photocatalytic activity to a higher extent [204,205]. Moreover, there are works showing that the visible photocatalytic activity is better when the quantity of the interstitial and substitutional N is equal [200].

Photocatalytic activity of the N-doped TiO₂ has been examined in various applications. In general, the N-doped TiO₂ photocatalysts were used for the removal of organic compounds, in particular dyes [164,167,170,174,175,182,185,196,206–208] and pharmaceuticals [170,174,209,210] from water. The other degraded pollutants were phenol [128], furfural [211], parabens [176], surfactants [212], and herbicides (paraquat [172], and bentazon [213]). The application of the N-doped TiO₂ photocatalysts for removal of contaminants such as acetaldehyde [214], benzene [215], ethylbenzene [216], NH₃ [117], and NO_x [217] from gaseous phase was also proposed. Some of the photocatalysts exhibited antibacterial properties, e.g., towards *Escherichia coli* [166,209,218,219] and against oral cariogenic biofilms [153]. Moreover, application of the N-doped TiO₂ for human breast cancer diagnostics [220] and treatment of cancers such as melanoma [221] was proposed.

Monteiro et al. [209] prepared a series of visible light-active N-doped TiO₂ photocatalysts by a simple impregnation method, well suited for a scale-up to mass production. They used urea and TiO₂ P25 as precursors. Photocatalytic activity of the obtained photocatalysts was tested by degradation of diphenhydramine hydrochloride (DP) under visible light irradiation and was found to depend on the amount of nitrogen dopant and calcination temperature. The optimal calcination temperature was found to be 380 °C. The photocatalyst prepared at the urea/TiO₂ ratio of 0.5 exhibited the highest photocatalytic efficiency (Figure 10). This was explained by the lowest band gap energy obtained for that photocatalyst (2.99 eV).

Xing et al. [174] used a common antibiotic CIP to evaluate the photocatalytic properties of the N-doped TiO₂ immobilized on the glass spheres. The photocatalytic activity experiments were carried out with 20 mL CIP aqueous solution (20 mg L⁻¹) and the supported photocatalyst loading was equal to 3 g L⁻¹. A 90% removal rate in 90 min under visible light irradiation from a 500 W xenon lamp ($\lambda > 420$ nm) was reported. Moreover, the removal rate of CIP in the five cycles of reuse was more than 90% in 120 min and almost no exfoliated photocatalyst was observed.

Delavari et al. [139] synthesized the N-doped titania nanotube arrays via electrochemical anodization method. The photocatalyst was applied to photocatalytic conversion of CO₂ and CH₄. With optimal experimental conditions of 250 W UV light power, 2 cm distance between UV lamp and reactor and initial amount of 10% CO₂, the efficiency of photoconversion was up to 41.5% and 62.2% for CO₂ and CH₄, respectively.

The N-doped TiO₂ was also used in the photocatalytic production of hydrogen [168,222]. Reddy et al. [168] prepared various N-doped TiO₂ photocatalysts using the hydrothermal method followed by calcination in air at 350 °C. Among them, the one with multiphase titania consisting of 69% anatase, 17% brookite and 14% rutile showed the highest photoactivity towards hydrogen production (10.5 mmol h⁻¹ g⁻¹). Preethi et al. [222] synthesized their photocatalyst by anodization method followed by annealing under 50 mL min⁻¹ NH₃ flow at 450 and 550 °C for 2 h. The obtained efficiency of H₂ generation was ~2–3 mmol h⁻¹ g⁻¹.

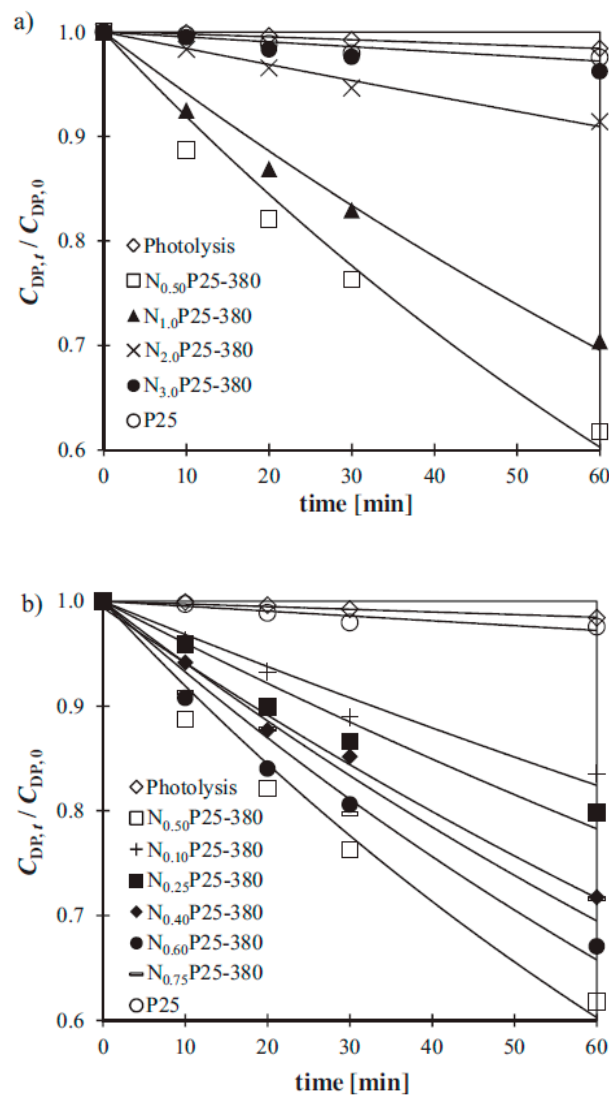


Figure 10. Photocatalytic degradation of DP (10 mg L^{-1}) under visible light illumination for TiO_2 P25 modified with different urea contents. Photocatalyst loading = 1.0 g L^{-1} . The curves represent the fitting of the pseudo-first order equation to the experimental data. Reproduced from [209] with permission from Elsevier.

The N-doped TiO_2 microsheets fabricated hydrothermally from TiN in the presence of HF and HCl were successfully applied for CO_2 photoreduction [60]. After 2 h of UV-vis or visible light irradiation, the production rate of CH_3OH reached $0.71 \mu\text{mol g}^{-1}$ and $0.28 \mu\text{mol g}^{-1}$, respectively, and was significantly higher than observed for TiO_2 P25 ($0.05 \mu\text{mol g}^{-1}$ and $0 \mu\text{mol g}^{-1}$, respectively).

The above overview confirms that the N-doped TiO_2 is the most widely investigated photocatalyst among all of the non-metal-doped titania with enhanced visible light photocatalytic activity. The incorporation of nitrogen into the TiO_2 structure is relatively easy due to its atomic size, comparable with that of oxygen. Various methods of modification of TiO_2 with nitrogen have been applied, including both the wet (hydrolysis, sol-gel, solvothermal, plasma enhanced electrolysis) and dry (magnetron sputtering, CVD, PLD) approach. The most common nitrogen sources are urea, ammonia, nitric acid, N_2 gas and TEA, although numerous other compounds were also applied. Nitrogen-doped TiO_2 exhibits a broad absorption in the visible region, which allows the utilization of a large part of the solar spectrum. This is caused by a reduction in the band gap resulting from the interstitial or substitutional incorporation of nitrogen in TiO_2 . The N-doped TiO_2 was proposed to be

applied for effective water and air purification, as well as energy production, or medical and antimicrobial applications.

5. S-Doped TiO₂

The application of sulfur as a TiO₂ dopant is considered to provide significant beneficial effects for the photocatalytic activity. In a considerable number of literature reports on the S-doped TiO₂, sulfur is introduced into the photocatalyst by using an organic precursor, thiourea [45,46,102,223–245]. Nevertheless, it should be emphasized here that some authors used this precursor for the preparation of co-doped S,N-TiO₂, C,S-TiO₂ or C,N-TiO₂. In this section, thiourea is considered as a precursor of the S-doped TiO₂ only. There are also other organic compounds applied as a source of sulfur, including dimethyl sulfoxide (DMSO) [246–248], 1,2-ethanedithiol (EDT) [249], thioacetamide [250], and thiourea dioxide [251]. Accordingly, there are reports on application of inorganic compounds containing sulfur, such as TiOSO₄ [252–254], CS₂ [236,255], TiS₂ [256–258], H₂S [259,260], H₂SO₄ [261], K₂S₂O₅ [262], Na₂SO₄ [263], sulfur powder [245,264–267], and sodium thiosulfate [268]. During a typical preparation of the S-doped TiO₂ photocatalysts, TiO₂ precursors are mostly titanium alkoxides (TTIP [45,223,224,227–230,242,249,250,260,261,265], TBOT [225,226,232–234,246,248,266]). Inorganic titanium sources can be Ti(OH)₄ [267], TiCl₄ [237–240,247,263], TiH₂ [251], TiO₂ P25 [46,231], TiC [269], or metallic Ti [235,236,255]. Wang et al. [256] used TiS₂ as a source of both sulfur and titanium. They applied the low-temperature hydrothermal oxidation of TiS₂ in pH neutral solvent to obtain an S-doped TiO₂ photocatalyst with a high photocatalytic activity. Another example of a compound acting as a precursor of both sulfur and titanium can be TiOSO₄ [252–254]. Table 5 presents an overview of the sulfur precursors and synthesis methods applied during the preparation of the S-doped TiO₂ photocatalysts.

Table 5. Selected examples of methods and precursors applied during preparation of the S-doped TiO₂ photocatalysts.

Method	TiO ₂ Precursor	Sulfur Source	References
Ball milling	TiO ₂ P25	Sulfur powder, thiourea	[245]
Electrochemical anodization	Titanium sheet	H ₂ S, K ₂ S ₂ O ₅	[259,262]
Flame spray pyrolysis	TTIP	H ₂ SO ₄	[261]
Hydrolysis	TiCl ₄ , TTIP, TiC	Na ₂ SO ₄ , thiourea	[242,263,269]
Hydrothermal	TiH ₂ , TiS ₂ , TTIP, TiOSO ₄	Thiourea dioxide, thiourea, TiS ₂ , TTIP, TiOSO ₄	[242,243,251,254,256,257]
Micro-plasma oxidation	Titanium sheet	Thiourea	[244]
Oxidant peroxide method (OPM)	Metallic Ti	CS ₂	[236]
Oxidation annealing	TiS ₂	TiS ₂	[258,270]
Sol-gel	TBOT, TTIP	Thiourea	[102,242,245,271]
Solvothermal	TBOT, TTIP	DMSO, thioacetamide	[248,250]
Sonothermal	TBOT	Sulfur powder	[266]
Thermochemical treatment	TTIP	H ₂ S	[260]
Ultrasound application	TTIP, TiOSO ₄	EDT, TiOSO ₄	[249,254]
Wet impregnation	TiO ₂ P25	Sodium thiosulfate	[268]

Various approaches have been employed for the doping of TiO₂ with sulfur. Some common methods were used, including hydrothermal [232,257], solvothermal [248], sol-gel [45, 102,223,224,227,228,230,234,247,271], sol-gel followed by hydrothermal treatment [229,242], sonothermal [249,266], wet impregnation [46,231,268], and intercalation [246].

Moreover, newer synthetic strategies have also been proposed. Pillai et al. [267] used continuous ball milling with moderate thermoannealing (Figure 11), which resulted in a unique S-doped TiO₂ nanostructure composed of macroporous channels with mesoporous cores. This environmentally friendly, solventless and template-free method requires titanium hydroxide and elemental sulfur as substrates.

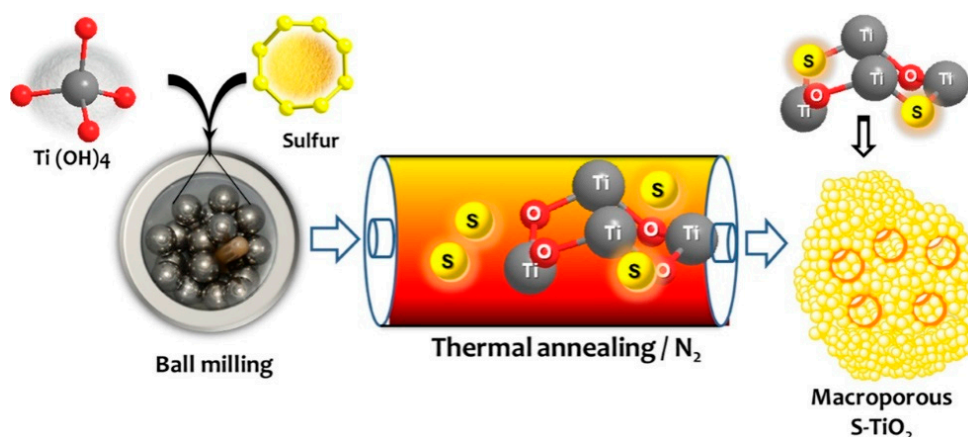


Figure 11. Schematic representation of the procedure of preparation of macroporous S-doped TiO₂ photocatalysts. Reprinted with permission from [267]. Copyright 2020 American Chemical Society.

Sharotri et al. [249] investigated the influence of sulfur doping on the phase transition of TiO₂. In order to study that, they prepared the S-doped TiO₂ photocatalysts calcined at 750 °C with different molar ratios of EDT (S source) to TiO₂ (1:0.1, 1:0.5 and 1:1). The results (Table 6) confirm that sulfur doping leads to a delay in the phase transition from anatase to rutile.

Table 6. Effect of S-dopant concentration on the crystallite phase of TiO₂. Calcination temperature: 750 °C [249].

EDT/TiO ₂ Molar Ratio	Phase Composition	
	Anatase (%)	Rutile (%)
1:0.1	11.9	88.1
1:0.5	58.2	41.8
1:1	89.5	10.5

There are two possible routes of sulfur doping-cationic or anionic. It has been reported that cationic doping takes place by titanium substitution with S⁴⁺ or S⁶⁺, while anionic doping occurs by oxygen substitution with S²⁻ [272]. The chemical state of the doped sulfur can be investigated by the XPS analysis (Figure 12). Generally, a peak at the BE values above 168 eV in the S 2p spectra can be assigned to sulfur on the higher oxidation state (S⁴⁺, S⁶⁺), substituting Ti atoms in the lattice of TiO₂ [236,260]. The peaks around 160–163 eV can indicate the Ti-S bonds' formation due to the substitution of O atoms in the TiO₂ lattice by S²⁻ [236,246,251,273].

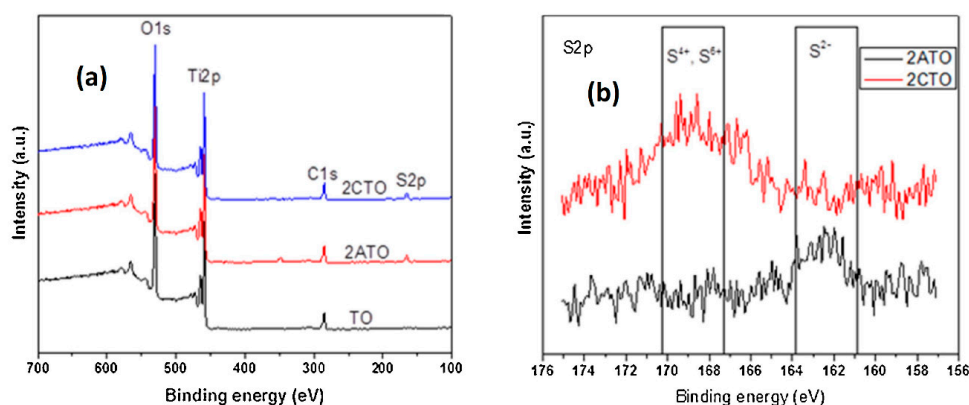


Figure 12. XPS survey spectra (a) of undoped (TO) and S-doped TiO₂ nanorods and S 2p region spectra (b) of anionic (2ATO) and cationic (2CTO) S-doped TiO₂ nanorods. Reproduced from [236] with permission from Elsevier.

The presence of cationic sulfur in the S-doped TiO₂ photocatalysts was confirmed in the literature by the peaks positioned at 168.3 [246], 168.5 [232], or 168.9 eV [233]. Zhu et al. [248] claimed that the peak at 168.5 eV, corresponding to S⁶⁺, can be further deconvoluted into two peaks at 168.5 and 169.7 eV (Figure 13), which can be attributed to S 2p_{3/2} and S 2p_{1/2}, respectively, with S 2p_{3/2} peak about twice the intensity or area higher than the S 2p_{1/2} peak. Doping S⁶⁺ into TiO₂ structure can form an impurity energy level above the VB, resulting in a reduction in the TiO₂ band gap [260].

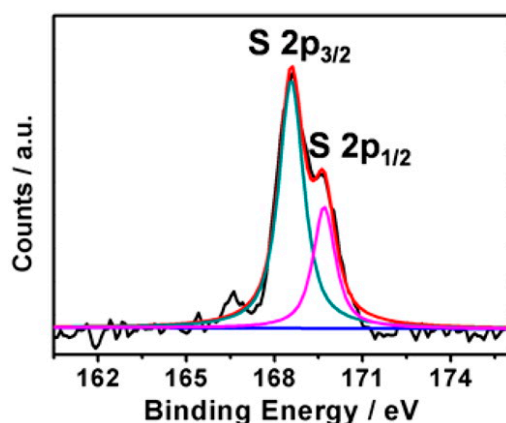


Figure 13. S 2p signals taken from the XPS spectrum of the S-doped TiO₂ NPs. Reprinted with permission from [248]. Copyright 2015 American Chemical Society.

Anionic sulfur doping is more difficult to achieve since the bond strength of the existing Ti-O bond (672.4 KJ/mol) is larger than Ti-S bond (418.0 KJ/mol). Additionally, the ionic radius of S²⁻ (1.7 Å) has a higher value than O²⁻ (1.22 Å) [246]. As a result, the incorporation of sulfur by substitution of Ti⁴⁺ with S⁶⁺ is energetically more favorable than the replacement of O²⁻ by S²⁻ [248].

Basera et al. [274] applied the density functional theory (DFT) to model the S-doped TiO₂, referring to various defect possibilities: (i) substitutional (S)_O, i.e., representing sulfur substituting oxygen, (ii) interstitial sulfur (SO)_O, and (iii) a combination of (S)_O and (SO)_O in which interstitial sulfur shares a lattice site with (S)_O forming (S₂)_O. The authors reported that under conditions poor in oxygen, the substitutional sulfur (S)_O is dominant, while under conditions rich in oxygen, the interstitial sulfur (SO)_O becomes more stable. In other words, the incorporation of (S)_O may be easier than (SO)_O under oxygen-poor conditions, which is due to a lower formation energy.

Bakar et al. [236] compared photodecomposition efficiency of methyl orange (MO) over 2ATO and 2CTO S-doped TiO₂. The photocatalysts were prepared via template free

and low-temperature OPM followed by crystallization through hydrothermal treatment. Thiourea was reported to be mainly responsible for cationic S-doping due to the substitution of Ti^{4+} by S^{6+} , while CS_2 promoted the anionic doping via substitution of O^{2-} by S^{2-} . Both, cationic and anionic S-doped photocatalysts revealed the enhanced visible light photocatalytic activity. However, S^{6+} was found to be responsible for reducing the TiO_2 crystallite size and in the cationic S-doped TiO_2 the photoinduced holes and chemisorbed hydroxyls played a major role during photocatalysis. On the other hand, the S^{2-} doping resulted in an increased TiO_2 crystallite size, and in anionic S-doped TiO_2 , the photoinduced holes and electrons played a nearly equal role in the photocatalytic activity.

The mechanism of photocatalysis in the presence of the cationic and anionic S-doped TiO_2 was proposed by various researchers [236,275]. Ma et al. [275] obtained the cationic doping by the application of thiourea as sulfur precursor, while the usage of CS_2 resulted in both cationic and anionic doping (Figure 14).

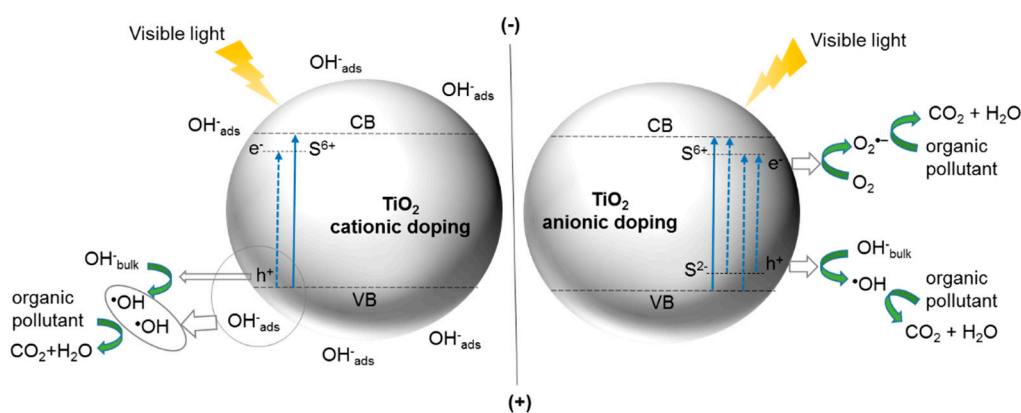


Figure 14. Schematic representation of the photocatalytic degradation mechanism over cationic and anionic S-doped TiO_2 (adapted from [275]).

The improvement of the photocatalytic activity of the cationic S-doped TiO_2 was attributed to [261,275]: (i) the formation of a midgap level under the CB due to the incorporation of S^{6+} , leading to the band gap narrowing and increase in the visible-light absorption; (ii) the enhanced adsorption of OH^- on the photocatalyst surface resulting from the created charge imbalance in the bulk of TiO_2 upon replacement of Ti^{4+} by S^{6+} . These adsorbed hydroxyl ions and the OH^- ions present in the bulk solution can be oxidized by h^+ to form highly oxidative $\bullet OH$ radicals; and (iii) the formation of Ti-O-S bonds, which due to the higher electronegativity of O atoms leads to a partial transfer of electrons from sulfur to oxygen. As a result, the electron-deficient S atoms can capture the e^- , which reduces the recombination of electron-hole pairs and improves the quantum efficiency. In the case of the cationic and anionic S-doped TiO_2 , the enhancement of the photoactivity was explained by: (i) the formation of Ti-O-S and O-Ti-S bands in the crystal lattice under the cationic and anionic S-doping, respectively, which introduce new impurity levels between the VB and CB. As a result, the formation of electron-hole pairs under the visible light radiation is improved; (ii) the generation of O_v and defects in the TiO_2 lattice, which contribute to the improvement of photoactivity by (a) enhancement of visible light absorption and (b) capture of electrons thus inhibiting the e^- - h^+ recombination; (iii) the increased generation of hydroxyl and superoxide radicals by the reaction of h^+ and e^- with the adsorbed H_2O and O_2 , respectively [261,275]. Moreover, an important role of the surface-adsorbed SO_4^{2-} groups in charge separation due to acting as electron traps was also proposed [261].

The photocatalytic activity of S-doped TiO_2 under visible light is usually investigated using dyes as model compounds. Table 7 presents the properties of different thiourea S-doped TiO_2 prepared using various titania precursors and the efficiency of methylene blue (MB) decomposition under visible light in the presence of these photocatalysts.

Table 7. Methylene blue (MB) decomposition under visible light irradiation in the presence of S-doped TiO₂ obtained using thiourea and various titania precursors.

Titania Precursor	Preparation Method	Treatment Temperature (°C)	S Content	Binding Energy (eV)	S _{BET} (m ² g ⁻¹)	E _{bg} (eV)	Irradiation Source	Initial Concentration of MB (mg L ⁻¹)	Degradation Rate	Ref.
TTIP	Sol-gel	600	-	-	47.6	-	Household lamp (2.5 W/m ²)	10	71.83%, 6 h	[276]
	Hydrolysis	120	0.64–0.80 wt.%	-	-	-	150 W high-pressure Xenon lamp	10	Up to 59%, 4 h	[277]
	Vapor-thermal	250	-	162.2 (S ²⁻), 164.0 (S), 165.2 (S ⁴⁺), 168.6 (S ⁶⁺)	99.1–125.2	-	300 W Xenon lamp	10	78.4–99.9%, 1 h	[278]
TBOT	Ultrasonic-assisted spray pyrolysis	400	-	-	-	2.85	570 W Xenon lamp	3.2	80%, 5 h	[225]
	Thermal CVD	180 and 250	S/Ti molar ratio of 0.5, 1, 2, 3, 4, and 5	163.5 (S ²⁻), 164.4 (S), 168.0 (S ⁶⁺)	81.7–210.9	2.4	300 W Xenon lamp	10	92.5–99.8%, 2 h	[226]
TiCl ₄	Sol-gel	500	4 mol%	173.1 (S ⁶⁺)	-	-	350 W Xenon lamp	9	~60%, 100 min	[238]
Ti(OH) ₂ O	Thermal hydrolysis	600	Ti(OH) ₂ O/thiourea molar ratio of 1:3	-	-	2.56	Visible light	8	~70%, 6 h	[241]
Metallic Ti	Low temperature and template free OPM	200	Ti/S molar ratio of 1:1, 1:2 and 1:3	168.4 (S ⁶⁺)	-	2.89	18 W Daylight lamp	10	Up to 92%, 4 h	[235]

Wang et al. [256] examined the effect of synthesis temperature on the visible light photocatalytic activity of the S-doped TiO₂ prepared by hydrothermal oxidation of TiS₂ (ST-120-4) or its high temperature calcination in air (ST-550-10). Rh B was used as a model compound. As can be seen from the plot (Figure 15), about 50% of Rh B was decomposed using TS-550-10 and 80% using TS-120-4 within 60 min. This difference in the photocatalytic activity was attributed to the significantly larger surface area of ST-120-4, afforded by the low-temperature hydrothermal synthesis. The surface area of ST-550-10 was 6.6 m² g⁻¹, while that of ST-120-4 was 46.4 m² g⁻¹, i.e., seven times greater.

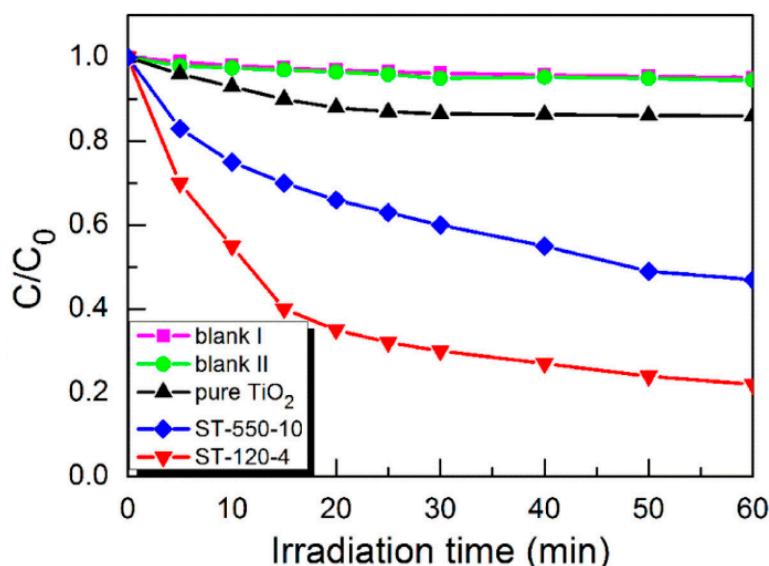


Figure 15. Normalized concentration (C/C_0) of Rh B as a function of illumination time for pure TiO₂, ST-120-4, ST-550-10, and blank references. Reproduced from [256] with permission.

Boningari et al. [261] investigated the photodegradation of acetaldehyde over a cationic S-doped TiO₂ in the presence of visible light. In order to obtain the photocatalysts, sulfuric acid at various concentrations (1–3 mol L⁻¹) was applied as S source, while TTIP was used as TiO₂ precursor. The presence of both S⁶⁺/S⁴⁺ oxidation states, corresponding to the BE of 167.5–167.9 and 169.1–169.6 eV, respectively, was noted. The highest content of S calculated on the basis of XPS was observed for the photocatalyst prepared using 2 mol L⁻¹ H₂SO₄ (8.9 at%). For this photocatalyst, the S⁶⁺/S⁴⁺ ratio was also the highest (5.61). Nevertheless, the most efficient total organic carbon (TOC) removal (ca. 60%) was found in the case of the photocatalyst fabricated from 3 mol L⁻¹ H₂SO₄ (containing 5.19 at% of S).

Bakar et al. [236] applied the anionic and cationic S-doped TiO₂ for the decomposition of colored MO and colorless Ph under visible light irradiation. The rate of MO decolorization after 240 min of the experiment reached 89.32% for 2ATO and 85.43% for 2CTO. A significant mineralization efficiency was also found for both photocatalysts. Moreover, the authors reported that the efficiency of Ph photodegradation and mineralization was similar to that observed for MO. It was also noted that the pristine TiO₂ exhibited no significant photoactivity under visible light.

Sraw et al. [268] prepared S-doped TiO₂ photocatalyst via wet impregnation method. The authors demonstrated the degradation process of two persistent and highly toxic organophosphorus pesticides, monocrotophos (MCP) and quinalphos (QP). The S-doped photocatalyst showed better performance under the sunlight than under UV irradiation. The removal efficiency of MCP (25 mg L⁻¹) was 95.36% and 68.21% for sunlight and UV, respectively. In the case of QP (20 mg L⁻¹), a similar effectiveness of decomposition was observed (98.09% and 68.67%, respectively). The increase in photocatalytic activity under the sunlight was due to the changes in the band gap energy of the photocatalyst caused by

doping with sulfur. Examination of different S:Ti ratios (Table 8) revealed that the optimum value was 0.7:1, in the case of which the band gap energy was lowered by about 10% compared to the undoped TiO₂. Moreover, the photocatalyst with the S:Ti ratio of 0.7:1 had the lowest average particle size (27.2 nm), as was determined by the transmission electron microscopy (TEM).

Table 8. Effect of S-dopant concentration on the E_{bg} and average particle size of S-doped TiO₂ [268].

Photocatalyst	E_{bg} (eV)	Average Particle Size by TEM (nm)
TiO ₂ P25	3.22	33.0
S:Ti = 0.5:1	3.18	32.2
S:Ti = 0.6:1	3.10	29.6
S:Ti = 0.7:1	2.90	27.2
S:Ti = 0.8:1	3.14	28.6

In another case [269], a photodegradation of atrazine was investigated. The applied S-doped TiO₂ photocatalysts were obtained from TiCl₄ and (NH₄)₂SO₄, and contained sulfur in S⁶⁺ state. The studies revealed higher effectiveness of atrazine oxidation by the solar/S-doped TiO₂ system in comparison with the solar/TiO₂ system. After 30 min of irradiation, the removal rate reached 60% and 40%, respectively. The authors also emphasized that lower water pH favored the photodegradation of herbicide, while the presence of humic acids (HA) decreased the decomposition rate due to the competition with the atrazine molecules for hydroxyl radicals and partial absorption of sunlight before it reached TiO₂.

In turn, Lin et al. [271] examined the S-doped TiO₂ synthesized from TTIP and thiourea, in terms of degradation of gaseous 1,2-dichloroethane. The S-doped TiO₂ photocatalysts exhibited superior photocatalytic activity under visible light compared to that of pure TiO₂. The conversion rate of 1,2-dichloroethane was 55.3 nmol min⁻¹ g⁻¹, whereas in the case of the undoped TiO₂ it was 2.16 nmol min⁻¹ g⁻¹ after 1 h of irradiation. Among all the examined photocatalysts, the highest efficiency of photodecomposition was found for the S-doped TiO₂ containing 2.46 wt.% of sulfur.

The S-doped TiO₂ synthesized by Baieissa [230] was applied for photooxidation of cyanide in water (KCN concentration: 25–200 mg L⁻¹). The photocatalytic activity of the S-doped TiO₂ increased with increasing sulfur content from 0 to 0.3 wt.%. In the case of the highest S content, the efficiency of photocatalytic oxidation of cyanide reached 100% after 30 min of irradiation with a blue fluorescent lamp (150 W). The stability of the photocatalyst was confirmed during five cycles of recycling and reuse.

Yi et al. [234] proposed the sol-gel method followed by calcination at 300 °C to prepare the S-doped TiO₂ for visible light photocatalytic degradation of diclofenac (DCF) (10 mg L⁻¹). The efficiency of DCF decomposition reached 93% after 4 h for 0.8 g L⁻¹ of photocatalyst. A significant role of h⁺, •OH, and O₂•⁻ in the DCF degradation was confirmed in the experiments involving various scavengers: (a) benzoquinone (BQ) as a superoxide radical scavenger, (b) AgNO₃ as electron capturer, (c) tert-butyl alcohol as an •OH scavenger, and (d) methanol (MeOH) and potassium iodide (KI) as both •OH and h⁺ scavengers.

Furthermore, the S-doped TiO₂ showed potential for application in antimicrobial field. Dunnill et al. [279] investigated the inhibition of *E. coli* growth in the presence of the S-doped TiO₂ films. The samples were irradiated with the white light source, typically used in the hospitals. After 24 h of irradiation, a 99.5% inhibition of bacterial growth (i.e., 2.3 log₁₀ reduction) was observed.

Other researchers [61] described a significant improvement in the photoreduction of CO₂ using S-doped TiO₂ under UV-A and visible light irradiation. A series of photocatalysts was obtained via simple sonothermal method using sulfur powder as a dopant source. For the most active S-doped TiO₂, the evolution of 6.25 μmol g⁻¹ of methane, 2.74 μmol g⁻¹ of

ethylene, $0.074 \mu\text{mol g}^{-1}$ of propylene and $0.030 \mu\text{mol g}^{-1}$ of propane after 24 h of UV-A irradiation in KOH solution was reported. Moreover, generation of methane and methanol in the acetonitrile-water mixture was observed under visible light, with the yield of 167.6 and $12,828.4 \mu\text{mol g}^{-1}$, respectively.

Based on the analysis of the literature data, it can be concluded that doping of TiO_2 with sulfur is not as common as doping it with nitrogen, but still is one of the major strategies of non-metal modification of TiO_2 aimed at improvement of its visible light photoactivity. The main source of sulfur is thiourea, although many other compounds have also been used, such as DMSO, TiOSO_4 , and sulfur powder. A majority of the photocatalysts were prepared with the use of titanium alkoxides as TiO_2 precursors. Among numerous synthesis methods, sol-gel and hydrothermal treatment are the most common approaches. The two possible routes of sulfur doping are cationic ($\text{S}^{6+}/\text{S}^{4+}$) or anionic (S^{2-}), with the former being more energetically favorable and thus more often reported. It was found that S-doped TiO_2 materials exhibit superior properties as antibacterial agents. Moreover, this type of photocatalyst was employed in the decolorization of dyes and decomposition of both organic and inorganic contaminants.

6. C,N-Co-Doped TiO_2

The C,N-co-doped TiO_2 can be obtained by application of various carbon and nitrogen sources. A summary of the precursors is shown in Table 9. Among all nitrogen precursors, ammonia was the most commonly used, while in the case of the carbon source, various researchers applied different compounds (Table 9). The most popular Ti sources were TTIP and TBOT. The modified photocatalysts were obtained by numerous approaches, including sol-gel, solvothermal and hydrothermal methods, calcination, pyrolysis, or even green bioinspired synthesis.

According to Ananpattarachai et al. [89] the C,N-co-doped TiO_2 combines the synergistic effect of the C-doped and N-doped TiO_2 . Due to the carbon doping, the pollutant could be easier adsorbed on the surface of TiO_2 . The carbonaceous specie I formed by the incorporated C atoms could act as a photosensitizer (C^*). After the excitation of this specie, electrons can be injected into the CB of TiO_2 . Further, these electrons could be transferred to O_2 adsorbed on the photocatalyst surface, leading to the formation of the superoxide anion radicals ($\text{O}_2^{\bullet-}$), which could be subsequently transformed to H_2O_2 and $\bullet\text{OH}$, and together with the oxidative species formed by the oxidation of H_2O and OH^- by holes participate in pollutants degradation (Figure 16). Nitrogen doping could lead to the narrowing of the band gap by creation of an intra band gap states (IB) above the VB, enabling the visible light absorption. Furthermore, nitrogen doping can result in a shift of the flat-band (FB) potential position to a higher level than in the case of an unmodified TiO_2 .

Table 9. A summary of the precursors applied for the synthesis of the C,N-co-doped TiO₂ and the examples of application of the photocatalysts.

Nitrogen Precursor	Carbon Precursor	TiO ₂ Precursor or Type	Synthesis Method	Pollutant (Initial Concentration)	Photodecomposition or Removal Efficiency and Conditions	Ref.
	Citric acid	TiCl ₄	Sol-gel	4-NP (7.0×10^{-2} mmol L ⁻¹)	87% in 420 min, visible light	[280]
	Ethanol	Amorphous TiO ₂	Calcination under gas flow	Reactive Red 198 (RR198) (500 mg L ⁻¹)	96% in 20 h, visible light	[281]
	Isopropanol			<i>Escherichia coli</i> (1.5×10^8 CFU mL ⁻¹)	100% of bacteria inactivated in 60 min, visible light	[282]
	Methanol			<i>Escherichia coli</i> (1.5×10^8 CFU mL ⁻¹)	100% of bacteria inactivated in 60 min, visible light	[282]
				RR198 (500 mg L ⁻¹)	54.6% in 100 h, visible light	[283]
				<i>Escherichia coli</i> (1.5×10^8 CFU mL ⁻¹)	100% of bacteria inactivated in 60 min, visible light	[282]
	Styrene	TBOT	Pyrolysis	Tetracycline hydrochloride (TCH) (10 mg L ⁻¹)	99.6% in 30 min, visible light	[284]
	Titanium ethoxide	Titanium ethoxide	Sol-gel	DCF (10, 30 and 50 mg L ⁻¹)	80% in 100 min, UV light	[285]
Ammonium nitrate	Acetylacetone	TTIP	Sol-gel	MB (10 mg L ⁻¹)	91.3% in 3 h, visible light	[286]
Extrapallial fluid (EPF) of blue mussels	EPF of blue mussels	TBOT	Green bioinspired synthesis	Microplastic (0.4 w/v%)	71.77 ± 1.88% in 50 h, visible light	[287]
Glycine	Glycine	Titanium(III) sulfate	Hydrothermal	Ibuprofen (IBP) (20 mg L ⁻¹)	100% in 360 min, visible light	[288]
Guanidine hydrochloride	Guanidine hydrochloride	Anatase TiO ₂	One-step microwave	MO (20 mg L ⁻¹)	Up to 94% in 2 h, visible light	[289–291]
Hexamethylenetetramine (HMT)	HMT	TiCl ₄	Solvothermal	Resorcinol (20 mg L ⁻¹)	Up to 96% within 90 min, visible light	[292]
		TTIP		Bisphenol A (BPA) (5 and 0.02 mg L ⁻¹)	Over 99% in 5 h and 95% in 2 h, white LED	[293,294]
		Methanol		NO _x (1 ppm)	~10% at 530 nm, ~23% at 445 nm, ~40% at 390 nm	[295]
Nitric acid	Tween 80	TTIP	Sol-gel	CIP and levofloxacin	78.2% and 96.7% in 2 h, visible light	[296]
N-lauroyl-L-glutamic acid	N-lauroyl-L-glutamic acid	Titanium (diisopropoxide) bis (2,4-pentanedionate)	Selfassembly soft-template	Ph (10 mg L ⁻¹)	92% in 150 min, visible light	[297]
N-methyl-formamide	N-methyl-formamide	TTIP	Sol-gel	Orange G (80 mg L ⁻¹)	99% in 1 h, visible light	[298]
PAN	PAN	TBOT	Hydrolysis and calcination	Rh B (20 mg L ⁻¹)	About 99% in 4 h, visible light	[299]
Polyaniline	Carbon tetrachloride	TiO ₂ NPs powder	Stirring and carbonization	Ph (20 mg L ⁻¹)	87% in 150 min, UV radiation	[300]
	Polyaniline	TBOT	Polymerization and sol-gel coating	Rh B (2.0×10^{-5} mol L ⁻¹) and Ph (10 mg L ⁻¹)	90% in 100 min and 84% in 150 min, visible light	[301]

Table 9. Cont.

Nitrogen Precursor	Carbon Precursor	TiO ₂ Precursor or Type	Synthesis Method	Pollutant (Initial Concentration)	Photodecomposition or Removal Efficiency and Conditions	Ref.
PVP	PVP	TTIP	Electrospinning and calcination	MB (2.0×10^{-5} mol L ⁻¹)	95% in 120 min, visible light	[302]
Tetrakis(dimethylamino) titanium (TDMAT)	Mesoporous carbon molecular sieves CMK-3	TDMAT	Stirring in autoclave	Rh B (10 mg L ⁻¹)	99.87% in 60 min, visible light	[303]
Triethanolamine (TELA)	TELA	TTIP	Sol-gel	2-chlorophenol (100 mg L ⁻¹)	94.39% in 90 min, visible light	[89]
Urea	Tetrabutylammonium hydroxide (TBAH)	TBOT	Sol-gel	MB (1.8×10^{-5} mol L ⁻¹)	Over 90% in 7 h, visible light	[304]
	Urea			<i>Microcystis aeruginosa</i> ($\sim 3.0 \times 10^6$ cells mL ⁻¹)	Up to 92.7% of bacteria inactivated in 12 h, visible light	[305]
	Ti foil	CBD	MO (5 mg L ⁻¹)	100% in 30 min, visible light	[306]	

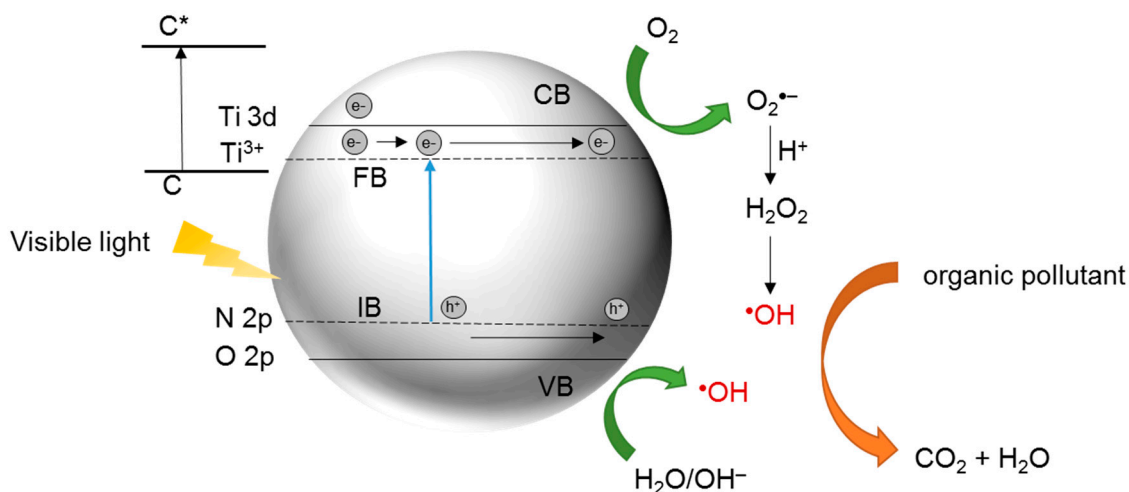


Figure 16. Schematic mechanism of photocatalysis in the presence of C,N-co-doped TiO₂ under visible light (adapted from [89]).

To investigate the state of N and C in the modified photocatalysts the XPS analysis is typically conducted. Table 10 presents a summary of the nitrogen and carbon species detected in the XPS spectra of the C,N-co-doped TiO₂. Usually, the N 1s signals in the range of ca. 396–402 eV are attributed to the presence of O-Ti-N bonds, indicating the substitutional incorporation of N atom into the TiO₂ lattice [89,280,298,300,302,303,305–308]. The presence of carbon is confirmed by the peaks ranging from 284.6 to 289.6 eV (Table 10). The most commonly reported signals are the peaks at 285.9–286.7 and 288.5–288.7 eV, which are mainly ascribed to C-O and C=O bonds [89,280,289,296,298,302,303,305,306], and the signals at 288.0–288.9 eV attributed to the Ti-O-C bonds [89,288,296,297,301,303,306].

Table 10. An overview of N 1s and C 1s signals reported in the XPS spectra of the C,N-co-doped TiO₂.

XPS Region	Chemical State	BE [eV]	References
N 1s	N-Ti-N	395.7	[297]
	Ti-N-Ti	397.98	[299]
	Ti-O-N	400–400.1	[289,306]
		401.7	[303]
	O-Ti-N	396.3–396.5	[306]
		397.1–397.7	[297,307]
		399.1–400.8	[89,280,289,296,300,302,303,305,308]
		395.7	[297]
	N-C	399.3	[297]
		~400	[298]
399.3		[297]	
N-N		399.3	[297]
C 1s	C-C (usually adventitious carbon)	284.6–285	[289,298,301,303,305,307]
	C-OH	285.6	[303]
		284.6	[280]
	C-N	284.6	[280]
		285.9	[301]
C=N	287	[301]	

Table 10. Cont.

XPS Region	Chemical State	BE [eV]	References
C 1s	C-O	285.9–286.7	[89,289,296,298,302,303,305]
		288	[306]
	Ti-C	281.8	[307,308]
		282.5	[292]
		284.6	[297]
		286	[306]
	C=O	288.5–288.7	[89,280,289,296,298,302,305]
		288.0–288.9	[89,296,297,301,303,306]
	Ti-O-C	289.6	[289]
		O-Ti-C	288.0–288.5

The visible light photocatalytic activity of the C,N-co-doped TiO₂ was evaluated mainly on the basis of the decomposition of dyes and phenolic compounds (Table 9). Ananpattarachai et al. [89] compared the photocatalytic activity of the C-doped TiO₂, N-doped TiO₂, and C,N-co-doped TiO₂ photocatalysts, prepared via sol-gel method with TTIP used as a TiO₂ precursor. ETA, DEA and TELA were applied as the carbon and nitrogen sources. The activity of the photocatalysts was tested in the 2-chlorophenol removal process under visible light. After 90 min of irradiation, the C,N-co-doped TiO₂ exhibited the highest removal efficiency of 94.39%, while for the C-doped and N-doped TiO₂, it was 79.74% and 69.36%, respectively. Under the same conditions, the photodegradation efficiency in the case of the undoped TiO₂ was about 24%. The best performance of the C,N-co-doped TiO₂ was accounted by a synergistic effect of carbon and nitrogen co-doping, which allowed to obtain the lowest band gap energy amongst all the prepared photocatalysts (2.80 eV).

Xiao et al. [284] applied the C-modified and N-doped TiO₂ hollow spheres for the degradation of tetracycline (TC) and TCH under simulated solar irradiation. The degradation rate constants k reached 0.1812 and 0.1785 min⁻¹, respectively. Moreover, the authors reported that after four cycles of reusing, the material exhibited almost unchanged TC degradation efficiency.

Recently, the pollution of the environment with microplastics has become a matter of concern. Ariza-Tarazona et al. [287] prepared C,N-co-doped TiO₂ photocatalysts and investigated the impact of pH and temperature on the degradation process of the high-density polyethylene (HDPE) microplastics under visible light. The influence of these factors is shown in Figure 17. The results prove that low pH and low temperature had a combined positive effect on the microplastics' degradation. This could be due to the presence of H⁺ ions facilitating the degradation process. Low temperature contributed to the microplastics' fragmentation, increasing their surface area and interaction with the photocatalyst. The authors obtained over 70% average mass loss at pH 3 and temperature of 0 °C.

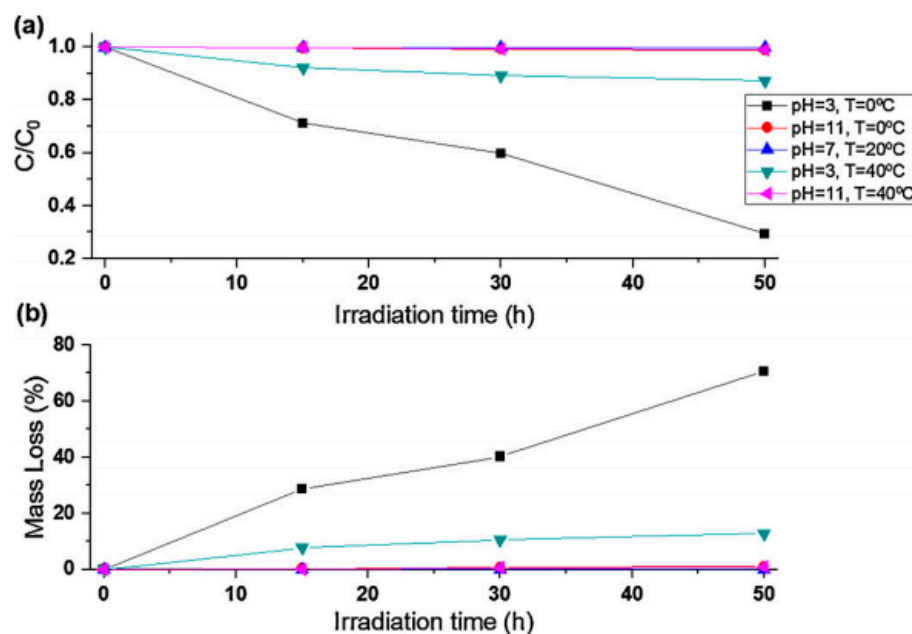


Figure 17. Photocatalytic degradation of microplastics under different experimental conditions: (a) microplastics relative concentration and (b) microplastics mass loss. Reproduced from [287] with permission from Elsevier.

Another proposed application is photocatalytic H₂ production. Zhang et al. [308] prepared the C,N-co-doped TiO₂ hollow spheres using TiCN as a precursor of anatase TiO₂ and a self-doping source of C and N. The photocatalyst was synthesized by a one-pot hydrothermal method. The resulting C,N-co-doped TiO₂ showed enhanced photocatalytic activity towards H₂ production under the visible light irradiation. The H₂ generation rate was 445 times higher than for pure TiO₂.

The modification of TiO₂ with nitrogen and carbon was also found to be an efficient approach to enhance its antibacterial activity [282]. The photocatalysts were prepared using gaseous NH₃ as a nitrogen source and aliphatic alcohols (methanol, ethanol and isopropanol) as carbon sources. The C,N-co-doped TiO₂ was incorporated into concrete plates. The plates were irradiated with an artificial solar light in the presence of *Escherichia coli* bacteria. A complete inactivation of bacteria after 60 min of irradiation was observed in the case of the photocatalysts treated at 100 °C in the presence of ethanol and isopropanol and treated at 300 °C in the presence of methanol. The authors reported that not only inactivation but also damage of the bacterial cells was achieved.

The review of the current state of the art revealed that the simultaneous doping with carbon and nitrogen is a predominately used mode of co-doping of TiO₂ with C, N and S non-metals. A majority of the photocatalysts were synthesized on the base of titanium alkoxides as TiO₂ precursors, similarly as in the case of C- and N-doped TiO₂. Numerous methods have been applied; some of them were common, such as sol-gel, solvothermal or calcination under gas flow, but there were also others such as pyrolysis, electrospinning, and CBD. Various alcohols are usually used as carbon sources. The most common nitrogen source is ammonia, although many other compounds were used, for example compounds containing amine groups such as glycine, HMT, or polyaniline. Moreover, some researchers used a single compound as both C and N source. Among others, PAN, TELA and urea were used for this purpose. The C,N-co-doped TiO₂ has been successfully applied to decompose various organic pollutants and hydrogen production. It was also used as an antibacterial agent.

7. C,S-Co-Doped TiO₂

The literature reports on the C,S-co-doped TiO₂ are very limited. There are only a few papers on that subject and a majority of them were published in the last 5 years. The summary of substrates and methods applied for the preparation of the C,S-co-doped TiO₂ is shown in Table 11.

Table 11. A summary of the precursors applied for C,S-co-doped TiO₂ synthesis and the examples of application of the photocatalysts.

Doping Source	TiO ₂ Precursor or Type	Synthesis Method	Pollutant (Initial Concentration)	Photodecomposition or Removal Efficiency and Conditions	Ref.
<i>Eichhornia crassipes</i> extract	TTIP	Green modification of sol-gel	Reactive Blue 19 (RB19) (6.10 mg L ⁻¹) and Reactive Red 76 (RR76) (4.49 mg L ⁻¹)	72.2% and 73.3% after 30 min, visible light	[102]
Carrageenans (kappa (κ-), iota (ι-) and lambda (λ-)) from red seaweeds	TTIP	Hydrothermal followed by calcination	RB5, MB and MO (25 mg L ⁻¹)	100% after <5, <5 and <20 min for κ-, ι- and λ- carrageenans, solar concentrator	[309]
Thiourea	Meta-titanic acid	Solid-phase	Rh B and MB	Up to about 60% (Rh B) and 50% (MB) after 30 min of contact with photocatalytic coatings, visible light	[156]
	TBOT	Solvothermal sol-gel	Doxycycline (DC)	43.1% after 1 h, visible light	[310]
1-octadecene and sulfur	TiCl ₄	Solvothermal	TCH (10 mg L ⁻¹)	86% after 1 h, visible light	[311]
Thiourea, carbon, citric acid and glycerol	Titanium ethoxide	Stirring followed by stepwise heating	Safranin T (ST) (30 mg L ⁻¹)	Rate constants: up to 4.04 × 10 ⁴ s ⁻¹ for UV and 0.63 × 10 ⁴ s ⁻¹ for vis	[157]
Thiourea, urea	TBOT	Hydrolysis	4-chlorophenol (1.5 × 10 ⁻⁴ mol L ⁻¹)	~35% in 3 h, visible light	[312]

Ivanov et al. [156], Khalyavka et al. [157], and Romanovska et al. [310] used the widely applied thiourea as a dopant of C and S. Although the authors [310] claimed their photocatalyst to be C,S-co-doped TiO₂, the XPS analysis revealed the signals characteristic for C, N and S (285, 400, and 170 eV, respectively). The calculated surface content of the non-metals was 16.7 at% for C, 0.4 at% for S and 0.3 at% for N. Nonetheless, since the elemental analysis showed no presence of nitrogen, the authors attributed the observed weak XPS signal in the N 1s region to the adsorption of gaseous N₂ and NH₃ from the atmosphere.

The entirely new approaches were proposed by El Nemr et al. [102] and Chaudhary et al. [309]. The method reported by El Nemr et al. [102] was an ecofriendly procedure based on the sol-gel synthesis under alkaline conditions in the presence of *Eichhornia crassipes* aqueous leaf extract, followed by calcination in air at 400 °C. Except for deionized water, no other solvents were applied. Chaudhary et al. [309] proposed the application of the sulfate rich seaweed polysaccharides, carrageenans, (kappa (κ-), iota (ι-) and lambda (λ-)) from red seaweeds as a source of sulfur and carbon, while TTIP was used as TiO₂ substrate. Sulfur was present in two oxidation states, S⁴⁺ and S⁰, corresponding to the XPS BE of 168 and 164.4 eV, respectively. It was observed that application of calcination at 600 °C led to a conversion of S⁰ to S⁴⁺, as was concluded from a disappearance of the 164.4 eV peak and the presence of an intense peak at ~168 eV. The authors concluded that no new Ti-S bond was formed at the expense of Ti-O bonds, and that the sulfate ions could form O-S-O bonds on the TiO₂ surface. The presence of C 1s peak at 287.4 eV was also observed and it was assigned to the graphitic carbon.

Ivanov et al. [156] proposed a more conventional approach in which metatitanic acid was applied as a TiO₂ precursor, while thiourea was the source of carbon and sulfur. A homogenous mixture of the substrates was calcined at 500 °C. The obtained C,S-co-doped TiO₂ contained sulfur exclusively in the oxidation state of +6 (XPS BE of 168.8 eV). In the

case of carbon, three peaks at BE of 285, 287 and 289 eV were observed. The signal at 285 eV was attributed to an external post-synthesis (not in vacuo) contamination. The other two peaks were assigned to C-O and C=O bonds indicating the presence of carbon substituting lattice Ti atoms and forming a Ti-O-C structure or C=O groups adsorbed on the photocatalyst surface. The surface content of sulfur and carbon was visibly higher (2.8 and 30.3 at%, respectively) than the content in the powder volume (0.36 and 5.07 at%, respectively).

Photocatalytic activity of the C,S-co-doped TiO₂ was analyzed mainly on the basis of the removal of various dyes, including Rh B [156,313], RB19 [102], RR76 [102], MB [156] and ST [157]. El Nemr et al. [102] investigated the photoactivity of the C,S-co-doped TiO₂ with reference to RB19 and RR76 decolorization in a real textile wastewater and the toxicity of the treated and untreated effluents. A 400 W halide lamp was used as a radiation source. The results were compared with those obtained in the presence of C-doped TiO₂ and S-doped TiO₂. It was reported that although all the doped photocatalysts exhibited higher photocatalytic activity than pure TiO₂, the efficiency of decolorization was higher for the C-doped TiO₂ than for the other photocatalysts. After 30 min of irradiation the concentration of RB19 decreased by 5.5%, 77.8%, 72.2%, and 73.3%, while the concentration of RR76 was lowered by 7.5%, 86.7%, 73.3%, and 63.3%, in the presence of TiO₂, C-TiO₂, C,S-TiO₂ and S-TiO₂, respectively. However, the analysis of chemical oxygen demand revealed that the highest degradation efficiency was obtained in the presence of C,S-co-doped TiO₂ (97%), while in the case of the C-doped TiO₂ and S-doped TiO₂, it amounted to 91%. The toxicity of the treated wastewater samples analyzed with reference to rotifer and *Artemia salina* was less than 4%, being significantly lower compared to that of the untreated wastewater (95–98%). On the basis of the tests conducted in the presence of scavengers, it was concluded that the main species participating in the decomposition of the dyes were photogenerated holes, not the hydroxyl radicals. Moreover, the obtained photocatalyst was successfully recovered and reused at least three times without significant decrease in photoactivity.

In another case [157], the dye ST was photocatalytically degraded under UV and visible (568 nm) light in the presence of a series of C,S-co-doped TiO₂ with various dopants content. The decolorization rates were in the range of 0.68–4.04 × 10⁴ s⁻¹ for UV and 0.20–0.63 × 10⁴ s⁻¹ for visible light, depending on the photocatalyst composition. In the case of the pure TiO₂, the decolorization rate was 2.58 × 10⁴ s⁻¹ for UV, while no visible decomposition was observed for vis. The authors concluded that the following effects were responsible for the enhanced dye removal: (i) interfacial bonding, (ii) defective sites, (iii) narrowing of the band gap, (iv) inhibition of electron-hole pair recombination in the presence of carbon and sulfur, (v) prolongation of the lifetime of the photogenerated charges, (vi) formation of doping electronic states and (vii) change in textural characteristics.

Hohol et al. [313] applied the C,S-co-doped TiO₂ as well as TiO₂ P25 as the modifiers of the cement mortars. The photocatalytic activity was analyzed on the basis of Rh B removal in the visible light. The sample containing 2 wt.% of the C,S-co-doped TiO₂ revealed the highest photocatalytic activity corresponding to the 87% removal efficiency after 2 h of irradiation. The cement mortars modified with 1 wt.% of the C,S-co-doped TiO₂, 2 wt.% of TiO₂ P25 and 1 wt.% of TiO₂ P25 showed a removal efficiency of 65, 44 and 37%, respectively.

The overview presented above reveals that the number of papers on C,S-co-doped TiO₂ is very limited. However, it is worth noting again here the case of thiourea precursor. As was already explained, this compound is used for the preparation of the S-doped TiO₂, C,S-co-doped TiO₂, or even C,N,S-tri-doped TiO₂, thus in some cases it is difficult to distinguish between these types of single- and multiple doping. Thus, further investigations on the C,S-co-doped TiO₂ are necessary. The studies should be especially related to the synthesis method and type of precursors, the structural and electronic properties of the photocatalysts and their effect on the photocatalytic activity analyzed with reference to other compounds than dyes.

8. N,S-Co-Doped TiO₂

The simultaneous doping with nitrogen and sulfur is considered as an efficient method to obtain a reduction in the band gap of TiO₂ [314]. Thiourea [231,247,276,315–320] as an S source and urea [87,231,315,316,318] or ammonium nitrate [276] as an N source are usually proposed. There are also reports on the application of ammonium sulfate [321] and ammonium thiocyanate [322] as both N and S precursors. Albrbar et al. [247] applied an aprotic solvent DMSO as a precursor for S-doping, while the annealing in ammonia stream was applied for N-doping.

Some authors performed a comparative evaluation of the non-metal doped TiO₂. The N,S-co-doped TiO₂ was compared with the N-doped and S-doped photocatalysts. A summary of these data is shown in Table 12. Sol-gel and wet impregnation were mainly applied as synthesis methods. In general, co-doping resulted in a smaller crystallite size of anatase and lower band gap energy values than observed in the case of the single-doped photocatalysts. The effect of the co-doping on the S_{BET} was dependent on the synthesis method. An increase in the specific surface area compared to the single co-doped photocatalysts was observed only in the case of the sol-gel approach.

Table 12. A comparison of the properties of the N-doped TiO₂, S-doped TiO₂ and N,S-co-doped TiO₂, synthesized by various methods with the use of different dopant sources.

No.	Photocatalyst	Doping Source	Synthesis Method	S _{BET} (m ² g ⁻¹)	Crystallite Size of Anatase (nm)	E _{bg} (eV)	Ref.
1	N-doped TiO ₂	Ammonia	Non-hydrolytic sol-gel	100.1	8.2	2.67	[87,231,315]
	S-doped TiO ₂	DMSO		69.7	10.5	3.07	
	N,S-co-doped TiO ₂	Ammonia and DMSO		144.8	5.1	2.32	
2	N-doped TiO ₂	Urea	Wet impregnation	55.35	18.8	2.79	[276]
	S-doped TiO ₂	Thiourea		50.16	18.5	2.65	
	N,S-co-doped TiO ₂	Urea and thiourea		45.74	16.9	2.68	
3	N-doped TiO ₂	Ammonium nitrate	Sol-gel	39.5	-	-	[231]
	S-doped TiO ₂	Thiourea		47.6	-	-	
	N,S-co-doped TiO ₂	Ammonium nitrate and thiourea		68.6	-	-	
4	N-doped TiO ₂	Dodecylamine	Sol-gel	-	10.32	2.95	[320]
	S-doped TiO ₂	Thiourea		-	10.83	3.00	
	N,S-co-doped TiO ₂	Dodecylamine and thiourea		-	9.59	2.89	
5	N-doped TiO ₂	Urea	Wet impregnation	143.61	13.7	2.99	[247]
	S-doped TiO ₂	Thiourea		158.30	14.1	3.08	
	N,S-co-doped TiO ₂	Urea and thiourea		97.11	13.8	2.96	

Figure 18 shows the effects of the N and S dopants on the visible light photocatalytic activity of the N,S-co-doped TiO₂ photocatalyst. According to Chung et al. [314], nitrogen forms a delocalized state in the band gap of TiO₂ leading to the enhanced solution bulk reaction by increasing the visible light absorption. On the other hand, sulfur promotes the adsorption of organic species present in the solution onto the surface of the N,S-co-doped TiO₂, thereby enhancing the surface reaction with cationic organic pollutants.

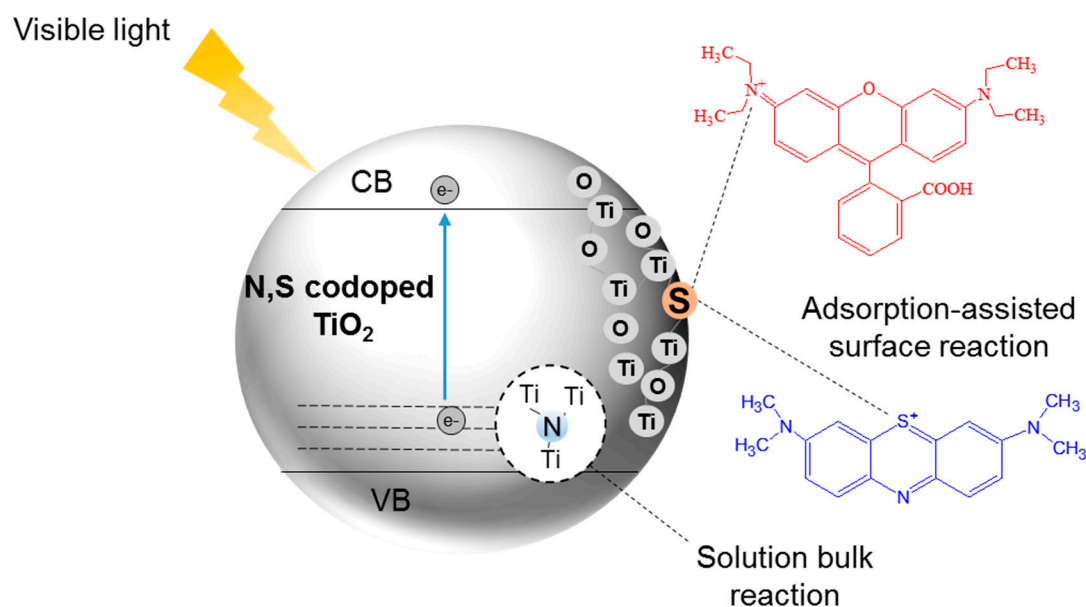


Figure 18. Schematic illustration of the suggested effects of the nitrogen and sulfur dopants on the enhanced visible light photocatalytic activity of the N,S-co-doped TiO₂ (adapted from [314,323–326]).

The XPS analysis of the N,S-co-doped TiO₂ synthesized by the non-hydrolytic sol-gel approach using DMSO and gaseous NH₃ as S and N precursors, respectively, revealed interstitial nitrogen doping and cationic sulfur doping by the substitution of Ti⁴⁺ with S⁴⁺ and S⁶⁺ [247]. The N 1s peak was observed at ~400 eV. The authors noticed that the interstitial doping of N³⁻ ion into TiO₂ lattice is typical for annealing of titania in ammonia atmosphere. The S 2p signal was in the form of a doublet with a maximum of the S 2p_{3/2} at 169.6 eV. It was also noted that annealing in ammonia suppresses the oxidation of sulfur, and as a result the substitution of Ti⁴⁺ with S⁴⁺ and S⁶⁺ is less favorable compared to calcination in air [247]. The presence of interstitial N and substitution of Ti⁴⁺ with S⁴⁺/S⁶⁺ was also reported in the case of application of ammonium thiocyanate as a dopant [322]. In contrast, Abu Bakar et al. [316] reported the absence of the interstitial nitrogen and the presence of the anionic N-doping in the case of N,S-co-doped TiO₂ obtained by the OPM-assisted hydrothermal procedure using ammonia, thiourea and urea as N and S precursors. The substitution of O atoms by N atoms in the TiO₂ lattice led to the formation of O-Ti-N bonds. The main form of sulfur was S⁶⁺ substituting Ti⁴⁺, as was found on the basis of the XPS peak at 168.7 eV. Moreover, a weak signal at the BE of 163.8 eV was observed indicating that anionic doping due to the replacement of oxygen by S²⁻ in the crystal lattice of TiO₂ also occurred. The above data clearly show that the synthesis route strongly affects the type of doping.

The photocatalytic activity of the N,S-co-doped TiO₂ was examined using dyes such as Rh B [314,316,324], MB [291], MO [317,322,326], reactive orange 16 (RO16) [247], as well as HA [87,231], Ph [276,316], TC [325], non-steroidal anti-inflammatory drugs such as ibuprofen (IBP) and naproxen (NPX) [323], anti-cancer drug 5-fluorouracil (5-FU) [327], or an organophosphorus flame retardant tris(1-chloro-2-propyl)phosphate (TCPP) [321]. Table 13 presents selected examples of the application of the N,S-co-doped TiO₂ photocatalysts in organic pollutants removal.

Table 13. Selected examples of precursors, methods applied during preparation and applications of the N,S-co-doped TiO₂ photocatalysts.

Nitrogen Precursor	Sulfur Precursor	TiO ₂ Precursor or Type	Synthesis Method	Pollutant (Initial Concentration)	Photo-Decomposition or Removal Efficiency and Conditions	Ref.
Ammonia	DMSO	TiCl ₄ and TTIP	Non-hydrolytic sol-gel	RO16 (20 mg L ⁻¹)	100% after 30 min, visible light	[247]
Ammonium nitrate	Thiourea	TTIP	Sol-gel	MB (10 mg L ⁻¹) and Ph (10 mg L ⁻¹)	78.64% after 6 h and 77.87% after 4 h, visible light	[276]
Ammonium sulfate	Ammonium sulfate	TBOT	Sol-gel impregnation	5-FU (10 mg L ⁻¹)	Ca. 90% after 90 min, simulated solar light	[327]
		TBOT	Sol-gel	MO (7 mg L ⁻¹)	96% after 3 h, sunlight	[326]
Thiourea	Thiourea	TiO ₂ P25	Mixing—calcination	TC (10 mg L ⁻¹)	91% after 20 min, visible light	[325]
		TiO ₂ powder (Tayca Corp., Japan)		<i>E. coli</i> (10 ⁴ CFU mL ⁻¹)	Total bacteria inactivation after 75 min, visible light	[319]
		Ti(SO ₄) ₂	Hydrothermal	MO (10 mg L ⁻¹)	92% after 6 h, sunlight	[317]
Urea	Thiourea	Ti(SO ₄) ₂	Hydrothermal	Atrazine (5 mg L ⁻¹)	Over 70% after 6 h, visible light	[318]

Eslami et al. [323] prepared the N,S-co-doped TiO₂ NPs and nanosheets through facile sol-gel and hydrothermal methods, respectively. They used thiourea as nitrogen and sulfur source, and TBOT as the TiO₂ precursor. The photocatalytic activity of the two types of the modified TiO₂ was examined in IBP and NPX decomposition under visible light (Figure 19). The NPs displayed better photocatalytic activity by degrading 85% of IBP and 99.3% of NPX, whereas 71.6% of IBP and 99.1% of NPX were degraded by nanosheet structures. Both photocatalysts exhibited higher degradation and mineralization efficiency than TiO₂ P25.

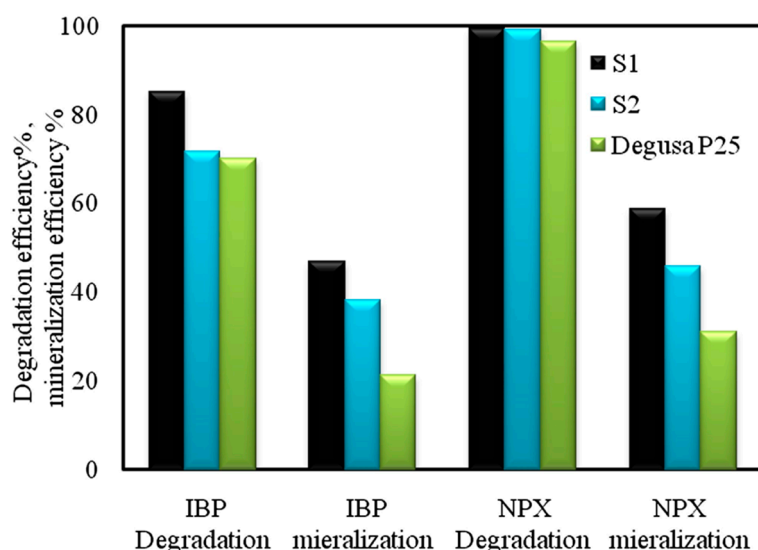


Figure 19. Comparison of degradation and mineralization of IBP and NPX under visible light in the presence of various photocatalysts (S1-N,S-co-doped TiO₂ NPs and S2-N,S-co-doped TiO₂ nanosheets). Process parameters: initial IBP or NPX concentration: 5 mg L⁻¹, photocatalyst loading 2 g L⁻¹, pH 6, irradiation time: 90 min. Reproduced from [323] with permission from John Wiley and Sons.

The N,S-co-doped TiO₂ nanowires (NWs) were synthesized by Zhang et al. [318] via hydrothermal approach using titanium sulfate, thiourea and urea as the precursors. The experiments exhibited that the N,S-co-doped NWs can be easily separated from aqueous suspension by a simple sedimentation within ca. 30 min, while TiO₂ P25 suspension

remains turbid at this time. Furthermore, the N,S-co-doped NWs were proved to maintain their photocatalytic activity during five cycles of atrazine degradation under visible light. The authors concluded that the ease of separation and the stable photocatalytic performance make the prepared photocatalyst an attractive candidate for the industrial water purification.

The influence of the climate conditions on the photocatalysis process with N,S-co-doped TiO₂ was studied by Khalilian et al. [326]. Thiourea was applied as a source of nitrogen and sulfur while TBOT was used as TiO₂ precursor. The authors compared the degradation efficiency of MO under natural sunlight irradiation in cloudy and clear sky. The MO decomposition rate was 96% after 3 h in clear sky conditions, while in the case of the cloudy sky it reached 90% after 4.5 h. A more significant difference was observed after a shorter irradiation time, e.g., after 1 h, the decolorization rate amounted to about 75% and 30%, respectively.

Ju et al. [317] applied hydrothermal treatment followed by calcination for the preparation of the N,S-co-doped TiO₂ photocatalysts from Ti(SO₄)₂ and thiourea as precursors. Various N/Ti atomic ratio and calcination temperature were used. The highest photocatalytic activity during MO removal under sunlight exhibited the photocatalyst obtained at 3% of N and calcined at 500 °C. The authors attributed the highest photoactivity of this photocatalyst to the small crystallite size of anatase (7 nm). The analysis of the influence of the pH of MO solution on its decolorization rate revealed the highest removal efficiency (92% after 6 h) at pH 4.

Yan et al. [324] prepared the N,S-co-doped TiO₂ films by S-doping with thiourea of the previously N-doped TiO₂ nanograss array films on Ti wire mesh obtained through moderate chemical oxidation. The films were applied for Rh B decolorization under visible light irradiation. The decomposition rate constants calculated for the undoped, N-doped and N,S co-doped TiO₂ amounted to 9.77×10^{-4} , 3.39×10^{-3} and 1.70×10^{-2} , respectively. These data show that the photocatalytic activity of the pure TiO₂ was increased by 2.5 times due to N-doping, while the subsequent S-doping enhanced it by 4.0 times. The N,S-co-doped TiO₂ film kept its photocatalytic activity under visible light during five cycles of reuse, while in the case of the N-doped TiO₂, a gradual deterioration of the photodecolorization rate was observed.

Birben et al. [231] compared the photocatalytic performance of the N-doped TiO₂, S-doped TiO₂ and S,N-co-doped TiO₂ synthesized according to the wet impregnation method with the use of TiO₂ P25 (about 80% anatase and 20% rutile) or Hombikat UV-100 (100% anatase) as TiO₂ sources. The photocatalytic activity of the prepared photocatalysts was assessed regarding the photocatalytic degradation of HA in terms of decolorization and mineralization. The experiment was conducted in the reactor equipped with a 250 W m⁻² Xenon lamp (wavelength range of 300–800 nm). Initial concentrations of HA and photocatalysts were 20 mg L⁻¹ and 0.25 g L⁻¹, respectively. The results reveal that the S,N-co-doped TiO₂ prepared with the use of Hombikat UV-100 had the highest photocatalytic degradation efficiency among all the examined photocatalysts. The pseudo-first order rate constants *k* calculated for color removal and mineralization amounted to 11.4×10^{-2} min⁻¹ and 6.80×10^{-2} min⁻¹, respectively. In the case of the S,N-co-doped TiO₂ P25, the photocatalytic performance was significantly worse (*k* = 2.28×10^{-2} min⁻¹ and 2.81×10^{-2} min⁻¹, respectively).

Another application of the N,S-co-doped TiO₂ photocatalyst was described by Antonopoulou et al. [321]. The authors prepared the photocatalysts via the sol-gel method using TBOT as a TiO₂ precursor and ammonium sulfate as a source of S and N. Different N,S:Ti molar ratios of 0.5, 1, and 1.5 were applied. The photocatalytic efficiency of the obtained materials was evaluated during photodegradation of an organophosphorus flame retardant TCPP under simulated solar light (Xenon lamp (2.2 kW) with 290 nm cut-off glass filter) and under visible light (>400 nm, 20 W led flood lamp emitting 1600 lumens). The highest photodegradation efficiency under visible light was observed in the case of the N,S-co-doped TiO₂ obtained with the equimolar N,S:Ti ratio. The pseudo-first order

rate constant k amounted to $0.64 \times 10^{-3} \text{ min}^{-1}$. For the simulated solar light, however, the photodegradation was more efficient in the presence of the single N-doped TiO_2 than in the case of the N,S-co-doped TiO_2 with the rate constants of 2.6×10^{-3} and $1.6 \times 10^{-3} \text{ min}^{-1}$, respectively. Nonetheless, the lowest photodegradation of TCP was observed for the undoped TiO_2 (0.01×10^{-3} and $0.31 \times 10^{-3} \text{ min}^{-1}$ for visible and simulated solar light, respectively).

The N,S-co-doped TiO_2 was also proposed to be applied in lithium storage. Jiao et al. [328] compared the lithium storage capacity of the undoped, N-doped, S-doped and N,S-co-doped TiO_2 as active anode materials. The N-doped TiO_2 revealed only slightly (3.5 times) higher storage capacity than the undoped TiO_2 , while the S-doped TiO_2 was characterized by even lower efficiency than TiO_2 . However, co-doping of TiO_2 with N and S led to a significantly (17 times) higher storage capacity compared to the undoped TiO_2 . The superior performance of the N,S-co-doped TiO_2 compared to the undoped and single doped TiO_2 was ascribed to its significantly improved electronic conductivity resulting from a modified electronic structure of the semiconductor due to a homogenous distribution of the N and S dopants.

The presented above overview shows that co-doping of TiO_2 with N and S can enhance the photocatalytic activity of titania under visible light due to the formation of new impurity levels. The N,S-co-doped TiO_2 photocatalysts were prepared mainly via sol-gel and wet impregnation approaches. The major reported source of sulfur is thiourea, while the applied nitrogen sources include primarily ammonia, ammonium nitrate and urea. It remains unclear what the role of thiourea is as a source of nitrogen in this context. Furthermore, the authors did not discuss the presence of carbon, which is another element in the thiourea structure. Hence, an additional research on this subject is essential. The N,S-co-doped TiO_2 photocatalysts were successfully employed in the photodecomposition of organic compounds, mostly dyes, but also pharmaceuticals and HA.

9. C,N,S-Tri-Doped TiO_2

Single doping of TiO_2 with carbon, nitrogen, or sulfur results in an improved photocatalytic activity under visible light. Tri-doping of TiO_2 has been proposed as a more efficient method of enhancement of photoactivity and extending the visible light absorption range of titania photocatalysts [7,8,329–337]. Sushma et al., in their review [39], summarized the progress on C,N,S-tri-doped TiO_2 in the years 2008–2015. They compared the characteristics of the photocatalysts regarding preparation method and further temperature treatment, the type of dopant as well as TiO_2 precursor, the band gap energy obtained from UV-vis/DR spectra and the dopant states acquired from XPS. The most common methods were sol-gel and hydrothermal treatment. TBOT and TTIP were often used as the TiO_2 precursors, while thiourea and cystine were the most frequently applied sources of C, N and S dopants. In Table 14, there is a continuation of the overview covering the articles from the year 2015 to the present.

It can be seen (Table 14) that the most widely used C, N and S dopant is still thiourea [7,8,329–334,338–341]. Moreover, cystine [335,336], L-cysteine [342], and urea [337] were used as the precursors. The incorporation of the non-metals into TiO_2 was usually confirmed on the basis of the XPS analysis. Most reports [8,330–339,341,342] indicated the occurrence of the peaks at about 285 eV, which could be related to the presence of carbonate species (Table 14). Additionally, some reports [7,8,330,331,334–337] revealed the presence of the peak at about 290 eV, related to the C=O bonds. Nitrogen was reported to be present in two major modes—substitutional (~ 399 eV) [7,8,331,333,335–338,341,342] and interstitial (~ 400 eV) [8,330–339,341]. Moreover, the adsorbed N_2 and NH_3 were also found [337]. In most of the reviewed articles [7,8,330,331,333–337], cationic doping of sulfur was observed. Sulfur existed in S^{6+} oxidation state, as was confirmed by the peaks at about 168 and 169 eV [7,8,331,333–339,341]. Anionic doping was reported by Wang et al. [342], who observed an XPS peak at about 163.3 eV corresponding to the S^{2-} oxidation state.

Table 14. Characteristics of the C,N,S-tri-doped TiO₂ obtained by various methods and using different precursors.

Year	Preparation Method	Precursors	Precursor Ratio (C, N, S Source to Ti Source)	Annealing Temperature, Time	E _{bg} (eV)	Doping Mode of C, N and S and Respective BE from XPS	Ref.
2015	Sol-gel	Thiourea, TTIP	20 mL TTIP, 15 wt.% thiourea	300, 400, 500 and 600 °C	NR	Carbon: adventitious carbon species (284.6 eV), graphite intercalation compounds (285.3 eV) and C-O (298.6 eV); Nitrogen: substituted oxygen lattice sites as O-Ti-N (396.5 eV) and interstitially doped into TiO ₂ lattice (400.5 eV); Sulfur: Ti ⁴⁺ substituted by S ⁶⁺ (169.4 eV)	[333]
2016	Sol-gel	Thiourea, TBOT	1:100	450 °C, 1 h	NR	Carbon: XPS peak at 285 eV; Nitrogen: XPS peak 400 eV; Sulfur: XPS peaks at 165 and 233 eV	[332]
2017	Hydrothermal (120 °C, 2 h)	Thiourea, TiC	0.63	-	NR	Carbon: C-O (286.5 eV) and C=O (288.6 eV) bonds; Nitrogen: interstitially doped as Ti-O-N (400.1 eV); Sulfur: formed Ti-O-S bonds due to cationic doping (168.5 eV)	[330]
2017	Hydrothermal (200 °C, 20 h)	Thiourea, anatase/brookite heterojunction TiO ₂	1:1	450 °C, 1 h	2.9	Carbon: carbonate species C-O (286.46 eV) and C=O (288.9 eV); Nitrogen: interstitially Ti-O-N and substitutionally O-Ti-N doped (400.9 eV); Sulfur: Ti ⁴⁺ substituted by S ⁶⁺ (168.6 eV)	[8]
2017	Hydrothermal (180 °C, 24 h)	Cystine, TBOT	1.7 mL TBOT, 0.5 g cystine	450 °C, 2 h	2.51–2.95	Carbon: hydrocarbons from precursor and adventitious carbon (284.6 eV), C-O (286.1 eV) and C=O (288.6 eV) species; Nitrogen: partially substituted oxygen lattice sites as O-Ti-N (399.7 eV) and interstitially doped as Ti-O-N (400.9 eV) Sulfur: Ti ⁴⁺ substituted by S ⁶⁺ (168.3 eV)	[335]
2017	Sonochemical (20 kHz, room temperature (RT))	Thiourea, TBOT	0.05:1, 0.2:1 and 0.5:1	300, 400 and 500 °C, 3 h	2.66	Carbon: elemental C on the surface (287.60 eV), C-O (289.40 eV) and C=O (291.50 eV) bonds; Nitrogen: N doped into the TiO ₂ lattice (396.00 eV); Sulfur: Ti ⁴⁺ substituted by S ⁶⁺ (171.50 eV)	[7]
2018	Hydrolysis (RT, 6 h)	Thiourea, TTIP	10 mL TTIP, 5 wt.% thiourea	400 °C	2.91	NR	[329]
2018	Thermal decomposition	Urea, Ti(SO ₄) ₂	N:Ti = 4:1	600 °C, 2 and 4 h	1.39–3.05	Carbon: C substituted oxygen atom in the TiO ₂ lattice forming Ti-C (281.7 eV), C formed complex unsaturated groups and carbonate species C=C or C-C (284.4 eV), C-O (287.5 eV) and C=O (289.1 eV); Nitrogen: N substituted oxygen atom O-Ti-N (~399 eV) and interstitially doped in the TiO ₂ lattice (~400 eV), adsorbed as N ₂ and NH ₃ (~401, ~402, ~404 and ~408 eV); Sulfur: S ⁶⁺ in TiO ₂ (168.38 and 169.48 eV)	[337]
2020	Sol-gel followed by dip coating	Thiourea, TBOT	10 mL TBOT, 2.5 mol% thiourea	450 °C, 2 h	NR	NR	[340]
2020	Hydrothermal (180 °C, 12 h)	Thiourea, TiOSO ₄	2:1	400, 500, 600 and 700 °C, 1 h	2.88	Carbon: elemental carbon formed by incomplete combustion (284.7 eV), C replaced Ti atoms in lattice forming Ti-O-C structure (286.4 eV), presence of C=O bond (289.0 eV) Nitrogen: N replaced O atoms (400.3 eV) Sulfur: S ⁶⁺ replaced Ti ⁴⁺ (168.7 eV and 169.5 eV)	[343]

NR—not reported.

A probable mechanism of the photocatalytic degradation of a colorless compound, DCF, with the use of the C,N,S-tri-doped TiO₂ was proposed by Ramandi et al. [7] (Figure 20). According to the authors, the doping of TiO₂ with C, N, and S could generate new impurity levels including the N 2p, S 2p and C 1s. Under sunlight irradiation, carbon acts as a photosensitizer, injecting an electron into the CB (compare Figure 16), whereas incorporation of nitrogen and sulfur leads to mixing of the O 2p orbitals of TiO₂

with N 2p and S 2p orbitals. As a result, the band gap is narrower compared to the undoped TiO₂, which allows the direct electron excitation into CB using the visible light. Additionally, the anionic superoxide radicals O₂^{•−} could be generated by a reduction of the adsorbed O₂ molecules with CB electrons, and afterwards hydroxyl radicals •OH can be formed. According to the authors [7], in the case of the C,N,S-tri-doped TiO₂, this route of hydroxyl radicals formation plays a significant role.

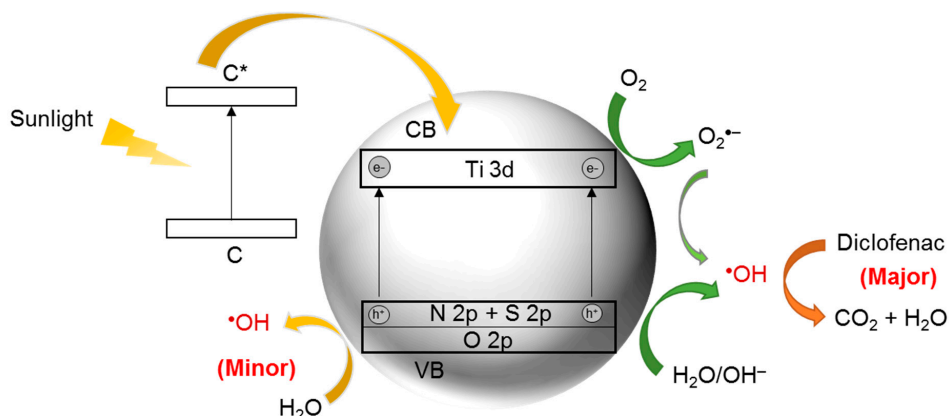


Figure 20. Schematic representation of the improvement of the photoactivity of C,S,N-tri-doped TiO₂ photocatalyst (adapted from [7]).

Another mechanism was proposed by Amreetha et al. [334] (Figure 21) in the case of a colorful compound—an organic dye Rh B. They suggested three pathways of the photodecolorization. The first pathway refers to the dye photosensitization process and is based on the excitation of the dye to the triplet excited state under the visible light irradiation. Furthermore, the dye molecules are converted to cationic dye radicals and the electrons are injected to the TiO₂ CB according to Equations (8)–(10):

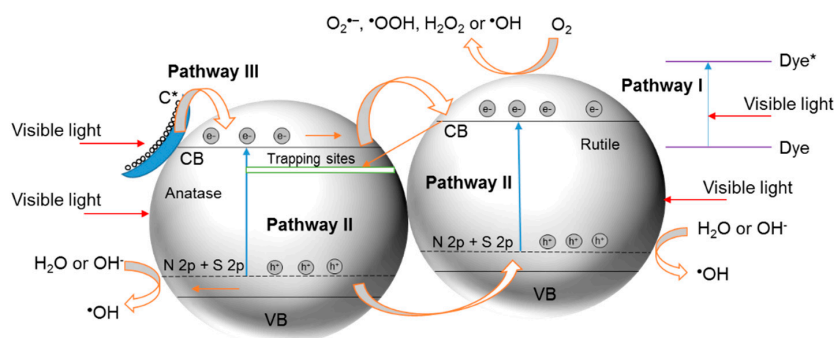
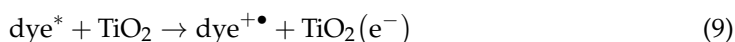


Figure 21. Electron migration in C,N,S-tri-doped TiO₂ with binary polymorphs (adapted from [334]).

Electrons contribute to the production of the anionic superoxide radicals O₂^{•−}, followed by the formation of hydroperoxyl radicals •OOH and then H₂O₂, which further dissociates into hydroxyl radicals •OH. The hydroxyl radicals participate in the decomposition and mineralization of the dye. The second pathway is similar to the mechanism proposed by Ramandi et al. [7]. However, Amreetha et al. [334] discussed it with reference to a mixed phase material composed of anatase and rutile. The electrons from the intermediate states created due to N and S doping (N 2p, S 2p) are excited to the CB of TiO₂. Due

to the presence of the mixed phases the charge separation occurs which limits the negative phenomenon of electron-hole recombination. There are two possible methods of electron transfer: (i) from the CB of anatase to the CB of rutile and (ii) from the CB edge of rutile to the lattice trapping sites of anatase localized below the CB of both anatase and rutile. At the same time, the hole transfer from the VB of anatase to the VB of rutile occurs. The third pathway assumes carbon to behave like a photosensitizer, which injects an electron into the CB (compare Figure 20).

Table 15 presents a brief summary of photocatalytic applications of the C,N,S-tri-doped TiO₂. It was used to decompose dyes such as Rh B [330,333], MB [337,340], MO [335] and Rose Bengal [329]. Another common application was the removal of pharmaceutical compounds such as DCF [7], IBP [8], and TC [338] from water. Chun et al. [332] used the C,N,S-tri-doped TiO₂ for the decomposition of volatile organic compounds (VOCs) such as benzene, toluene, ethyl benzene and o-xylene. Tri-doped TiO₂ was also applied for decomposition of NO_x [339,342].

Table 15. A brief summary of photocatalytic applications of C,N,S-tri-doped TiO₂.

Model Compound	Type of Radiation	Experiment Conditions	Degradation Rate	Ref.
Rh B	Visible	300 W Xenon lamp with a 420 nm cut-off filter Rh B: 10 mg·L ⁻¹ Photocatalyst: 1 g L ⁻¹	68% Rh B decomposed after 10 min, complete decolorization after 60 min	[330]
MB	Visible	500 W Xenon lamp equipped with a UV cutoff filter. MB: 20 mg L ⁻¹ Photocatalyst: 1 g L ⁻¹	91.9% MB decomposed after 60 min	[337]
MO	Visible	300 W Xenon lamp with a 420 nm cut-off filter MO: 10 mg L ⁻¹ Photocatalyst: 1 g L ⁻¹	Up to 92.13% MO decomposed within 180 min	[335]
Rose Bengal	Sunlight	Sunny day under clear sky conditions at Tirunelveli between 11 a.m. to 2 p.m. Rose Bengal: 20 mg L ⁻¹ Photocatalyst: 1 g L ⁻¹	Complete decolorization after 60 min	[329]
DCF	Sunlight	Sunny days in April 2015 with the intensity of 750 lx DCF: 25 mg L ⁻¹ Photocatalyst: 1 g L ⁻¹	Up to 69.81% DCF decomposed within 90 min	[7]
IBP	Visible	LED lamp (λ _{max} = 420 nm, intensity = 1 mW cm ⁻² , height 31.8 cm) IBP: 20 mg L ⁻¹ Photocatalyst: 0.5 g L ⁻¹	Mineralization of TOC: 95.2%, complete decomposition after 5 h	[8]
TC	Visible	6 W cold white visible lamp with a 420 nm cut-off filter TC: 5 mg L ⁻¹ Photocatalyst: 0.5 g L ⁻¹	97% TC removed after 3 h	[338]
NO _x	Visible	Two 15 W fluorescent light tubes with emission between 400–700 nm NO: 400 ± 50 ppb Relative humidity: 60 ± 10% Flow rate: 1.140 ± 0.027 L min ⁻¹	Up to 18% NO _x degraded	[339]
NO	Simulated solar light	300 W tungsten halogen lamp NO: 400 ppb Relative humidity: 70% Flow rate: 4 L min ⁻¹	Up to 25% NO degraded after 30 min	[342]
VOCs	Visible	8 W fluorescent daylight lamp VOCs: 0.1 ppm Relative humidity: 45% Flow rate: 1 L min ⁻¹	70, 87, ~100, and ~100% of decomposition for benzene, toluene, ethyl benzene and o-xylene, respectively	[332]
Toluene	UV	8 W fluorescent lamp Toluene: 1 mL toluene vapor Photocatalyst: 6 g dispersed on a borosilicate Petri dish in a Teflon sampling bag	Above 95% of toluene degraded after 4 h	[340]

Khedr et al. [8] revealed about 40 times higher initial rate of IBP photodegradation under visible light with application of the C,N,S-tri-doped TiO₂ (1.779 μmol min⁻¹) in comparison with the undoped TiO₂ (0.043 μmol min⁻¹). The efficiency of mineralization was 95.2% and 2.8% for the tri-doped and unmodified photocatalysts, respectively.

Wang et al. [338] prepared several C,N,S-tri-doped TiO₂ photocatalysts via sol-gel method using different thiourea to Ti molar ratio (0.03:1, 0.05:1, 0.10:1 and 0.15:1) and various calcination temperature (350, 450, 550 and 650 °C). The authors tested the photocatalytic activity of the obtained photocatalysts in the TC removal process under visible light irradiation. The highest photocatalytic activity (97% removal after 3 h) exhibited the photocatalyst calcined at 450 °C with the thiourea to Ti molar ratio of 0.05:1. The surface content of the non-metals in that photocatalyst was 12.56 at% of C, 1.60 at% of S, and 0.54 at% of N, as was found from the XPS analysis. For comparison, the commercial TiO₂ P25 achieved 26% removal efficiency. The authors attributed the superior performance of the C,N,S-tri-doped TiO₂ to the synergistic effects of (i) the high adsorption of TC associated with the high specific surface area of the photocatalyst, (ii) the narrowing of the band gap resulting from the C,N,S tri-doping, (iii) the presence of carbonaceous species which acted as a photosensitizer, and (iii) the good crystallinity of the anatase phase.

The C,N,S-tri-doped single crystal black TiO₂ nanosheets with exposed {001} facets synthesized by the hydrothermal in situ solid state reduction approach were applied for the photocatalytic decolorization of MO and evolution of hydrogen under visible light. After 180 min of irradiation, the MO decomposition rate reached 92.13% and was significantly higher than that obtained in the presence of the undoped TiO₂ (42.38%). Similarly, the highest H₂ evolution rate (149.7 μmol h⁻¹ g⁻¹) was observed for the C,N,S-tri-doped single crystal black TiO₂. The authors asserted the high stability of the photocatalyst, confirmed by the constant hydrogen evolution rate during five cycles of reuse [335].

Bengtsson et al. [339] applied the C,N,S-tri-doped TiO₂ synthesized from TTIP and thiourea for the degradation of NO_x in air under visible light. The influence of the calcination temperature (400–650 °C) and thiourea content on the properties and activity of the photocatalysts was especially investigated. It was found that the increase in the calcination temperature improved the photoactivity under visible light, while in the case of UV irradiation, the correlation was not clear. Moreover, it was reported that a key role in the decomposition of NO_x under visible light was played by the presence of nitrogen doped in the TiO₂ structure. On the contrary, an increase in sulfur content resulted in a decrease in the efficiency of NO_x degradation. The effect of the carbon amount was ambiguous and it was postulated that an optimal content exists (16–20 at.%), above and below which the presence of carbon has a negative influence on the photoactivity. Moreover, no correlation between the band gap and the photocatalytic activity under visible light was observed.

The data presented above show that in recent years, only a few groups of researchers worked on the C,N,S-tri-doped TiO₂ photocatalysts. Most of them used thiourea as the C, N and S source. Thiourea was also utilized for the preparation of S-doped, C,S-co-doped and N,S-co-doped TiO₂. Thus, it remains vague as to what is the role of this precursor in the synthesis of single- and co-doped photocatalysts. The C,N,S-tri-doped TiO₂ was obtained mainly through sol-gel and hydrothermal procedures, although wet impregnation and sonochemical approaches were also proposed. Regardless of the synthesis method, sulfur was typically incorporated in the TiO₂ crystal lattice in the S⁶⁺ oxidation state, as was concluded on the basis of the XPS analysis. Incorporation of carbon was usually confirmed by the peaks related to the presence of C–O and C=O species. In the case of nitrogen, both doping modes, i.e., substitutional or interstitial, were reported, depending on the preparation procedure. The C,N,S-tri-doped TiO₂ materials have been proved to exhibit a superior photocatalytic performance towards the photodecomposition of organic compounds such dyes and pharmaceuticals in water, as well as the photodegradation of VOCs or NO_x in air.

10. Conclusions and Perspectives

The present review is focused on the progress of the research on the doping, co-doping and tri-doping of TiO₂ with C, N, or S. It confirms the great potential of this approach for the fabrication of visible light-active photocatalysts. The influence of the methods of the photocatalysts synthesis, including the applied precursors and process parameters, on the physicochemical properties and photoactivity of the doped TiO₂ is discussed. Moreover, the mechanisms of photocatalysis in the presence of the single-, co- or tri-doped TiO₂ are presented. Numerous applications of the non-metal doped TiO₂ are also summarized, including the removal of organic compounds from water/wastewater, treatment of air, production of hydrogen, lithium storage, or inactivation of bacteria.

The most widespread approaches of the synthesis of the C, N or S-doped TiO₂ photocatalysts are sol-gel, hydrothermal, solvothermal and wet impregnation methods, while the major precursors of TiO₂, carbon, nitrogen and sulfur are titanium alkoxides, sugars, urea, and thiourea, respectively. However, great ambiguity in the case of the application of thiourea as a modifying agent exists. Thiourea has been used as the source of sulfur in S-doped, C,S-co-doped, and N,S-co-doped TiO₂ or as the source of carbon and sulfur in the C,S-co-doped TiO₂, while for the C,N,S-tri-doped TiO₂ it was the precursor of all three non-metals. Thus, it remains vague as to what the role of thiourea is and which of the three mentioned above non-metals are built in the structure of the modified TiO₂ photocatalysts. This leads to the conclusion that further thorough research regarding the effect of not only thiourea, but also other C, N and S sources on the structure and properties of the doped TiO₂ is essential.

Numerous studies have shown that the incorporation of non-metals into TiO₂ usually results in the narrowing of the band gap due to the formation of new impurity levels (C 2p, N 2p, S 2p) above the VB of the semiconductor. As a result, a red shift of optical absorption leading to an enhancement of the visible light photocatalytic activity is commonly reported. Moreover, the presence of C, N, or S could also contribute to the increase in the specific surface area or the improvement in crystallinity, thus additionally enhancing the photocatalytic performance.

The most common method of doping of TiO₂ is modification with nitrogen. This issue has been widely investigated over the years. Presently, there is growing interest in the doping of TiO₂ with more than one non-metal, including C,N-, C,S-, and N,S-co-doping or C,N,S-tri-doping. Two possible modes of nitrogen incorporation can occur, depending on the preparation conditions, i.e., interstitial (Ti-O-N) and substitutional (O-Ti-N) doping. In the case of sulfur, anionic (as S²⁻) or cationic (as S⁴⁺ or S⁶⁺) doping is possible, with the latter case being more energetically favorable and, thus, more commonly reported. The modification with carbon includes the widest range of species that could possibly be formed, such as Ti-C, C-C, C-N, C=N, C=O or C-O, etc. The reported pathways of C-doping include: (i) substitution of lattice oxygen with carbon (formation of Ti-C bonds); (ii) replacement of Ti by C (formation of C-O bonds); or (iii) stabilization of C at the interstitial position. The various mechanisms of doping affect the properties of the photocatalysts, although clear correlations between the modification procedure and the type of doping difficult to find. Therefore, more extensive investigations regarding this issue are necessary, especially when the photocatalysts with designed properties are considered.

It is not possible to unambiguously indicate the most advantageous mode of non-metal doping of TiO₂. Each of them has some advantages and disadvantages. Moreover, a clear correlation between the doping mode and the physicochemical properties or photoactivity of the modified TiO₂ is difficult to find. Co-doping and tri-doping of TiO₂ can result in combining the properties of the particular single doped TiO₂, leading to the enhancement of photoactivity. However, such improvement usually requires the employment of more reagents and more complicated synthesis procedures. Moreover, only a few authors compared the co-doped or tri-doped photocatalysts with single doped ones, while most of the others referred their results to an undoped TiO₂. On the other hand, comparing the photocatalysts obtained by different authors would not be reliable since various conditions

of experiments were applied, e.g., light sources and intensity, type and concentration of model pollutant, or dose of photocatalysts. Therefore, simple and reliable standard methods for testing of photocatalytic activity that will be widely applied by scientists around the world are a key issue to enable the comparison of the results obtained in different laboratories. That would contribute to defining the correlations and development of methods for designing the highly active photocatalysts.

A majority of applications of doped photocatalysts refer to the removal of pollutants from water and wastewater. The C-, N-, and S-doped photocatalysts were applied mainly for the decomposition of various dyes. Considering that the main aim of modification of TiO₂ with the non-metals is the enhancement of its visible light photoactivity, such an attempt is not appropriate, as was already widely discussed in the literature. This is because of the dye sensitization effect. Therefore, it is very important to study the photocatalytic activity with the application of colorless compounds, such as phenols, pharmaceuticals, etc. Moreover, the determination of mineralization efficiency apart from decomposition rates is also important. A detailed evaluation of the mechanisms of the visible light photocatalysis, with reference to the by-product formation or the role of various ROS is also of high significance. Finally, the toxicity of the treated solutions should be carefully examined as one of the most important parameters reflecting the treatment efficiency and environmental safety. The important research should also focus on applications of doped photocatalysts other than water/wastewater treatment. The visible light photocatalytic air treatment, hydrogen production, CO₂ photoreduction, and bacterial inactivation are still not thoroughly examined.

The enhanced photocatalytic activity under visible light irradiation makes the doped TiO₂ a promising material for low-cost photocatalytic processes. Nonetheless, although the modified photocatalysts show superior properties compared to the undoped TiO₂, more investigations are still needed to develop the production methods at the industrial scale. The crucial matter is to obtain stable and reusable photocatalysts using simple and economically feasible procedures.

Author Contributions: Conceptualization, A.P., S.M.; writing—original draft preparation, review and editing A.P., M.J., K.S. and S.M.; visualization, A.P. and M.J.; supervision, S.M.; funding acquisition, S.M. All authors have read and agreed to the published version of the manuscript.

Funding: This work was supported by the National Science Centre, Poland under project No. 2019/33/B/ST8/00252.

Institutional Review Board Statement: Not applicable.

Informed Consent Statement: Not applicable.

Data Availability Statement: Not applicable.

Conflicts of Interest: The authors declare no conflict of interest.

Abbreviations and Symbols

2ATO	anionic S-doped TiO ₂ nanorods
2CTO	cationic S-doped TiO ₂ nanorods
4-NP	4-nitrophenol
5-FU	5-fluorouracil
Asc-TiO ₂	TiO ₂ modified with citric acid as carbon source
BE	binding energy
BPA	bisphenol A
BQ	benzoquinone
CB	conduction band
CBD	chemical bath deposition
C/C ₀	normalized concentration
CDs	carbon dots

CIP	ciprofloxacin
Cit-TiO ₂	TiO ₂ modified with citric acid as carbon source
CTCNF	C-doped TiO ₂ /carbon nanofibrous film
CTF	C-doped TiO ₂ flakes
CTS	C-doped TiO ₂ sheets
CVD	chemical vapor deposition
DC	doxycycline
DCF	diclofenac
DEA	diethanolamine
DFT	density functional theory
DMF	<i>N,N</i> -dimethylformamide
DMSO	dimethyl sulfoxide
DP	diphenhydramine hydrochloride
d _{TiO₂}	crystallite size estimated from XRD
e ⁻	electron
E _{bg}	band gap energy
EDA	ethylenediamine
EDT	1,2-ethanedithiol
EDTA-Na ₂	ethylenediaminetetraacetic acid disodium salt
EPF	extrapallial fluid
ETA	ethanolamine
FB	flat-band
h ⁺	hole
HA	humic acids
HDA	1,6-diaminohexane
HDPE	high-density polyethylene
HMT	hexamethylenetetramine
IB	intra band gap states
IBP	ibuprofen
k	pseudo-first order rate constant
MB	methylene blue
MCP	monocrotophos
MO	methyl orange
MWCNT	multi-walled carbon nanotubes
N _i	interstitial nitrogen state
N _s	substitutional nitrogen state
NHE	normal hydrogen electrode
NPs	nanoparticles
NPX	naproxen
NWs	nanowires
O _{lat}	lattice oxygen
O _{sur}	surface adsorbed oxygen
O _v	oxygen vacancy
OPM	oxidant peroxide method
PAN	polyacrylonitrile
PLD	pulsed laser deposition
Ph	phenol
PS	polystyrene
PVP	polyvinylpyrrolidone
QP	quinalphos
r-GO	reduced graphene oxide
RB19	reactive blue 19
Rh B	rhodamine b
RO16	reactive orange 16
ROS	reactive oxygen species

RR198	reactive red 198
RR76	reactive red 76
RT	room temperature
S _{BET}	specific surface area estimated with the Brunauer–Emmett–Teller (BET) method
(S) _O	substitutional sulfur
(SO) _O	interstitial sulfur
(S ₂) _O	interstitial sulfur sharing a lattice site with substitutional sulfur
ST	safranin T
TAA	anatase TiO ₂ from Sigma Aldrich
TBAH	tetrabutylammonium hydroxide
TBOT	titanium(IV) butoxide
TC	tetracycline
TCH	tetracycline hydrochloride
TCPP	tris(1-chloro-2-propyl)phosphate
TDMAT	tetrakis(dimethylamino)titanium
TEA	triethylamine
TELA	triethanolamine
TEM	transmission electron microscopy
TiO ₂ P25	Aeroxide [®] TiO ₂ P25 from Evonik, Germany
TOC	total organic carbon
TTIP	titanium isopropoxide
UV-vis/DR	UV-vis diffuse reflectance (spectroscopy)
VB	valence band
VOCs	volatile organic compound
XPS	X-ray photoelectron spectroscopy
XRD	X-ray diffraction

References

- Mittal, A.; Mari, B.; Sharma, S.; Kumari, V.; Maken, S.; Kumari, K.; Kumar, N. Non-metal Modified TiO₂: A Step towards Visible Light Photocatalysis. *J. Mater. Sci. Mater. Electron.* **2019**, *30*, 3186–3207. [\[CrossRef\]](#)
- Cuerda-Correa, E.M.; Alexandre-Franco, M.F.; Fernández-González, C. Advanced Oxidation Processes for the Removal of Antibiotics from Water. An Overview. *Water* **2019**, *12*, 102. [\[CrossRef\]](#)
- Saibu, S.; Adebuseye, S.A.; Oyetibo, G.O. Aerobic Bacterial Transformation and Biodegradation of Dioxins: A Review. *Bioresour. Bioprocess.* **2020**, *7*. [\[CrossRef\]](#)
- Kumari, V.; Mittal, A.; Jindal, J.; Yadav, S.; Kumar, N. S-, N- and C-doped ZnO as Semiconductor Photocatalysts: A Review. *Front. Mater. Sci.* **2019**, *13*, 1–22. [\[CrossRef\]](#)
- Din, M.I.; Khalid, R.; Hussain, Z. Recent Research on Development and Modification of Nontoxic Semiconductor for Environmental Application. *Sep. Purif. Rev.* **2020**, 1–18. [\[CrossRef\]](#)
- Al-Mamun, M.R.; Kader, S.; Islam, M.S.; Khan, M.Z.H. Photocatalytic Activity Improvement and Application of UV-TiO₂ Photocatalysis in Textile Wastewater Treatment: A Review. *J. Environ. Chem. Eng.* **2019**, *7*, 103248. [\[CrossRef\]](#)
- Ramandi, S.; Entezari, M.H.; Ghows, N. Sono-Synthesis of Solar Light Responsive S–N–C–Tri Doped TiO₂ Photo-Catalyst under Optimized Conditions for Degradation and Mineralization of Diclofenac. *Ultrason. Sonochem.* **2017**, *38*, 234–245. [\[CrossRef\]](#)
- Khedr, T.M.; El-Sheikh, S.M.; Hakki, A.; Ismail, A.A.; Badawy, W.A.; Bahnemann, D.W. Highly Active Non-metals Doped Mixed-Phase TiO₂ for Photocatalytic Oxidation of Ibuprofen under Visible Light. *J. Photoch. Photobiol. A.* **2017**, *346*, 530–540. [\[CrossRef\]](#)
- Nasirian, M.; Lin, Y.P.; Bustillo-Lecompte, C.F.; Mehrvar, M. Enhancement of Photocatalytic Activity of Titanium Dioxide Using Non-metal Doping Methods under Visible Light: A Review. *Int. J. Environ. Sci. Technol.* **2017**, *15*, 2009–2032. [\[CrossRef\]](#)
- Islam, S.; Nagpure, S.; Kim, D.; Rankin, S. Synthesis and Catalytic Applications of Non-metal Doped Mesoporous Titania. *Inorganics* **2017**, *5*, 15. [\[CrossRef\]](#)
- Sanchez-Martinez, A.; Ceballos-Sanchez, O.; Koop-Santa, C.; López-Mena, E.R.; Orozco-Guareño, E.; García-Guaderrama, M. N-doped TiO₂ Nanoparticles Obtained by a Facile Coprecipitation Method at Low Temperature. *Ceram. Int.* **2018**, *44*, 5273–5283. [\[CrossRef\]](#)
- Lazar, M.; Varghese, S.; Nair, S. Photocatalytic Water Treatment by Titanium Dioxide: Recent Updates. *Catalysts* **2012**, *2*, 572–601. [\[CrossRef\]](#)
- Chen, J.; Qiu, F.; Xu, W.; Cao, S.; Zhu, H. Recent Progress in Enhancing Photocatalytic Efficiency of TiO₂-based Materials. *Appl. Catal. A-Gen.* **2015**, *495*, 131–140. [\[CrossRef\]](#)

14. Devi, L.G.; Kavitha, R. A Review on Non Metal Ion Doped Titania for the Photocatalytic Degradation of Organic Pollutants under UV/Solar Light: Role of Photogenerated Charge Carrier Dynamics in Enhancing the Activity. *Appl. Catal. B-Environ.* **2013**, *140–141*, 559–587. [[CrossRef](#)]
15. Al Jitan, S.; Palmisano, G.; Garlisi, C. Synthesis and Surface Modification of TiO₂-based Photocatalysts for the Conversion of CO₂. *Catalysts* **2020**, *10*, 227. [[CrossRef](#)]
16. Basavarajappa, P.S.; Patil, S.B.; Ganganagappa, N.; Reddy, K.R.; Raghu, A.V.; Reddy, C.V. Recent Progress in Metal-doped TiO₂, Non-metal Doped/Codoped TiO₂ and TiO₂ Nanostructured Hybrids for Enhanced Photocatalysis. *Int. J. Hydrogen Energ.* **2020**, *45*, 7764–7778. [[CrossRef](#)]
17. Asahi, R.; Morikawa, T.; Irie, H.; Ohwaki, T. Nitrogen-Doped Titanium Dioxide as Visible-Light-Sensitive Photocatalyst: Designs, Developments, and Prospects. *Chem. Rev.* **2014**, *114*, 9824–9852. [[CrossRef](#)]
18. Rammohan, G.; Nadagouda, M. Green Photocatalysis for Degradation of Organic Contaminants: A Review. *COC* **2013**, *17*, 2338–2348. [[CrossRef](#)]
19. Teh, C.M.; Mohamed, A.R. Roles of Titanium Dioxide and Ion-Doped Titanium Dioxide on Photocatalytic Degradation of Organic Pollutants (Phenolic Compounds and Dyes) in Aqueous Solutions: A Review. *J. Alloys Compd.* **2011**, *509*, 1648–1660. [[CrossRef](#)]
20. Ismail, A.A.; Bahnemann, D.W. Mesoporous Titania Photocatalysts: Preparation, Characterization and Reaction Mechanisms. *J. Mater. Chem.* **2011**, *21*, 11686. [[CrossRef](#)]
21. Akpan, U.G.; Hameed, B.H. The Advancements in Sol–Gel Method of Doped-TiO₂ Photocatalysts. *Appl. Catal. A Gen.* **2010**, *375*, 1–11. [[CrossRef](#)]
22. Ajmal, A.; Majeed, I.; Malik, R.N.; Idriss, H.; Nadeem, M.A. Principles and Mechanisms of Photocatalytic Dye Degradation on TiO₂ based Photocatalysts: A Comparative Overview. *RSC Adv.* **2014**, *4*, 37003–37026. [[CrossRef](#)]
23. Ahmed, S.; Rasul, M.G.; Martens, W.N.; Brown, R.; Hashib, M.A. Heterogeneous Photocatalytic Degradation of Phenols in Wastewater: A Review on Current Status and Developments. *Desalination* **2010**, *261*, 3–18. [[CrossRef](#)]
24. Wang, W.; Chen, M.; Huang, D.; Zeng, G.; Zhang, C.; Lai, C.; Zhou, C.; Yang, Y.; Cheng, M.; Hu, L.; et al. An Overview on Nitride and Nitrogen-doped Photocatalysts for Energy and Environmental Applications. *Compos. Part B Eng.* **2019**, *172*, 704–723. [[CrossRef](#)]
25. Kaur, N.; Shahi, S.K.; Shahi, J.S.; Sandhu, S.; Sharma, R.; Singh, V. Comprehensive Review and Future Perspectives of Efficient N-doped, Fe-doped and (N,Fe)-co-doped Titania as Visible Light Active Photocatalysts. *Vacuum* **2020**, *178*, 109429. [[CrossRef](#)]
26. Samokhvalov, A. Hydrogen by Photocatalysis with Nitrogen Codoped Titanium Dioxide. *Renew. Sustain. Energ. Rev.* **2017**, *72*, 981–1000. [[CrossRef](#)]
27. Ansari, S.A.; Khan, M.M.; Ansari, M.O.; Cho, M.H. Nitrogen-doped Titanium Dioxide (N-doped TiO₂) for Visible Light Photocatalysis. *New J. Chem.* **2016**, *40*, 3000–3009. [[CrossRef](#)]
28. Bakar, S.A.; Ribeiro, C. Nitrogen-doped Titanium Dioxide: An Overview of Material Design and Dimensionality Effect over Modern Applications. *J. Photoch. Photobiol. C* **2016**, *27*, 1–29. [[CrossRef](#)]
29. Gomes, J.; Lincho, J.; Domingues, E.; Quinta-Ferreira, R.; Martins, R. N–TiO₂ Photocatalysts: A Review of Their Characteristics and Capacity for Emerging Contaminants Removal. *Water* **2019**, *11*, 373. [[CrossRef](#)]
30. Zhang, W.; Jia, B.; Wang, Q.; Dionysiou, D. Visible-light Sensitization of TiO₂ Photocatalysts via Wet Chemical N-doping for the Degradation of Dissolved Organic Compounds in Wastewater Treatment: A Review. *J. Nanopart. Res.* **2015**, *17*. [[CrossRef](#)]
31. Spadavecchia, F.; Ceotto, M.; Presti, L.L.; Aieta, C.; Biraghi, I.; Meroni, D.; Ardizzone, S.; Cappelletti, G. Second Generation Nitrogen Doped Titania Nanoparticles: A Comprehensive Electronic and Microstructural Picture. *Chin. J. Chem.* **2014**, *32*, 1195–1213. [[CrossRef](#)]
32. Gomathi Devi, L.; Kavitha, R. Review on Modified N–TiO₂ for Green Energy Applications under UV/Visible Light: Selected Results and Reaction Mechanisms. *RSC Adv.* **2014**, *4*, 28265–28299. [[CrossRef](#)]
33. Dunnill, C.W.; Parkin, I.P. Nitrogen-Doped TiO₂ thin Films: Photocatalytic Applications for Healthcare Environments. *Dalton Trans.* **2011**, *40*, 1635–1640. [[CrossRef](#)] [[PubMed](#)]
34. Thompson, T.L.; Yates, J.T., Jr. TiO₂-Based Photocatalysis: Surface Defects, Oxygen and Charge Transfer. *Top. Catal.* **2005**, *35*, 197–210. [[CrossRef](#)]
35. Lamo, M.P.B.; Nowotny, J. Water Purification Using Solar Energy: Effect of Sulphur on Photocatalytic Properties of TiO₂. *Energy Mater.* **2009**, *4*, 150–158. [[CrossRef](#)]
36. Shi, Z.-J.; Ma, M.-G.; Zhu, J.-F. Recent Development of Photocatalysts Containing Carbon Species: A Review. *Catalysts* **2018**, *9*, 20. [[CrossRef](#)]
37. Mestre, A.S.; Carvalho, A.P. Photocatalytic Degradation of Pharmaceuticals Carbamazepine, Diclofenac, and Sulfamethoxazole by Semiconductor and Carbon Materials: A Review. *Molecules* **2019**, *24*, 3702. [[CrossRef](#)]
38. Zhao, X.; Zhang, G.; Zhang, Z. TiO₂-Based Catalysts for Photocatalytic Reduction of Aqueous Oxyanions: State-of-the-Art and Future Prospects. *Environ. Int.* **2020**, *136*, 105453. [[CrossRef](#)]
39. Sushma, C.; Kumar, S.G. C–N–S Tridoping into TiO₂ matrix for Photocatalytic Applications: Observations, Speculations and Contradictions in the Codoping Process. *Inorg. Chem. Front.* **2017**, *4*, 1250–1267. [[CrossRef](#)]
40. Linsebigler, A.L.; Lu, G.; Yates, J.T. Photocatalysis on TiO₂ Surfaces: Principles, Mechanisms, and Selected Results. *Chem. Rev.* **1995**, *95*, 735–758. [[CrossRef](#)]

41. Hoffmann, M.R.; Martin, S.T.; Choi, W.; Bahnemann, D.W. Environmental Applications of Semiconductor Photocatalysis. *Chem. Rev.* **1995**, *95*, 69–96. [[CrossRef](#)]
42. Banerjee, S.; Pillai, S.C.; Falaras, P.; O’Shea, K.E.; Byrne, J.A.; Dionysiou, D.D. New Insights into the Mechanism of Visible Light Photocatalysis. *J. Phys. Chem. Lett.* **2014**, *5*, 2543–2554. [[CrossRef](#)] [[PubMed](#)]
43. Fujishima, A.; Zhang, X.; Tryk, D. TiO₂ Photocatalysis and Related Surface Phenomena. *Surf. Sci. Rep.* **2008**, *63*, 515–582. [[CrossRef](#)]
44. Fujishima, A.; Rao, T.N.; Tryk, D.A. Titanium Dioxide Photocatalysis. *J. Photoch. Photobiol. C* **2000**, *1*, 1–21. [[CrossRef](#)]
45. Ahmed, S.; Rasul, M.G.; Brown, R.; Hashib, M.A. Influence of Parameters on the Heterogeneous Photocatalytic Degradation of Pesticides and Phenolic Contaminants in Wastewater: A Short Review. *J. Environ. Manag.* **2011**, *92*, 311–330. [[CrossRef](#)]
46. Ramanathan, R.; Bansal, V. Ionic Liquid Mediated Synthesis of Nitrogen, Carbon and Fluorine-codoped Rutile TiO₂ Nanorods for Improved UV and Visible Light Photocatalysis. *RSC Adv.* **2015**, *5*, 1424–1429. [[CrossRef](#)]
47. Chen, M.; Chu, J.-W. NO_x Photocatalytic Degradation on Active Concrete Road Surface—From Experiment to Real-Scale Application. *J. Clean. Prod.* **2011**, *19*, 1266–1272. [[CrossRef](#)]
48. Su, T.; Shao, Q.; Qin, Z.; Guo, Z.; Wu, Z. Role of Interfaces in Two-Dimensional Photocatalyst for Water Splitting. *ACS Catal.* **2018**, *8*, 2253–2276. [[CrossRef](#)]
49. Razzaq, A.; Sinhamahapatra, T.-H.; Kang, C.A.; Grimes, J.-S.; Yu, S.-I. Efficient Solar Light Photoreduction of CO₂ to Hydrocarbon Fuels via Magnesiumthermally Reduced TiO₂ Photocatalyst. *Appl. Catal. B-Environ.* **2017**, *215*, 28–35. [[CrossRef](#)]
50. Spadaro, L.; Arena, F.; Negro, P.; Palella, A. Sunfuels from CO₂ Exhaust Emissions: Insights Into the Role of Photoreactor Configuration by the Study in Laboratory and Industrial Environment. *J. CO₂ Util.* **2018**, *26*, 445–453. [[CrossRef](#)]
51. Tahir, B.; Tahir, M.; Amin, N.S. Gold-Indium Modified TiO₂ Nanocatalysts for Photocatalytic CO₂ Reduction with H₂ as Reductant in a Monolith Photoreactor. *Appl. Surf. Sci.* **2015**, *338*, 1–14. [[CrossRef](#)]
52. Hu, B.; Guild, C.; Suib, S.L. Thermal, Electrochemical, and Photochemical Conversion of CO₂ to Fuels and Value-Added Products. *J. CO₂ Util.* **2013**, *1*, 18–27. [[CrossRef](#)]
53. Tahir, M.; Amin, N.S. Advances in Visible Light Responsive Titanium Oxide-Based Photocatalysts for CO₂ Conversion to Hydrocarbon Fuels. *Energ. Convers. Manag.* **2013**, *76*, 194–214. [[CrossRef](#)]
54. Spadaro, L.; Arena, F.; Palella, A. Which Future Route in the Methanol Synthesis? Photocatalytic Reduction of CO₂, the New Challenge in the Solar Energy Exploitation. In *Methanol: Science and Engineering*; Dalena, F., Basile, A., Eds.; Elsevier: Amsterdam, The Netherlands, 2018. [[CrossRef](#)]
55. Abdullah, H.; Khan, M.M.; Ong, H.R.; Yaakob, Z. Modified TiO₂ Photocatalyst for CO₂ Photocatalytic Reduction: An Overview. *J. CO₂ Util.* **2017**, *22*, 15–32. [[CrossRef](#)]
56. Carp, O.; Huisman, C.L.; Reller, A. Photoinduced Reactivity of Titanium Dioxide. *Prog. Solid State Chem.* **2004**, *32*, 33–177. [[CrossRef](#)]
57. Kočí, K.; Obalová, L.; Matějová, L.; Plachá, D.; Lacný, Z.; Jirkovský, J.; Šolcová, O. Effect of TiO₂ Particle Size on the Photocatalytic Reduction of CO₂. *Appl. Catal. B-Environ.* **2009**, *89*, 494–502. [[CrossRef](#)]
58. Adekoya, D.; Tahir, M.; Amin, N.A. Recent Trends in Photocatalytic Materials for Reduction of Carbon Dioxide to Methanol. *Renew. Sustain. Energy Rev.* **2019**, *116*, 109389. [[CrossRef](#)]
59. Wang, P.; Yin, G.; Bi, Q.; Huang, X.; Du, X.; Zhao, W.; Huang, F.-Q. Efficient Photocatalytic Reduction of CO₂ Using Carbon-Doped Amorphous Titanium Oxide. *Chem. Cat. Chem.* **2018**, *10*, 3854–3861. [[CrossRef](#)]
60. Akple, M.S.; Low, J.; Qin, Z.; Wageh, S.; Al-Ghamdi, A.A.; Yu, J.; Liu, S. Nitrogen-Doped TiO₂ Microsheets with Enhanced Visible Light Photocatalytic Activity for CO₂ Reduction. *Chin. J. Catal.* **2015**, *36*, 2127–2134. [[CrossRef](#)]
61. Habisreutinger, S.N.; Schmidt-Mende, L.; Stolarczyk, J.K. Photocatalytic Reduction of CO₂ on TiO₂ and Other Semiconductors. *Angew. Chem. Int. Ed.* **2013**, *52*, 7372–7408. [[CrossRef](#)]
62. Friedmann, D.; Hakki, A.; Kim, H.; Choi, W.; Bahnemann, D. Heterogeneous Photocatalytic Organic Synthesis: State-of-the-Art and Future Perspectives. *Green Chem.* **2016**, *18*, 5391–5411. [[CrossRef](#)]
63. Qiu, H.; Fang, S.; Huang, G.; Bi, J. A Novel Application of In₂S₃ for Visible-Light-Driven Photocatalytic Inactivation of Bacteria: Kinetics, Stability, Toxicity and Mechanism. *Environ. Res.* **2020**, *190*, 110018. [[CrossRef](#)] [[PubMed](#)]
64. Pan, J.; Shen, S.; Zhou, W.; Tang, J.; Ding, H.; Wang, J.; Chen, L.; Au, C.-T.; Yin, S.-F. Recent Progress in Photocatalytic Hydrogen Evolution. *Acta Phys. Chim. Sin.* **2020**, *36*, 1–9. [[CrossRef](#)]
65. Sakar, M.; Mithun Prakash, R.; Do, T.-O. Insights into the TiO₂-Based Photocatalytic Systems and Their Mechanisms. *Catalysts* **2019**, *9*, 680. [[CrossRef](#)]
66. Fang, Y.; Zheng, Y.; Fang, T.; Chen, Y.; Zhu, Y.; Liang, Q.; Sheng, H.; Li, Z.; Chen, C.; Wang, X. Photocatalysis: An Overview of Recent Developments and Technological Advancements. *Sci. China Chem.* **2019**, *63*, 149–181. [[CrossRef](#)]
67. Matos, J.; Miralles-Cuevas, S.; Ruiz-Delgado, A.; Oller, I.; Malato, S. Development of TiO₂-C Photocatalysts for Solar Treatment of Polluted Water. *Carbon* **2017**, *122*, 361–373. [[CrossRef](#)]
68. Shi, J.-W.; Wang, Z.; He, C.; Li, G.; Niu, C. Carbon-Doped Titania Flakes with an Octahedral Bipyramid Skeleton Structure for the Visible-Light Photocatalytic Mineralization of Ciprofloxacin. *RSC Adv.* **2015**, *5*, 98361–98365. [[CrossRef](#)]
69. Shi, J.-W.; Liu, C.; He, C.; Li, J.; Xie, C.; Yang, S.; Chen, J.-W.; Li, S.; Niu, C. Carbon-doped Titania Nanoplates with Exposed {001} Facets: Facile Synthesis, Characterization and Visible-Light Photocatalytic Performance. *RSC Adv.* **2015**, *5*, 17667–17675. [[CrossRef](#)]

70. Chauhan, A.; Sharma, M.; Kumar, S.; Thirumalai, S.; Kumar, R.V.; Vaish, R. TiO₂@C Core@shell Nanocomposites: A Single Precursor Synthesis of Photocatalyst for Efficient Solar Water Treatment. *J. Hazard. Mater.* **2020**, *381*, 120883. [[CrossRef](#)]
71. Kuang, L.; Zhang, W. Enhanced Hydrogen Production by Carbon-doped TiO₂ Decorated with Reduced Graphene Oxide (RGO) under Visible Light Irradiation. *RSC Adv.* **2016**, *6*, 2479–2488. [[CrossRef](#)]
72. Jia, G.; Wang, Y.; Cui, X.; Zheng, W. Highly Carbon-doped TiO₂ Derived from MXene Boosting the Photocatalytic Hydrogen Evolution. *ACS Sustain. Chem. Eng.* **2018**, *6*, 13480–13486. [[CrossRef](#)]
73. Shim, J.; Seo, Y.-S.; Oh, B.-T.; Cho, M. Microbial Inactivation Kinetics and Mechanisms of Carbon-doped TiO₂ (C-TiO₂) under Visible Light. *J. Hazard. Mater.* **2016**, *306*, 133–139. [[CrossRef](#)] [[PubMed](#)]
74. Marszewski, M.; Marszewska, J.; Pylypenko, S.; Jaroniec, M. Synthesis of Porous Crystalline Doped Titania Photocatalysts Using Modified Precursor Strategy. *Chem. Mater.* **2016**, *28*, 7878–7888. [[CrossRef](#)]
75. Yuan, Y.; Qian, X.; Han, H.; Chen, Y. Synthesis of Carbon Modified TiO₂ Photocatalysts with High Photocatalytic Activity by a Facile Calcinations Assisted Solvothermal Method. *J. Mater. Sci. Mater. Electron.* **2017**, *28*, 10028–10034. [[CrossRef](#)]
76. Shaban, Y.A.; Fallata, H.M. Sunlight-Induced Photocatalytic Degradation of Acetaminophen over Efficient Carbon Doped TiO₂ (CTiO₂) Nanoparticles. *Res. Chem. Intermed.* **2019**, *45*, 2529–2547. [[CrossRef](#)]
77. de Luna, M.D.G.; Lin, J.C.-T.; Gotostos, M.J.N.; Lu, M.-C. Photocatalytic Oxidation of Acetaminophen Using Carbon Self-doped Titanium Dioxide. *Sustain. Environ. Res.* **2016**, *26*, 161–167. [[CrossRef](#)]
78. Purbia, R.; Borah, R.; Paria, S. Carbon-Doped Mesoporous Anatase TiO₂ Multi-Tubes Nanostructures for Highly Improved Visible Light Photocatalytic Activity. *Inorg. Chem.* **2017**, *56*, 10107–10116. [[CrossRef](#)]
79. Nawawi, W.I.; Ani, A.Y.; Ishak, M.A.M.; Ramli, A.; Azami, M.S.; Zaid, F.; Bakar, F.; Zaharudin, R. Modification and Characterization of C-doped TiO₂ Photocatalyst for Photodegradation of Reactive Red (RR4). *Desalin. Water Treat.* **2018**, *113*, 254–261. [[CrossRef](#)]
80. Rajamanickam, A.T.; Thirunavukkarasu, P.; Dhanakodi, K. A Simple Route to Synthesis of Carbon Doped TiO₂ Nanostructured Thin Film for Enhanced Visible-Light Photocatalytic Activity. *J. Mater. Sci. Mater. Electron.* **2015**, *26*, 4038–4045. [[CrossRef](#)]
81. Huang, Y.; Ho, W.; Lee, S.; Zhang, L.; Li, G.; Yu, J.C. Effect of Carbon Doping on the Mesoporous Structure of Nanocrystalline Titanium Dioxide and Its Solar-Light-Driven Photocatalytic Degradation of NO_x. *Langmuir* **2008**, *24*, 3510–3516. [[CrossRef](#)]
82. Ding, Y.; Nagpal, P. Standalone Anion- and Co-doped Titanium Dioxide Nanotubes for Photocatalytic and Photoelectrochemical Solar-to-Fuel Conversion. *Nanoscale* **2016**, *8*, 17496–17505. [[CrossRef](#)] [[PubMed](#)]
83. Jiang, L.; Huang, Y.; Liu, T. Enhanced Visible-Light Photocatalytic Performance of Electrospun Carbon-doped TiO₂/Halloysite Nanotube Hybrid Nanofibers. *J. Colloid Interf. Sci.* **2015**, *439*, 62–68. [[CrossRef](#)] [[PubMed](#)]
84. An, N.; Ma, Y.; Liu, J.; Ma, H.; Yang, J.; Zhang, Q. Enhanced Visible-light Photocatalytic Oxidation Capability of Carbon-doped TiO₂ via Coupling with Fly Ash. *Chin. J. Catal.* **2018**, *39*, 1890–1900. [[CrossRef](#)]
85. Zhang, J.; Huang, G.-F.; Li, D.; Zhou, B.-X.; Chang, S.; Pan, A.; Huang, W.-Q. Facile Route to Fabricate Carbon-doped TiO₂ Nanoparticles and Its Mechanism of Enhanced Visible Light Photocatalytic Activity. *Appl. Phys. A* **2016**, *122*. [[CrossRef](#)]
86. Qiu, B.; Zhong, C.; Xing, M.; Zhang, J. Facile Preparation of C-modified TiO₂ Supported on MCF for High Visible-Light-Driven Photocatalysis. *RSC Adv.* **2015**, *5*, 17802–17808. [[CrossRef](#)]
87. Birben, N.C.; Uyguner-Demirel, C.S.; Sen-Kavurmaci, S.; Gürkan, Y.Y.; Türkten, N.; Kılıç, M.; Çınar, Z.; Bekbolet, M. Photocatalytic Performance of Anion Doped TiO₂ on the Degradation of Complex Organic Matrix. *J. Adv. Oxid. Technol.* **2016**, *19*. [[CrossRef](#)]
88. Choi, Y.; Umebayashi, T.; Yoshikawa, M. Fabrication and Characterization of C-Doped Anatase TiO₂ photocatalysts. *J. Mater. Sci.* **2004**, *39*, 1837–1839. [[CrossRef](#)]
89. Ananpattarachai, J.; Seraphin, S.; Kajitvichyanukul, P. Formation of Hydroxyl Radicals and Kinetic Study of 2-Chlorophenol Photocatalytic Oxidation Using C-doped TiO₂, N-doped TiO₂, and C,N Co-doped TiO₂ under Visible Light. *Environ. Sci. Pollut. Res.* **2015**, *23*, 3884–3896. [[CrossRef](#)]
90. Tijani, J.O.; Mouele, M.E.S.; Tottito, T.C.; Fatoba, O.O.; Petrik, L.F. Degradation of 2-Nitrophenol by Dielectric Barrier Discharge System: The Influence of Carbon Doped TiO₂ Photocatalyst Supported on Stainless Steel Mesh. *Plasma Chem. Plasma P* **2017**, *37*, 1343–1373. [[CrossRef](#)]
91. Tijani, J.O.; Fatoba, O.O.; Totito, T.C.; Roos, W.D.; Petrik, L.F. Synthesis and Characterization of Carbon Doped TiO₂ Photocatalysts Supported on Stainless Steel Mesh by Sol-Gel Method. *Carbon Lett.* **2017**, *22*, 48–59. [[CrossRef](#)]
92. Zhang, Y.; Zhao, Z.; Chen, J.; Cheng, L.; Chang, J.; Sheng, W.; Hu, C.; Cao, S. C-doped Hollow TiO₂ Spheres: In Situ Synthesis, Controlled Shell Thickness, and Superior Visible-Light Photocatalytic Activity. *Appl. Catal. B-Environ.* **2015**, *165*, 715–722. [[CrossRef](#)]
93. Li, J.; Gao, L.; Gan, W. Bioinspired C/TiO₂ Photocatalyst for Rhodamine B Degradation under Visible Light Irradiation. *Front. Agr. Sci. Eng.* **2017**, *4*, 459. [[CrossRef](#)]
94. Mohamed, M.A.; Salleh, W.N.W.; Jaafar, J.; Mohd Hir, Z.A.; Rosmi, M.S.; Mutalib, M.A.; Ismail, A.F.; Tanemura, M. Regenerated Cellulose Membrane as Bio-Template for in-Situ Growth of Visible-light Driven C-modified Mesoporous Titania. *Carbohydr. Polym.* **2016**, *146*, 166–173. [[CrossRef](#)]
95. Mani, A.D.; Reddy, P.M.K.; Srinivaas, M.; Ghosal, P.; Xanthopoulos, N.; Subrahmanyam, C. Facile Synthesis of Efficient Visible Active C-doped TiO₂ Nanomaterials with High Surface Area for the Simultaneous Removal of Phenol and Cr(VI). *Mater. Res. Bull.* **2015**, *61*, 391–399. [[CrossRef](#)]

96. Yang, Y.; Ni, D.; Yao, Y.; Zhong, Y.; Ma, Y.; Yao, J. High Photocatalytic Activity of Carbon Doped TiO₂ Prepared by Fast Combustion of Organic Capping Ligands. *RSC Adv.* **2015**, *5*, 93635–93643. [[CrossRef](#)]
97. Habibi, S.; Jamshidi, M. Sol–Gel Synthesis of Carbon-doped TiO₂ Nanoparticles Based on Microcrystalline Cellulose for Efficient Photocatalytic Degradation of Methylene Blue under Visible Light. *Environ. Technol.* **2019**, *41*, 3233–3247. [[CrossRef](#)]
98. Payormhorm, J.; Idem, R. Synthesis of C-Doped TiO₂ by Sol-Microwave Method for Photocatalytic Conversion of Glycerol to Value-Added Chemicals under Visible Light. *Appl. Catal. A Gen.* **2020**, *590*, 117362. [[CrossRef](#)]
99. Ouyang, W.; Santiago, A.R.P.; Cerdán-Gómez, K.; Luque, R. Nanoparticles within Functional Frameworks and Their Applications in Photo(Electro)Catalysis. In *Photoactive Inorganic Nanoparticles*; Elsevier: Amsterdam, The Netherlands, 2019; pp. 109–138. [[CrossRef](#)]
100. Song, L.; Jing, W.; Chen, J.; Zhang, S.; Zhu, Y.; Xiong, J. High Reusability and Durability of Carbon-doped TiO₂/Carbon Nanofibrous Film as Visible-Light-Driven Photocatalyst. *J. Mater. Sci.* **2018**, *54*, 3795–3804. [[CrossRef](#)]
101. Qian, H.; Hou, Q.; Duan, E.; Niu, J.; Nie, Y.; Bai, C.; Bai, X.; Ju, M. Honeycombed Au@C-TiO_{2-x} Catalysts for Enhanced Photocatalytic Mineralization of Acid Red 3R under Visible Light. *J. Hazard. Mater.* **2020**, *391*, 122246. [[CrossRef](#)]
102. El Nemr, A.; Helmy, E.T.; Gomaa, E.A.; Eldafrawy, S.; Mousa, M. Photocatalytic and Biological Activities of Undoped and Doped TiO₂ Prepared by Green Method for Water Treatment. *J. Environ. Chem. Eng.* **2019**, *7*, 103385. [[CrossRef](#)]
103. Xie, C.; Yang, S.; Shi, J.; Niu, C. Highly Crystallized C-doped Mesoporous Anatase TiO₂ with Visible Light Photocatalytic Activity. *Catalysts* **2016**, *6*, 117. [[CrossRef](#)]
104. Xie, C.; Yang, S.; Li, B.; Wang, H.; Shi, J.-W.; Li, G.; Niu, C. C-Doped Mesoporous Anatase TiO₂ Comprising 10 nm Crystallites. *J. Colloid Interf. Sci.* **2016**, *476*, 1–8. [[CrossRef](#)] [[PubMed](#)]
105. Wu, J.; Jiang, X.; Zhang, Y.; Fu, Q.; Pan, C. Preparation of High-concentration Substitutional Carbon-doped TiO₂ Film via a Two-step Method for High-performance Photocatalysis. *RSC Adv.* **2018**, *8*, 36691–36696. [[CrossRef](#)]
106. Shaban, Y.A. Solar Light-Induced Photodegradation of Chrysene in Seawater in the Presence of Carbon-modified n-TiO₂ Nanoparticles. *Arab. J. Chem.* **2019**, *12*, 652–663. [[CrossRef](#)]
107. Di Valentin, C.; Pacchioni, G.; Selloni, A. Theory of Carbon Doping of Titanium Dioxide. *Chem. Mater.* **2005**, *17*, 6656–6665. [[CrossRef](#)]
108. Saharudin, K.A.; Sreekantan, S.; Lai, C.W. Fabrication and Photocatalysis of Nanotubular C-doped TiO₂ Arrays: Impact of Annealing Atmosphere on the Degradation Efficiency of Methyl Orange. *Mat. Sci. Semicon. Proc.* **2014**, *20*, 1–6. [[CrossRef](#)]
109. Shao, J.; Sheng, W.; Wang, M.; Li, S.; Chen, J.; Zhang, Y.; Cao, S. In Situ Synthesis of Carbon-doped TiO₂ Single-Crystal Nanorods with a Remarkably Photocatalytic Efficiency. *Appl. Catal. B-Environ.* **2017**, *209*, 311–319. [[CrossRef](#)]
110. Ohtani, B. Photocatalysis A to Z—What We Know and What We Do Not Know in a Scientific Sense. *J. Photoch. Photobiol. C.* **2010**, *11*, 157–178. [[CrossRef](#)]
111. Dong, F.; Guo, S.; Wang, H.; Li, X.; Wu, Z. Enhancement of the Visible Light Photocatalytic Activity of C-Doped TiO₂ Nanomaterials Prepared by a Green Synthetic Approach. *J. Phys. Chem. C* **2011**, *115*, 13285–13292. [[CrossRef](#)]
112. Bergamonti, L.; Predieri, G.; Paz, Y.; Fornasini, L.; Lottici, P.P.; Bondioli, F. Enhanced Self-cleaning Properties of N-doped TiO₂ Coating for Cultural Heritage. *Microchem. J.* **2017**, *133*, 1–12. [[CrossRef](#)]
113. Preethi, L.K.; Antony, R.P.; Mathews, T.; Walczak, L.; Gopinath, C.S. A Study on Doped Heterojunctions in TiO₂ Nanotubes: An Efficient Photocatalyst for Solar Water Splitting. *Sci. Rep.* **2017**, *7*. [[CrossRef](#)] [[PubMed](#)]
114. Calisir, M.D.; Gungor, M.; Demir, A.; Kilic, A.; Khan, M.M. Nitrogen-doped TiO₂ Fibers for Visible-Light-Induced Photocatalytic Activities. *Ceram. Int.* **2020**, *46*, 16743–16753. [[CrossRef](#)]
115. Liu, T.; Chen, W.; Liu, X.; Zhu, J.; Lu, L. Well-Dispersed Ultrafine Nitrogen-doped TiO₂ with Polyvinylpyrrolidone (PVP) Acted as N-source and Stabilizer for Water Splitting. *J. Energy Chem.* **2016**, *25*, 1–9. [[CrossRef](#)]
116. Wang, T.; Yan, X.; Zhao, S.; Lin, B.; Xue, C.; Yang, G.; Ding, S.; Yang, B.; Ma, C.; Yang, G.; et al. A Facile One-Step Synthesis of Three-Dimensionally Ordered Macroporous N-Doped TiO₂ with Ethanediamine as the Nitrogen Source. *J. Mater. Chem. A* **2014**, *2*, 15611–15619. [[CrossRef](#)]
117. Sirivallop, A.; Areerob, T.; Chiarakorn, S. Enhanced Visible Light Photocatalytic Activity of N and Ag Doped and Co-doped TiO₂ Synthesized by Using an In-Situ Solvothermal Method for Gas Phase Ammonia Removal. *Catalysts* **2020**, *10*, 251. [[CrossRef](#)]
118. Breeson, A.C.; Sankar, G.; Goh, G.K.L.; Palgrave, R.G. Rutile to Anatase Phase Transition Induced by N Doping in Highly Oriented TiO₂ Films. *Phys. Chem. Chem. Phys.* **2016**, *18*, 24722–24728. [[CrossRef](#)]
119. Siuzdak, K.; Szkoda, M.; Sawczak, M.; Lisowska-Oleksiak, A. Novel Nitrogen Precursors for Electrochemically Driven Doping of Titania Nanotubes Exhibiting Enhanced Photoactivity. *New J. Chem.* **2015**, *39*, 2741–2751. [[CrossRef](#)]
120. May IX, L.A.; Estrella González, A.; Cipagauta-Díaz, S.; Gómez, R. Effective Electron–Hole Separation over N-doped TiO₂ Materials for Improved Photocatalytic Reduction of 4-nitrophenol Using Visible Light. *J. Chem. Technol. Biotechnol.* **2020**. [[CrossRef](#)]
121. Cheng, Z.-L.; Han, S. Preparation and Photoelectrocatalytic Performance of N-doped TiO₂/NaY Zeolite Membrane Composite Electrode Material. *Water Sci. Technol.* **2015**, *73*, 486–492. [[CrossRef](#)]
122. Huang, L.; Fu, W.; Fu, X.; Zong, B.; Liu, H.; Bala, H.; Wang, X.; Sun, G.; Cao, J.; Zhang, Z. Facile and Large-Scale Preparation of N doped TiO₂ Photocatalyst with High Visible Light Photocatalytic Activity. *Mater. Lett.* **2017**, *209*, 585–588. [[CrossRef](#)]
123. Cheng, X.; Yu, X.; Xing, Z.; Yang, L. Synthesis and Characterization of N-doped TiO₂ and Its Enhanced Visible-Light Photocatalytic Activity. *Arab. J. Chem.* **2016**, *9*, S1706–S1711. [[CrossRef](#)]

124. Zeng, H.; Xie, J.; Xie, H.; Su, B.-L.; Wang, M.; Ping, H.; Wang, W.; Wang, H.; Fu, Z. Bioprocess-Inspired Synthesis of Hierarchically Porous Nitrogen-Doped TiO₂ with High Visible-Light Photocatalytic Activity. *J. Mater. Chem. A* **2015**, *3*, 19588–19596. [[CrossRef](#)]
125. Ariza-Tarazona, M.C.; Villarreal-Chiu, J.F.; Barbieri, V.; Siligardi, C.; Cedillo-González, E.I. New Strategy for Microplastic Degradation: Green Photocatalysis Using a Protein-Based Porous N-TiO₂ Semiconductor. *Ceram. Int.* **2019**, *45*, 9618–9624. [[CrossRef](#)]
126. Xu, X.; Song, W. Enhanced H₂ Production Activity under Solar Irradiation over N-doped TiO₂ Prepared Using Pyridine as a Precursor: A Typical Sample of N-doped TiO₂ Series. *Mater. Technol.* **2016**, *32*, 52–63. [[CrossRef](#)]
127. Zhou, X.; Peng, F.; Wang, H.; Yu, H.; Yang, J. Preparation of Nitrogen Doped TiO₂ Photocatalyst by Oxidation of Titanium Nitride with H₂O₂. *Mater. Res. Bull.* **2011**, *46*, 840–844. [[CrossRef](#)]
128. Huang, J.-G.; Zhao, X.-G.; Zheng, M.-Y.; Li, S.; Wang, Y.; Liu, X.-J. Preparation of N-Doped TiO₂ by Oxidizing TiN and Its Application on Phenol Degradation. *Water Sci. Technol.* **2013**, *68*, 934–939. [[CrossRef](#)]
129. Nguyen-Le, M.-T.; Lee, B.-K. Novel Fabrication of a Nitrogen-doped Mesoporous TiO₂-Nanorod Titanate Heterojunction to Enhance the Photocatalytic Degradation of Dyes under Visible Light. *RSC Adv.* **2016**, *6*, 31347–31350. [[CrossRef](#)]
130. Assayehegn, E.; Solaiappan, A.; Chebude, Y.; Alemayehu, E. Fabrication of Tunable Anatase/Rutile Heterojunction N/TiO₂ Nanophotocatalyst for Enhanced Visible Light Degradation Activity. *Appl. Surf. Sci.* **2020**, *515*, 145966. [[CrossRef](#)]
131. Assayehegn, E.; Solaiappan, A.; Chebudie, Y.; Alemayehu, E. Influence of Temperature on Preparing Mesoporous Mixed Phase N/TiO₂ Nanocomposite with Enhanced Solar Light Photocatalytic Activity. *Front. Mater. Sci.* **2019**, *13*, 352–366. [[CrossRef](#)]
132. Fang, Q.; Tang, J.; Zou, H.; Cai, T.; Deng, Q. Preparation of N-doped Mesoporous TiO₂ Using Nitromethane as Nitrogen Source and Their High Photocatalytic Performance. *Synth. React. Inorg. Met. Chem.* **2015**, *46*, 766–774. [[CrossRef](#)]
133. Lee, S.-H.; Yamasue, E.; Okumura, H.; Ishihara, K.N. Effect of Oxygen and Nitrogen Concentration of Nitrogen Doped TiO_x Film as Photocatalyst Prepared by Reactive Sputtering. *Appl. Catal. A-Gen.* **2009**, *371*, 179–190. [[CrossRef](#)]
134. Marques, J.; Gomes, T.D.; Forte, M.A.; Silva, R.F.; Tavares, C.J. A New Route for the Synthesis of Highly-Active N-doped TiO₂ Nanoparticles for Visible Light Photocatalysis Using Urea as Nitrogen Precursor. *Catal. Today* **2019**, *326*, 36–45. [[CrossRef](#)]
135. Pu, X.; Hu, Y.; Cui, S.; Cheng, L.; Jiao, Z. Preparation of N-doped and Oxygen-deficient TiO₂ Microspheres via a Novel Electron Beam-Assisted Method. *Solid State Sci.* **2017**, *70*, 66–73. [[CrossRef](#)]
136. Quesada-Cabrera, R.; Sotelo-Vázquez, C.; Quesada-González, M.; Melián, E.P.; Chadwick, N.; Parkin, I.P. On the Apparent Visible-Light and Enhanced UV-Light Photocatalytic Activity of Nitrogen-doped TiO₂ Thin Films. *J. Photoch. Photobiol. A.* **2017**, *333*, 49–55. [[CrossRef](#)]
137. Karim, A.V.; Shrivastav, A. Degradation of Ciprofloxacin Using Photo, Sono, and Sonophotocatalytic Oxidation with Visible Light and Low-Frequency Ultrasound: Degradation Kinetics and Pathways. *Chem. Eng. J.* **2020**, *392*, 124853. [[CrossRef](#)]
138. Huang, W.; Cheng, H.; Feng, J.; Shi, Z.; Bai, D.; Li, L. Synthesis of Highly Water-Dispersible N-doped Anatase Titania Based on Low Temperature Solvent-Thermal Method. *Arab. J. Chem.* **2018**, *11*, 871–879. [[CrossRef](#)]
139. Delavari, S.; Amin, N.A.S.; Ghaedi, M. Photocatalytic Conversion and Kinetic Study of CO₂ and CH₄ over Nitrogen-doped Titania Nanotube Arrays. *J. Clean. Prod.* **2016**, *111*, 143–154. [[CrossRef](#)]
140. Islam, S.Z.; Rankin, S.E. Hydrazine-Based Synergistic Ti(III)/N Doping of Surfactant-Templated TiO₂ Thin Films for Enhanced Visible Light Photocatalysis. *Mater. Chem. Phys.* **2016**, *182*, 382–393. [[CrossRef](#)]
141. Pikuda, O.; Garlisi, C.; Scandura, G.; Palmisano, G. Micro-Mesoporous N-doped Brookite-Rutile TiO₂ as Efficient Catalysts for Water Remediation under UV-free Visible LED Radiation. *J. Catal.* **2017**, *346*, 109–116. [[CrossRef](#)]
142. Fiorenza, R.; Di Mauro, A.; Cantarella, M.; Gulino, A.; Spitaleri, L.; Privitera, V.; Impellizzeri, G. Molecularly Imprinted N-doped TiO₂ Photocatalysts for the Selective Degradation of o-Phenylphenol Fungicide from Water. *Mat. Sci. Semicon. Proc.* **2020**, *112*, 105019. [[CrossRef](#)]
143. Ananpattarachai, J.; Kajitvichyanukul, P. Photocatalytic Degradation of p,p'-DDT under UV and Visible Light Using Interstitial N-doped TiO₂. *J. Environ. Sci. Heal. B* **2015**, *50*, 247–260. [[CrossRef](#)]
144. Ananpattarachai, J.; Boonto, Y.; Kajitvichyanukul, P. Visible Light Photocatalytic Antibacterial Activity of Ni-doped and N-doped TiO₂ on *Staphylococcus aureus* and *Escherichia coli* Bacteria. *Environ. Sci. Pollut. Res.* **2015**, *23*, 4111–4119. [[CrossRef](#)]
145. Nursam, N.M.; Tan, J.Z.Y.; Wang, X.; Li, W.; Xia, F.; Caruso, R.A. Mesoporous Nitrogen-Modified Titania with Enhanced Dye Adsorption Capacity and Visible Light Photocatalytic Activity. *Chem. Sel.* **2016**, *1*, 4868–4878. [[CrossRef](#)]
146. Szkoda, M.; Siuzdak, K.; Lisowska-Oleksiak, A. Non-Metal Doped TiO₂ Nanotube Arrays for High Efficiency Photocatalytic Decomposition of Organic Species in Water. *Phys. E* **2016**, *84*, 141–145. [[CrossRef](#)]
147. Pablos, C.; Marugán, J.; van Grieken, R.; Dunlop, P.; Hamilton, J.; Dionysiou, D.; Byrne, J. Electrochemical Enhancement of Photocatalytic Disinfection on Aligned TiO₂ and Nitrogen doped TiO₂ Nanotubes. *Molecules* **2017**, *22*, 704. [[CrossRef](#)] [[PubMed](#)]
148. Mehdizadeh, P.; Tavangar, Z.; Shabani, N.; Hamadian, M. Visible Light Activity of Nitrogen-doped TiO₂ by Sol-Gel Method Using Various Nitrogen Sources. *J. Nanostruct.* **2020**, *10*, 307–316. [[CrossRef](#)]
149. Kamaludin, R.; Mohamad Puad, A.S.; Othman, M.H.D.; Kadir, S.H.S.A.; Harun, Z. Incorporation of N-doped TiO₂ into Dual Layer Hollow Fiber (DLHF) Membrane for Visible Light-Driven Photocatalytic Removal of Reactive Black 5. *Polym. Test.* **2019**, *78*, 105939. [[CrossRef](#)]
150. Ramchiary, A.; Samdarshi, S.K. Hydrogenation Based Disorder-Engineered Visible Active N-doped Mixed Phase Titania. *Sol. Energ. Mat. Sol. C* **2015**, *134*, 381–388. [[CrossRef](#)]

151. Tobaldi, D.M.; Pullar, R.C.; Gualtieri, A.F.; Otero-Irurueta, G.; Singh, M.K.; Seabra, M.P.; Labrincha, J.A. Nitrogen-modified Nano-titania: True Phase Composition, Microstructure and Visible-Light Induced Photocatalytic NO Abatement. *J. Solid State Chem.* **2015**, *231*, 87–100. [[CrossRef](#)]
152. Choi, A.Y.; Han, C.-H. FTIR Investigation of Sonochemically N-doped TiO₂ Nano Powder. *J. Nanosci. Nanotechnol.* **2016**, *16*, 11109–11112. [[CrossRef](#)]
153. Esteban Florez, F.L.; Hiers, R.D.; Larson, P.; Johnson, M.; O'Rear, E.; Rondinone, A.J.; Khajotia, S.S. Antibacterial Dental Adhesive Resins Containing Nitrogen-doped Titanium Dioxide Nanoparticles. *Mater. Sci. Eng. C* **2018**, *93*, 931–943. [[CrossRef](#)] [[PubMed](#)]
154. Khore, S.K.; Tellabati, N.V.; Apte, S.K.; Naik, S.D.; Ojha, P.; Kale, B.B.; Sonawane, R.S. Green Sol–Gel Route for Selective Growth of 1D Rutile N–TiO₂: A Highly Active Photocatalyst for H₂ Generation and Environmental Remediation under Natural Sunlight. *RSC Adv.* **2017**, *7*, 33029–33042. [[CrossRef](#)]
155. Li, X.; Zhang, G.; Wang, X.; Liu, W.; Yu, K.; Liang, C. Facile Synthesis of Nitrogen-doped Titanium Dioxide with Enhanced Photocatalytic Properties. *Mater. Res. Express* **2019**, *6*, 115019. [[CrossRef](#)]
156. Ivanov, S.; Barylyak, A.; Besaha, K.; Bund, A.; Bobitski, Y.; Wojnarowska-Nowak, R.; Yaremchuk, I.; Kus-Liśkiewicz, M. Synthesis, Characterization, and Photocatalytic Properties of Sulfur- and Carbon-Codoped TiO₂ Nanoparticles. *Nanoscale Res. Lett.* **2016**, *11*. [[CrossRef](#)] [[PubMed](#)]
157. Khalyavka, T.; Bondarenko, M.; Shcherban, N.; Petrik, I.; Melnyk, A. Effect of the C and S Additives on Structural, Optical, and Photocatalytic Properties of TiO₂. *Appl. Nanosci.* **2018**, *9*, 695–702. [[CrossRef](#)]
158. Zou, X.; Shang, X.; Wang, R.; Zhang, J.; Pan, Q.; Guo, Y. Sulfur and Carbon Co-doped TiO₂ Composite Fabricated by Lignosulphonate and Its Suitability for Removal of Cadmium. *Clean Soil Air Water* **2019**, *47*, 1800446. [[CrossRef](#)]
159. Minnekhanov, A.A.; Le, N.T.; Konstantinova, E.A.; Kashkarov, P.K. Influence of Defects on Photoconductivity and Photocatalytic Activity of Nitrogen-doped Titania. *Appl. Magn. Reson.* **2017**, *48*, 335–345. [[CrossRef](#)]
160. Chen, Y.; Luo, X.; Luo, Y.; Xu, P.; He, J.; Jiang, L.; Li, J.; Yan, Z.; Wang, J. Efficient Charge Carrier Separation in L-Alanine Acids Derived N-TiO₂ Nanospheres: The Role of Oxygen Vacancies in Tetrahedral Ti⁴⁺ Sites. *Nanomaterials* **2019**, *9*, 698. [[CrossRef](#)]
161. Batra, R.; Sharotri, N.; Sud, D. Ultrasound Assisted Synthesis of Visible Light Responsive Nitrogen Doped TiO₂ Nano Photocatalyst. *AMR* **2013**, *856*, 22–24. [[CrossRef](#)]
162. Wang, X.-K.; Wang, C.; Guo, W.-L.; Wang, J.-G. A Novel Single-Step Synthesis of N-Doped TiO₂ via a Sonochemical Method. *Mater. Res. Bull.* **2011**, *46*, 2041–2044. [[CrossRef](#)]
163. Wang, H.; Gao, X.; Duan, G.; Yang, X.; Liu, X. Facile Preparation of Anatase–Brookite–Rutile Mixed-Phase N-doped TiO₂ with High Visible-Light Photocatalytic Activity. *J. Environ. Chem. Eng.* **2015**, *3*, 603–608. [[CrossRef](#)]
164. Huang, W.C.; Ting, J.-M. Novel Nitrogen-Doped Anatase TiO₂ Mesoporous Bead Photocatalysts for Enhanced Visible Light Response. *Ceram. Int.* **2017**, *43*, 9992–9997. [[CrossRef](#)]
165. Mahy, J.; Cerfontaine, V.; Poelman, D.; Devred, F.; Gaigneaux, E.; Heinrichs, B.; Lambert, S. Highly Efficient Low-Temperature N-doped TiO₂ Catalysts for Visible Light Photocatalytic Applications. *Materials* **2018**, *11*, 584. [[CrossRef](#)] [[PubMed](#)]
166. Makropoulou, T.; Panagiotopoulou, P.; Venieri, D. N-doped TiO₂ Photocatalysts for Bacterial Inactivation in Water. *J. Chem. Technol. Biotechnol.* **2018**, *93*, 2518–2526. [[CrossRef](#)]
167. Chen, X.; Kuo, D.-H.; Lu, D. N-doped Mesoporous TiO₂ Nanoparticles Synthesized by Using Biological Renewable Nanocrystalline Cellulose as Template for the Degradation of Pollutants under Visible and Sun Light. *Chem. Eng. J.* **2016**, *295*, 192–200. [[CrossRef](#)]
168. Reddy, P.A.K.; Reddy, P.V.L.; Kim, K.-H.; Kumar, M.K.; Manvitha, C.; Shim, J.-J. Novel Approach for the Synthesis of Nitrogen-Doped Titania with Variable Phase Composition and Enhanced Production of Hydrogen under Solar Irradiation. *J. Ind. Eng. Chem.* **2017**, *53*, 253–260. [[CrossRef](#)]
169. Li, X.; Liu, P.; Mao, Y.; Xing, M.; Zhang, J. Preparation of Homogeneous Nitrogen-Doped Mesoporous TiO₂ Spheres with Enhanced Visible-light Photocatalysis. *Appl. Catal. B-Environ.* **2015**, *164*, 352–359. [[CrossRef](#)]
170. Kowalska, K.; Maniakova, G.; Carotenuto, M.; Sacco, O.; Vaiano, V.; Lofrano, G.; Rizzo, L. Removal of Carbamazepine, Diclofenac and Trimethoprim by Solar Driven Advanced Oxidation Processes in a Compound Triangular Collector Based Reactor: A Comparison between Homogeneous and Heterogeneous Processes. *Chemosphere* **2020**, *238*, 124665. [[CrossRef](#)] [[PubMed](#)]
171. Singha, K.; Ghosh, S.C.; Panda, A.B. N-Doped Yellow TiO₂ Hollow Sphere-Mediated Visible-Light-Driven Efficient Esterification of Alcohol and N-Hydroxyimides to Active Esters. *Chem. Asian J.* **2019**, *14*, 3205–3212. [[CrossRef](#)]
172. Suwannaruang, T.; Kamonsuangkasem, K.; Kidkhunthod, P.; Chirawatkul, P.; Saiyasombat, C.; Chanlek, N.; Wantala, K. Influence of Nitrogen Content Levels on Structural Properties and Photocatalytic Activities of Nanorice-like N-doped TiO₂ with Various Calcination Temperatures. *Mater. Res. Bull.* **2018**, *105*, 265–276. [[CrossRef](#)]
173. Ibukun, O.; Jeong, H.K. Enhancement of Photocatalytic Activities of Nitrogen-doped Titanium Dioxide by Ambient Plasma. *Chem. Phys. Lett.* **2020**, *744*, 137234. [[CrossRef](#)]
174. Xing, X.; Du, Z.; Zhuang, J.; Wang, D. Removal of Ciprofloxacin from Water by Nitrogen Doped TiO₂ Immobilized on Glass Spheres: Rapid Screening of Degradation Products. *J. Photoch. Photobiol. A* **2018**, *359*, 23–32. [[CrossRef](#)]
175. Pandiangan, I.F.D.; Sutanto, H.; Nurhasanah, I. Effect of Annealing Temperature on Optical Properties and Photocatalytic Properties of TiO₂:N 8% Thin Film for Rhodamine B Degradation. *Mater. Res. Express* **2018**, *5*, 086404. [[CrossRef](#)]

176. Fernandes, E.; Contreras, S.; Medina, F.; Martins, R.C.; Gomes, J. N-doped Titanium Dioxide for Mixture of Parabens Degradation Based on Ozone Action and Toxicity Evaluation: Precursor of Nitrogen and Titanium Effect. *Process Saf. Environ.* **2020**, *138*, 80–89. [[CrossRef](#)]
177. Kusano, D.; Emori, M.; Sakama, H. Influence of Electronic Structure on Visible Light Photocatalytic Activity of Nitrogen-doped TiO₂. *RSC Adv.* **2017**, *7*, 1887–1898. [[CrossRef](#)]
178. Konstantinova, E.A.; Zaitsev, V.B.; Minnekhanov, A.A.; Le, N.T.; Kashkarov, P.K. The Effect of Spin Center Parameters on the Photoactivity of Nanocrystalline Titanium Dioxide in the Visible Spectral Range. *Crystallogr. Rep.* **2020**, *65*, 130–137. [[CrossRef](#)]
179. Than, L.D.; Luong, N.S.; Ngo, V.D.; Tien, N.M.; Dung, T.N.; Nghia, N.M.; Loc, N.T.; Thu, V.T.; Lam, T.D. Highly Visible Light Activity of Nitrogen Doped TiO₂ Prepared by Sol–Gel Approach. *J. Electron. Mater.* **2016**, *46*, 158–166. [[CrossRef](#)]
180. Fornasini, L.; Bergamonti, L.; Bondioli, F.; Bersani, D.; Lazzarini, L.; Paz, Y.; Lottici, P.P. Photocatalytic N-doped TiO₂ for Self-cleaning of Limestones. *Eur. Phys. J. Plus* **2019**, *134*. [[CrossRef](#)]
181. Jang, I.; Leong, H.J.; Noh, H.; Kang, T.; Kong, S.; Oh, S.-G. Preparation of N-functionalized TiO₂ Particles Using One-Step Sol–Gel Method and Their Photocatalytic Activity. *J. Ind. Eng. Chem.* **2016**, *37*, 380–389. [[CrossRef](#)]
182. Kamaludin, R.; Othman, M.H.D.; Kadir, S.H.S.A.; Ismail, A.F.; Rahman, M.A.; Jaafar, J. Visible-Light-Driven Photocatalytic N-doped TiO₂ for Degradation of Bisphenol A (BPA) and Reactive Black 5 (RB5) Dye. *Water Air Soil Pollut.* **2018**, *229*. [[CrossRef](#)]
183. Mohamed, M.A.; Salleh, W.N.W.; Jaafar, J.; Ismail, A.F.; Nor, N.A.M. Photodegradation of Phenol by N-doped TiO₂ Anatase/Rutile Nanorods Assembled Microsphere under UV and Visible Light Irradiation. *Mater. Chem. Phys.* **2015**, *162*, 113–123. [[CrossRef](#)]
184. Mohamed, M.A.; Salleh, W.N.W.; Jaafar, J.; Ismail, A.F. Structural Characterization of N-doped Anatase–Rutile Mixed Phase TiO₂ Nanorods Assembled Microspheres Synthesized by Simple Sol–Gel Method. *J. Sol. Gel. Sci. Technol.* **2015**, *74*, 513–520. [[CrossRef](#)]
185. Zhang, W.; Zou, L.; Dionysio, D. A Parametric Study of Visible-Light Sensitive TiO₂ photocatalysts Synthesis via a Facile Sol–Gel N-doping Method. *J. Exp. Nanosci.* **2014**, *10*, 1153–1165. [[CrossRef](#)]
186. Samsudin, E.M.; Abd Hamid, S.B. Effect of Band Gap Engineering in Anionic-doped TiO₂ Photocatalyst. *Appl. Surf. Sci.* **2017**, *391*, 326–336. [[CrossRef](#)]
187. Zhang, D.; Wang, J. Modification of the Optical and Electronic Properties of TiO₂ by N Anion-doping for Augmentation of the Visible Light Assisted Photocatalytic Performance. *J. Struct. Chem.* **2018**, *59*, 1353–1361. [[CrossRef](#)]
188. Zhao, B.; Wang, X.; Zhang, Y.; Gao, J.; Chen, Z.; Lu, Z. Synergism of Oxygen Vacancies, Ti³⁺ and N Dopants on the Visible-Light Photocatalytic Activity of N-doped TiO₂. *J. Photochem. Photobiol. A* **2019**, *382*, 111928. [[CrossRef](#)]
189. Kim, T.H.; Go, G.-M.; Cho, H.-B.; Song, Y.; Lee, C.-G.; Choa, Y.-H. A Novel Synthetic Method for N doped TiO₂ Nanoparticles Through Plasma-Assisted Electrolysis and Photocatalytic Activity in the Visible Region. *Front. Chem.* **2018**, *6*. [[CrossRef](#)] [[PubMed](#)]
190. Sun, Z.; Pichugin, V.F.; Evdokimov, K.E.; Konishchev, M.E.; Syrtanov, M.S.; Kudiyarov, V.N.; Li, K.; Tverdokhlebov, S.I. Effect of Nitrogen-Doping and Post Annealing on Wettability and Band Gap Energy of TiO₂ Thin Film. *Appl. Surf. Sci.* **2020**, *500*, 144048. [[CrossRef](#)]
191. Jin, Y.J.; Linghu, J.; Chai, J.; Chua, C.S.; Wong, L.M.; Feng, Y.P.; Yang, M.; Wang, S. Defect Evolution Enhanced Visible-Light Photocatalytic Activity in Nitrogen-doped Anatase TiO₂ Thin Films. *J. Phys. Chem. C* **2018**, *122*, 16600–16606. [[CrossRef](#)]
192. Farkas, B.; Heszler, P.; Budai, J.; Oszkó, A.; Ottosson, M.; Geretovszky, Z. Optical, Compositional and Structural Properties of Pulsed Laser Deposited Nitrogen-Doped Titanium-Dioxide. *Appl. Surf. Sci.* **2018**, *433*, 149–154. [[CrossRef](#)]
193. Zhao, Z.; Kou, T.; Zhang, L.; Zhai, S.; Wang, W.; Wang, Y. Dealloying Induced N-doping in Spindle-like Porous Rutile TiO₂ for Enhanced Visible Light Photocatalytic Activity. *Corros. Sci.* **2018**, *137*, 204–211. [[CrossRef](#)]
194. Krivtsov, I.; Ilkaeva, M.; Salas-Colera, E.; Amghouz, Z.; García, J.R.; Díaz, E.; Ordóñez, S.; Villar-Rodil, S. Consequences of Nitrogen Doping and Oxygen Enrichment on Titanium Local Order and Photocatalytic Performance of TiO₂ Anatase. *J. Phys. Chem. C* **2017**, *121*, 6770–6780. [[CrossRef](#)]
195. Kovalevskiy, N.; Selishchev, D.; Svintsitskiy, D.; Selishcheva, S.; Berezin, A.; Kozlov, D. Synergistic Effect of Polychromatic Radiation on Visible Light Activity of N-doped TiO₂ Photocatalyst. *Catal. Commun.* **2020**, *134*, 105841. [[CrossRef](#)]
196. Cao, Y.; Xing, Z.; Shen, Y.; Li, Z.; Wu, X.; Yan, X.; Zou, J.; Yang, S.; Zhou, W. Mesoporous Black Ti³⁺ /N-TiO₂ Spheres for Efficient Visible-Light-Driven Photocatalytic Performance. *Chem. Eng. J.* **2017**, *325*, 199–207. [[CrossRef](#)]
197. Di Valentin, C.; Pacchioni, G.; Selloni, A.; Livraghi, S.; Giamello, E. Characterization of Paramagnetic Species in N-doped TiO₂ Powders by EPR Spectroscopy and DFT Calculations. *J. Phys. Chem. B* **2005**, *109*, 11414–11419. [[CrossRef](#)]
198. Boningari, T.; Inturi, S.N.R.; Suidan, M.; Smirniotis, P.G. Novel One-Step Synthesis of Nitrogen-doped TiO₂ by Flame Aerosol Technique for Visible-Light Photocatalysis: Effect of Synthesis Parameters and Secondary Nitrogen (N) Source. *Chem. Eng. J.* **2018**, *350*, 324–334. [[CrossRef](#)]
199. Dong, F.; Zhao, W.; Wu, Z.; Guo, S. Band Structure and Visible Light Photocatalytic Activity of Multi-Type Nitrogen Doped TiO₂ Nanoparticles Prepared by Thermal Decomposition. *J. Hazard. Mater.* **2009**, *162*, 763–770. [[CrossRef](#)] [[PubMed](#)]
200. Dawson, M.; Soares, G.B.; Ribeiro, C. Influence of Calcination Parameters on the Synthesis of N-doped TiO₂ by the Polymeric Precursors Method. *J. Solid State Chem.* **2014**, *215*, 211–218. [[CrossRef](#)]
201. Bjelajac, A.; Petrović, R.; Popović, M.; Rakočević, Z.; Socol, G.; Mihailescu, I.N.; Janačković, D. Doping of TiO₂ Nanotubes with Nitrogen by Annealing in Ammonia for Visible Light Activation: Influence of Pre- and Post-Annealing in Air. *Thin Solid Films* **2019**, *692*, 137598. [[CrossRef](#)]

202. Peng, F.; Cai, L.; Yu, H.; Wang, H.; Yang, J. Synthesis and Characterization of Substitutional and Interstitial Nitrogen-doped Titanium Dioxides with Visible Light Photocatalytic Activity. *J. Solid State Chem.* **2008**, *181*, 130–136. [[CrossRef](#)]
203. Azami, M.S.; Nawawi, W.I.; Shukri, D.S.M. Formation of Predominant Interstitial N-TiO₂ Using Physical Preparation under Microwave Irradiation for Reactive Red 4 Dye Removal. *Desalin. Water Treat.* **2017**, *92*, 172–180. [[CrossRef](#)]
204. Zhou, Y.; Liu, Y.; Liu, P.; Zhang, W.; Xing, M.; Zhang, J. A Facile Approach to Further Improve the Substitution of Nitrogen into Reduced TiO₂ – with an Enhanced Photocatalytic Activity. *Appl. Catal. B-Environ.* **2015**, *170–171*, 66–73. [[CrossRef](#)]
205. Lee, S.; Cho, I.-S.; Lee, D.K.; Kim, D.W.; Noh, T.H.; Kwak, C.H.; Park, S.; Hong, K.S.; Lee, J.-K.; Jung, H.S. Influence of Nitrogen Chemical States on Photocatalytic Activities of Nitrogen-doped TiO₂ Nanoparticles under Visible Light. *J. Photoch. Photobiol. A* **2010**, *213*, 129–135. [[CrossRef](#)]
206. Huang, J.; Song, H.; Chen, C.; Yang, Y.; Xu, N.; Ji, X.; Li, C.; You, J.-A. Facile Synthesis of N-doped TiO₂ Nanoparticles Caged in MIL-100(Fe) for Photocatalytic Degradation of Organic Dyes under Visible Light Irradiation. *J. Environ. Chem. Eng.* **2017**, *5*, 2579–2585. [[CrossRef](#)]
207. Borges, K.A.; Santos, L.M.; Paniago, R.M.; Barbosa Neto, N.M.; Schneider, J.; Bahnemann, D.W.; Patrocínio, A.O.T.; Machado, A.E.H. Characterization of a Highly Efficient N-doped TiO₂ Photocatalyst Prepared via Factorial Design. *New J. Chem.* **2016**, *40*, 7846–7855. [[CrossRef](#)]
208. Le, P.; Hieu, L.; Lam, T.-N.; Hang, N.; Truong, N.; Tuyen, L.; Phong, P.; Leu, J. Enhanced Photocatalytic Performance of Nitrogen-doped TiO₂ Nanotube Arrays Using a Simple Annealing Process. *Micromachines* **2018**, *9*, 618. [[CrossRef](#)]
209. Monteiro, R.A.R.; Miranda, S.M.; Vilar, V.J.P.; Pastrana-Martínez, L.M.; Tavares, P.B.; Boaventura, R.A.R.; Faria, J.L.; Pinto, E.; Silva, A.M.T. N-Modified TiO₂ Photocatalytic Activity towards Diphenhydramine Degradation and *Escherichia coli* Inactivation in Aqueous Solutions. *Appl. Catal. B Environ.* **2015**, *162*, 66–74. [[CrossRef](#)]
210. Kuźmiński, K.; Morawski, A.W.; Janus, M. Adsorption and Photocatalytic Degradation of Anionic and Cationic Surfactants on Nitrogen-Modified TiO₂. *J. Surfactants Deterg.* **2018**, *21*, 909–921. [[CrossRef](#)]
211. Veisi, F.; Zazouli, M.A.; Ebrahimzadeh, M.A.; Charati, J.Y.; Dezfoli, A.S. Photocatalytic Degradation of Furfural in Aqueous Solution by N-doped Titanium Dioxide Nanoparticles. *Environ. Sci. Pollut. Res.* **2016**, *23*, 21846–21860. [[CrossRef](#)]
212. Janus, M.; Mađraszewski, S.; Zając, K.; Kusiak-Nejman, E.; Morawski, A.W.; Stephan, D. Photocatalytic Activity and Mechanical Properties of Cements Modified with TiO₂/N. *Materials* **2019**, *12*, 3756. [[CrossRef](#)]
213. Mungondori, H.H.; Tichagwa, L.; Katwire, D.M.; Aoyi, O. Preparation of Photo-Catalytic Copolymer Grafted Asymmetric Membranes (N-TiO₂-PMAA-g-PVDF/PAN) and Their Application on the Degradation of Bentazon in Water. *Iran. Polym. J.* **2016**, *25*, 135–144. [[CrossRef](#)]
214. Khalilzadeh, A.; Fatemi, S. Spouted Bed Reactor for VOC Removal by Modified Nano-TiO₂ Photocatalytic Particles. *Chem. Eng. Res. Des.* **2016**, *115*, 241–250. [[CrossRef](#)]
215. Sun, P.; Zhang, J.; Liu, W.; Wang, Q.; Cao, W. Modification to L-H Kinetics Model and Its Application in the Investigation on Photodegradation of Gaseous Benzene by Nitrogen-doped TiO₂. *Catalysts* **2018**, *8*, 326. [[CrossRef](#)]
216. Kamaei, M.; Rashedi, H.; Dastgheib, S.; Tasharrofi, S. Comparing Photocatalytic Degradation of Gaseous Ethylbenzene Using N-doped and Pure TiO₂ Nano-catalysts Coated on Glass Beads under Both UV and Visible Light Irradiation. *Catalysts* **2018**, *8*, 466. [[CrossRef](#)]
217. Rokicka, P.; Markowska-Szczupak, A.; Kowalczyk, Ł.; Kowalska, E.; Morawski, A.W. Influence of Titanium Dioxide Modification on the Antibacterial Properties. *Pol. J. Chem. Technol.* **2016**, *18*, 56–64. [[CrossRef](#)]
218. Kawashita, M.; Endo, N.; Watanabe, T.; Miyazaki, T.; Furuya, M.; Yokota, K.; Abiko, Y.; Kanetaka, H.; Takahashi, N. Formation of Bioactive N-doped TiO₂ on Ti with Visible Light-Induced Antibacterial Activity Using NaOH, Hot Water, and Subsequent Ammonia Atmospheric Heat Treatment. *Colloid. Surf. B.* **2016**, *145*, 285–290. [[CrossRef](#)]
219. Kassahun, S.K.; Kiflie, Z.; Kim, H.; Gadisa, B.T. Effects of Operational Parameters on Bacterial Inactivation in Vis-LEDs Illuminated N-doped TiO₂ Based Photoreactor. *J. Environ. Chem. Eng.* **2020**, *8*, 104374. [[CrossRef](#)]
220. Surmacki, J. Nitrogen-Doped Titanium Dioxide Nanoparticles Modified by an Electron Beam for Improving Human Breast Cancer Detection by Raman Spectroscopy: A Preliminary Study. *Diagnostics* **2020**, *10*, 757. [[CrossRef](#)]
221. Mohammadalipour, Z.; Rahmati, M.; Khataee, A.; Moosavi, M.A. Differential Effects of N-TiO₂ Nanoparticle and Its Photo-activated Form on Autophagy and Necroptosis in Human Melanoma A375 Cells. *J. Cell Physiol.* **2020**, *235*, 8246–8259. [[CrossRef](#)]
222. Preethi, L.K.; Antony, R.P.; Mathews, T.; Loo, S.C.J.; Wong, L.H.; Dash, S.; Tyagi, A.K. Nitrogen Doped Anatase-Rutile Heterostructured Nanotubes for Enhanced Photocatalytic Hydrogen Production: Promising Structure for Sustainable Fuel Production. *Int. J. Hydrogen Energ.* **2016**, *41*, 5865–5877. [[CrossRef](#)]
223. Shvadchina, Y.O.; Cherepivskaya, M.K.; Vakulenko, V.F.; Sova, A.N.; Stolyarova, I.V.; Prikhodko, R.V. The Study of Properties and Catalytic Activity of Titanium Dioxide Doped with Sulphur. *J. Water Chem. Technol.* **2015**, *37*, 283–288. [[CrossRef](#)]
224. Lin, Y.-H.; Hsueh, H.-T.; Chang, C.-W.; Chu, H. The Visible Light-Driven Photodegradation of Dimethyl Sulfide on S-doped TiO₂: Characterization, Kinetics, and Reaction Pathways. *Appl. Catal. B-Environ.* **2016**, *199*, 1–10. [[CrossRef](#)]
225. Hosseinzadeh, G.; Rasoulnezhad, H.; Ghasemian, N.; Hosseinzadeh, R. Ultrasonic-Assisted Spray Pyrolysis Technique for Synthesis of Transparent S-doped TiO₂ Thin Film. *J. Aust. Ceram. Soc.* **2018**, *55*, 387–394. [[CrossRef](#)]
226. Sun, X.-Y.; Sun, X.; Zhang, X.; Qian, N.-X.; Wang, M.; Ma, Y.-Q. Improved Adsorption and Degradation Performance by S-doping of (001)-TiO₂. *Beilstein J. Nanotechnol.* **2019**, *10*, 2116–2127. [[CrossRef](#)] [[PubMed](#)]

227. Taherinia, M.; Nasiri, M.; Abedini, E.; Pouretedal, H.R. Comparing the Photocatalytic Activity of N-doped and S-doped Titanium Dioxide Nanoparticles for Water Splitting under Sunlight Radiation. *J. Iran. Chem. Soc.* **2018**, *15*, 1301–1310. [[CrossRef](#)]
228. Esquivel-Escalante, K.; Nava-Mendoza, R.; Velázquez-Castillo, R. Crystal structure determination of the S/TiO₂ system and the correlation with its photocatalytic properties. *J. Nanosci. Nanotechnol.* **2016**, *16*, 967–972. [[CrossRef](#)]
229. Ramacharyulu, P.V.R.K.; Nimbalkar, D.B.; Kumar, J.P.; Prasad, G.K.; Ke, S.-C. N-doped, S-doped TiO₂ nanocatalysts: Synthesis, Characterization and Photocatalytic Activity in the Presence of Sunlight. *RSC Adv.* **2015**, *5*, 37096–37101. [[CrossRef](#)]
230. Baieissa, E.S. Synthesis and Characterization of Sulfur-Titanium Dioxide Nanocomposites for Photocatalytic Oxidation of Cyanide Using Visible Light Irradiation. *Chin. J. Catal.* **2015**, *36*, 698–704. [[CrossRef](#)]
231. Birben, N.C.; Uyguner-Demirel, C.S.; Sen-Kavurmaci, S.; Gurkan, Y.Y.; Turkten, N.; Cinar, Z.; Bekbolet, M. Comparative Evaluation of Anion Doped Photocatalysts on the Mineralization and Decolorization of Natural Organic Matter. *Catal. Today* **2015**, *240*, 125–131. [[CrossRef](#)]
232. Chen, X.; Sun, H.; Zhang, J.; Guo, Y.; Kuo, D.-H. Cationic S-doped TiO₂/SiO₂ Visible-Light Photocatalyst Synthesized by Co-hydrolysis Method and Its Application for Organic Degradation. *J. Mol. Liq.* **2019**, *273*, 50–57. [[CrossRef](#)]
233. McManamon, C.; O'Connell, J.; Delaney, P.; Rasappa, S.; Holmes, J.D.; Morris, M.A. A Facile Route to Synthesis of S-doped TiO₂ Nanoparticles for Photocatalytic Activity. *J. Mol. Catal. A-Chem.* **2015**, *406*, 51–57. [[CrossRef](#)]
234. Yi, C.; Liao, Q.; Deng, W.; Huang, Y.; Mao, J.; Zhang, B.; Wu, G. The Preparation of Amorphous TiO₂ Doped with Cationic S and Its Application to the Degradation of DCFs under Visible Light Irradiation. *Sci. Total Environ.* **2019**, *684*, 527–536. [[CrossRef](#)] [[PubMed](#)]
235. Abu Bakar, S.; Ribeiro, C. An Insight Toward the Photocatalytic Activity of S Doped 1-D TiO₂ Nanorods Prepared via Novel Route: As Promising Platform for Environmental Leap. *J. Mol. Catal. A-Chem.* **2016**, *412*, 78–92. [[CrossRef](#)]
236. Bakar, S.A.; Ribeiro, C. A Comparative Run for Visible-Light-Driven Photocatalytic Activity of Anionic and Cationic S-doped TiO₂ Photocatalysts: A Case Study of Possible Sulfur Doping through Chemical Protocol. *J. Mol. Catal. A-Chem.* **2016**, *421*, 1–15. [[CrossRef](#)]
237. Chen, X.; Sun, H.; Zelekew, O.A.; Zhang, J.; Guo, Y.; Zeng, A.; Kuo, D.-H.; Lin, J. Biological Renewable Hemicellulose-Template for Synthesis of Visible Light Responsive Sulfur-doped TiO₂ for Photocatalytic Oxidation of Toxic Organic and As(III) Pollutants. *Appl. Surf. Sci.* **2020**, *525*, 146531. [[CrossRef](#)]
238. Meng, Q.; Liu, B.; Liu, H.; Cai, Y.; Dong, L. Effects of S and Ta Codoping on Photocatalytic Activity of Rutile TiO₂. *J. Sol-Gel Sci. Technol.* **2018**, *86*, 631–639. [[CrossRef](#)]
239. Anitha, B.; Ravidhas, C.; Venkatesh, R.; Raj, A.M.E.; Ravichandran, K.; Subramanian, B.; Sanjeeviraja, C. Self Assembled Sulfur Induced Interconnected Nanostructure TiO₂ Electrode for Visible Light Photoresponse and Photocatalytic Application. *Phys. E* **2017**, *91*, 148–160. [[CrossRef](#)]
240. Chen, X.; Kuo, D.-H.; Lu, D. Visible Light Response and Superior Dispersed S-doped TiO₂ Nanoparticles Synthesized via Ionic Liquid. *Adv. Powder Technol.* **2017**, *28*, 1213–1220. [[CrossRef](#)]
241. Nam, S.-H.; Kim, T.K.; Boo, J.-H. Physical Property and Photo-Catalytic Activity of Sulfur Doped TiO₂ Catalysts Responding to Visible Light. *Catal. Today* **2012**, *185*, 259–262. [[CrossRef](#)]
242. Ramacharyulu, P.V.R.K.; Praveen Kumar, J.; Prasad, G.K.; Sreedhar, B. Sulphur Doped Nano TiO₂: Synthesis, Characterization and Photocatalytic Degradation of a Toxic Chemical in Presence of Sunlight. *Mater. Chem. Phys.* **2014**, *148*, 692–698. [[CrossRef](#)]
243. Yu, J.C.; Ho, W.; Yu, J.; Yip, H.; Wong, P.K.; Zhao, J. Efficient Visible-Light-Induced Photocatalytic Disinfection on Sulfur-Doped Nanocrystalline Titania. *Environ. Sci. Technol.* **2005**, *39*, 1175–1179. [[CrossRef](#)] [[PubMed](#)]
244. Zhongchen, Y.; Song, W.; Lu, H.; Zhuan, L.; Yuanlin, N. Photocatalytic Property of Nanostructured S Doped TiO₂ Films Prepared by the Micro Plasma Method. *Rare Met. Mater. Eng.* **2015**, *44*, 1629–1632. [[CrossRef](#)]
245. Randeniya, L.K.; Murphy, A.B.; Plumb, I.C. A Study of S-Doped TiO₂ for Photoelectrochemical Hydrogen Generation from Water. *J. Mater. Sci.* **2007**, *43*, 1389–1399. [[CrossRef](#)]
246. Bu, X.; Wang, Y.; Li, J.; Zhang, C. Improving the Visible Light Photocatalytic Activity of TiO₂ by Combining Sulfur Doping and Rectorite Carrier. *J. Alloys Compd.* **2015**, *628*, 20–26. [[CrossRef](#)]
247. Albrbar, A.J.; Djokić, V.; Bjelajac, A.; Kovač, J.; Ćirković, J.; Mitrić, M.; Janačković, D.; Petrović, R. Visible-Light Active Mesoporous, Nanocrystalline N,S-doped and Co-doped Titania Photocatalysts Synthesized by Non-Hydrolytic Sol-Gel Route. *Ceram. Int.* **2016**, *42*, 16718–16728. [[CrossRef](#)]
248. Zhu, M.; Zhai, C.; Qiu, L.; Lu, C.; Paton, A.S.; Du, Y.; Goh, M.C. New Method to Synthesize S-doped TiO₂ with Stable and Highly Efficient Photocatalytic Performance under Indoor Sunlight Irradiation. *ACS Sustain. Chem. Eng.* **2015**, *3*, 3123–3129. [[CrossRef](#)]
249. Sharotri, N.; Sud, D. A Greener Approach to Synthesize Visible Light Responsive Nanoporous S-doped TiO₂ with Enhanced Photocatalytic Activity. *New J. Chem.* **2015**, *39*, 2217–2223. [[CrossRef](#)]
250. Kovačić, M.; Perović, K.; Papac, J.; Tomić, A.; Matoh, L.; Žener, B.; Brodar, T.; Capan, I.; Surca, A.K.; Kušić, H.; et al. One-Pot Synthesis of Sulfur-doped TiO₂/Reduced Graphene Oxide Composite (S-TiO₂/RGO) with Improved Photocatalytic Activity for the Removal of Diclofenac from Water. *Materials* **2020**, *13*, 1621. [[CrossRef](#)]
251. Huang, Z.; Gao, Z.; Gao, S.; Wang, Q.; Wang, Z.; Huang, B.; Dai, Y. Facile Synthesis of S-doped Reduced TiO_{2-x} with Enhanced Visible-Light Photocatalytic Performance. *Chin. J. Catal.* **2017**, *38*, 821–830. [[CrossRef](#)]
252. Xing, Z.; Li, Z.; Wu, X.; Wang, G.; Zhou, W. In-Situ S-doped Porous Anatase TiO₂ Nanopillars for High-Efficient Visible-Light Photocatalytic Hydrogen Evolution. *Int. J. Hydrog. Energy* **2016**, *41*, 1535–1541. [[CrossRef](#)]

253. Li, M.; Xing, Z.; Jiang, J.; Li, Z.; Kuang, J.; Yin, J.; Wan, N.; Zhu, Q.; Zhou, W. In-Situ Ti³⁺/S Doped High Thermostable Anatase TiO₂ Nanorods as Efficient Visible-Light-Driven Photocatalysts. *Mater. Chem. Phys.* **2018**, *219*, 303–310. [CrossRef]
254. Mohan Kumar, K.; Godavarthi, S.; Karthik, T.V.K.; Mahendhiran, M.; Hernandez-Eligio, A.; Hernandez-Como, N.; Agarwal, V.; Martinez Gomez, L. Green Synthesis of S-doped Rod Shaped Anatase TiO₂ Microstructures. *Mater. Lett.* **2016**, *183*, 211–214. [CrossRef]
255. Bakar, S.A.; Ribeiro, C. Rapid and Morphology Controlled Synthesis of Anionic S-doped TiO₂ Photocatalysts for the Visible-Light-Driven Photodegradation of Organic Pollutants. *RSC Adv.* **2016**, *6*, 36516–36527. [CrossRef]
256. Wang, F.; Li, F.; Zhang, L.; Zeng, H.; Sun, Y.; Zhang, S.; Xu, X. S-TiO₂ with Enhanced Visible-Light Photocatalytic Activity Derived from TiS₂ in Deionized Water. *Mater. Res. Bull.* **2017**, *87*, 20–26. [CrossRef]
257. Ho, W.; Yu, J.C.; Lee, S. Low-Temperature Hydrothermal Synthesis of S-Doped TiO₂ with Visible Light Photocatalytic Activity. *J. Solid State Chem.* **2006**, *179*, 1171–1176. [CrossRef]
258. Umabayashi, T.; Yamaki, T.; Itoh, H.; Asai, K. Band Gap Narrowing of Titanium Dioxide by Sulfur Doping. *Appl. Phys. Lett.* **2002**, *81*, 454–456. [CrossRef]
259. Shin, S.W.; Lee, J.Y.; Ahn, K.-S.; Kang, S.H.; Kim, J.H. Visible Light Absorbing TiO₂ Nanotube Arrays by Sulfur Treatment for Photoelectrochemical Water Splitting. *J. Phys. Chem. C* **2015**, *119*, 13375–13383. [CrossRef]
260. Bento, R.T.; Correa, O.V.; Pillis, M.F. Photocatalytic Activity of Undoped and Sulfur-doped TiO₂ Films Grown by MOCVD for Water Treatment under Visible Light. *J. Eur. Ceram. Soc.* **2019**, *39*, 3498–3504. [CrossRef]
261. Boningari, T.; Inturi, S.N.R.; Suidan, M.; Smirniotis, P.G. Novel One-Step Synthesis of Sulfur Doped-TiO₂ by Flame Spray Pyrolysis for Visible Light Photocatalytic Degradation of Acetaldehyde. *Chem. Eng. J.* **2018**, *339*, 249–258. [CrossRef]
262. Momeni, M.M.; Ghayeb, Y.; Ghonchehi, Z. Visible Light Activity of Sulfur-doped TiO₂ Nanostructure Photoelectrodes Prepared by Single-Step Electrochemical Anodizing Process. *J. Solid State Electrochem.* **2015**, *19*, 1359–1366. [CrossRef]
263. Wang, Z.; Liu, X.; Li, W.; Wang, H.; Li, H. Enhancing the Photocatalytic Degradation of Salicylic Acid by Using Molecular Imprinted S-Doped TiO₂ under Simulated Solar Light. *Ceram. Int.* **2014**, *40*, 8863–8867. [CrossRef]
264. Sun, S.; Zhang, J.; Gao, P.; Wang, Y.; Li, X.; Wu, T.; Wang, Y.; Chen, Y.; Yang, P. Full Visible-Light Absorption of TiO₂ Nanotubes Induced by Anionic S₂²⁻ Doping and Their Greatly Enhanced Photocatalytic Hydrogen Production Abilities. *Appl. Catal. B Environ.* **2017**, *206*, 168–174. [CrossRef]
265. Adiansyah, A.; Purba, I.E.; Tarigan, M.; Lisnadiyanti, L.; Yusnaidar, Y.; Mahendra, I.P. Preparation of S-doped TiO₂ via Sol-Gel/Hydrothermal Method and Its Activity as Photodegradation of RB05. *RJC* **2020**, *13*, 757–760. [CrossRef]
266. Olowoyo, J.O.; Kumar, M.; Jain, S.L.; Shen, S.; Zhou, Z.; Mao, S.S.; Vorontsov, A.V.; Kumar, U. Reinforced Photocatalytic Reduction of CO₂ to Fuel by Efficient S-TiO₂: Significance of Sulfur Doping. *Int. J. Hydrog. Energy* **2018**, *43*, 17682–17695. [CrossRef]
267. Pillai, V.V.; Lonkar, S.P.; Alhassan, S.M. Template-Free, Solid-State Synthesis of Hierarchically Macroporous S-doped TiO₂ Nano-photocatalysts for Efficient Water Remediation. *ACS Omega* **2020**, *5*, 7969–7978. [CrossRef] [PubMed]
268. Sraw, A.; Kaur, T.; Pandey, Y.; Verma, A.; Sobti, A.; Wanchoo, R.K.; Toor, A.P. Photocatalytic Degradation of Monocrotophos and Quinalphos Using Solar-Activated S-Doped TiO₂. *Int. J. Environ. Sci. Technol.* **2020**, *17*, 4895–4908. [CrossRef]
269. Liu, C.; Chen, W.; Sheng, Y.; Li, L. Atrazine Degradation in Solar Irradiation/S-Doped Titanium Dioxide Treatment. In Proceedings of the 2009 3rd International Conference on Bioinformatics and Biomedical Engineering, Beijing, China, 11–13 June 2009. [CrossRef]
270. Umabayashi, T.; Yamaki, T.; Tanaka, S.; Asai, K. Visible Light-Induced Degradation of Methylene Blue on S-Doped TiO₂. *Chem. Lett.* **2003**, *32*, 330–331. [CrossRef]
271. Lin, Y.-H.; Chou, S.-H.; Chu, H. A Kinetic Study for the Degradation of 1,2-Dichloroethane by S-Doped TiO₂ under Visible Light. *J. Nanopart. Res.* **2014**, *16*. [CrossRef]
272. Vorontsov, A.V.; Valdés, H. Insights into the Visible Light Photocatalytic Activity of S-doped Hydrated TiO₂. *Int. J. Hydrogen Energy* **2019**, *44*, 17963–17973. [CrossRef]
273. Etghani, S.A.; Ansari, E.; Mohajerzadeh, S. Evolution of Large Area TiS₂-TiO₂ Heterostructures and S-doped TiO₂ Nano-sheets on Titanium Foils. *Sci. Rep.* **2019**, *9*. [CrossRef]
274. Basera, P.; Saini, S.; Arora, E.; Singh, A.; Kumar, M.; Bhattacharya, S. Stability of Non-metal Dopants to Tune the Photo-Absorption of TiO₂ at Realistic Temperatures and Oxygen Partial Pressures: A Hybrid DFT Study. *Sci. Rep.* **2019**, *9*. [CrossRef] [PubMed]
275. Ma, D.; Xin, Y.; Gao, M.; Wu, J. Fabrication and Photocatalytic Properties of Cationic and Anionic S-doped TiO₂ Nanofibers by Electrospinning. *Appl. Catal. B-Environ.* **2014**, *147*, 49–57. [CrossRef]
276. Syafiuddin, A.; Hadibarata, T.; Zon, N.F. Characterization of Titanium Dioxide Doped with Nitrogen and Sulfur and Its Photocatalytic Appraisal for Degradation of Phenol and Methylene Blue. *J. Chin. Chem. Soc. Taip.* **2017**, *64*, 1333–1339. [CrossRef]
277. Khang, N.C.; Van, D.Q.; Thuy, N.M.; Minh, N.V.; Minh, P.N. Remarkably Enhanced Photocatalytic Activity by Sulfur-doped Titanium Dioxide in Nanohybrids with Carbon Nanotubes. *J. Phys. Chem. Solids* **2016**, *99*, 119–123. [CrossRef]
278. Wang, M.; Zhang, X.; Rao, R.; Qian, N.X.; Ma, Y.Q. Study on Vapor-Thermal Synthesis and Sulfur-doping of TiO₂/Graphene Composites. *Appl. Surf. Sci.* **2020**, *507*, 144856. [CrossRef]
279. Dunnill, C.W.; Aiken, Z.A.; Kafizas, A.; Pratten, J.; Wilson, M.; Morgan, D.J.; Parkin, I.P. White Light Induced Photocatalytic Activity of Sulfur-Doped TiO₂ Thin Films and Their Potential for Antibacterial Application. *J. Mater. Chem.* **2009**, *19*, 8747. [CrossRef]

280. Osin, O.A.; Yu, T.; Cai, X.; Jiang, Y.; Peng, G.; Cheng, X.; Li, R.; Qin, Y.; Lin, S. Photocatalytic Degradation of 4-Nitrophenol by C,N-TiO₂: Degradation Efficiency vs. Embryonic Toxicity of the Resulting Compounds. *Front. Chem.* **2018**, *6*. [[CrossRef](#)]
281. Janus, M.; Bubacz, K.; Zatorska, J.; Kusiak-Nejman, E.; Czyżewski, A.; Morawski, A.W. Preliminary Studies of Photocatalytic Activity of Gypsum Plasters Containing TiO₂ Co-modified with Nitrogen and Carbon. *Pol. J. Chem. Technol.* **2015**, *17*, 96–102. [[CrossRef](#)]
282. Janus, M.; Kusiak-Nejman, E.; Rokicka-Konieczna, P.; Markowska-Szczupak, A.; Zając, K.; Morawski, A.W. Bacterial Inactivation on Concrete Plates Loaded with Modified TiO₂ Photocatalysts under Visible Light Irradiation. *Molecules* **2019**, *24*, 3026. [[CrossRef](#)]
283. Janus, M.; Zatorska, J.; Czyżewski, A.; Bubacz, K.; Kusiak-Nejman, E.; Morawski, A.W. Self-Cleaning Properties of Cement Plates Loaded with N,C-modified TiO₂ Photocatalysts. *Appl. Surf. Sci.* **2015**, *330*, 200–206. [[CrossRef](#)]
284. Xiao, Y.; Sun, X.; Li, L.; Chen, J.; Zhao, S.; Jiang, C.; Yang, L.; Cheng, L.; Cao, S. Simultaneous Formation of a C/N-TiO₂ Hollow Photocatalyst with Efficient Photocatalytic Performance and Recyclability. *Chin. J. Catal.* **2019**, *40*, 765–775. [[CrossRef](#)]
285. Buda, W.; Czech, B. Preparation and Characterization of C,N-Codoped TiO₂ Photocatalyst for the Degradation of Diclofenac from Wastewater. *Water Sci. Technol.* **2013**, *68*, 1322–1328. [[CrossRef](#)] [[PubMed](#)]
286. Krishnan, J.; Nerissa, E.; Hadi, A. Synthesis, Characterization and Efficiency of N, C-TiO₂ as an Active Visible Light Photocatalyst. *AMM* **2014**, *661*, 63–67. [[CrossRef](#)]
287. Ariza-Tarazona, M.C.; Villarreal-Chiu, J.F.; Hernández-López, J.M.; Rivera De la Rosa, J.; Barbieri, V.; Siligardi, C.; Cedillo-González, E.I. Microplastic Pollution Reduction by a Carbon and Nitrogen-doped TiO₂: Effect of pH and Temperature in the Photocatalytic Degradation Process. *J. Hazard. Mater.* **2020**, *395*, 122632. [[CrossRef](#)] [[PubMed](#)]
288. El-Sheikh, S.M.; Khedr, T.M.; Hakki, A.; Ismail, A.A.; Badawy, W.A.; Bahnemann, D.W. Visible Light Activated Carbon and Nitrogen Co-doped Mesoporous TiO₂ as Efficient Photocatalyst for Degradation of Ibuprofen. *Sep. Purif. Technol.* **2017**, *173*, 258–268. [[CrossRef](#)]
289. Li, F.; Zhou, J.; Du, C.; Li, W.; Wang, Y.; He, G.; He, Q. Preparation and Photocatalytic Properties of Porous C and N Co-doped TiO₂ Deposited on Brick by a Fast, One-Step Microwave Irradiation Method. *J. Environ. Sci.* **2017**, *60*, 24–32. [[CrossRef](#)] [[PubMed](#)]
290. Du, C.; Zhou, J.; Li, F.; Li, W.; Wang, Y.; He, Q. Extremely Fast Dark Adsorption Rate of Carbon and Nitrogen Co-doped TiO₂ Prepared by a Relatively Fast, Facile and Low-Cost Microwave Method. *Appl. Phys. A* **2016**, *122*. [[CrossRef](#)]
291. Zhou, J.; Li, F.; Du, C.; Liu, J.; Wang, Y.; Li, W.; He, G.; He, Q. Photodegradation Performance and Recyclability of a Porous Nitrogen and Carbon Co-doped TiO₂/Activated Carbon Composite Prepared by an Extremely Fast One-Step Microwave Method. *RSC Adv.* **2016**, *6*, 84457–84463. [[CrossRef](#)]
292. Al-Hajji, L.A.; Ismail, A.A.; Alseidi, M.; Almutawa, F.; Ahmad, S.; Bumajdad, A. Green Approach and Ease Synthesis of C/N-codoped TiO₂ Nanocrystals for Photodegradation of Endocrine. *J. Nanopart. Res.* **2020**, *22*. [[CrossRef](#)]
293. Wang, X.; Lim, T.-T. Effect of Hexamethylenetetramine on the Visible-Light Photocatalytic Activity of C–N Codoped TiO₂ for Bisphenol A Degradation: Evaluation of Photocatalytic Mechanism and Solution Toxicity. *Appl. Catal. A-Gen.* **2011**, *399*, 233–241. [[CrossRef](#)]
294. Wang, X.; Lim, T.-T. Solvothermal Synthesis of C–N Codoped TiO₂ and Photocatalytic Evaluation for Bisphenol A Degradation Using a Visible-Light Irradiated LED Photoreactor. *Appl. Catal. B-Environ.* **2010**, *100*, 355–364. [[CrossRef](#)]
295. Komatsuda, S.; Asakura, Y.; Vequizo, J.J.M.; Yamakata, A.; Yin, S. Enhanced Photocatalytic NO Decomposition of Visible-Light Responsive F-TiO₂/(N,C)-TiO₂ by Charge Transfer between F-TiO₂ and (N,C)-TiO₂ through Their Doping Levels. *Appl. Catal. B-Environ.* **2018**, *238*, 358–364. [[CrossRef](#)]
296. Huang, X.; Yang, W.; Zhang, G.; Yan, L.; Zhang, Y.; Jiang, A.; Xu, H.; Zhou, M.; Liu, Z.; Tang, H.; et al. Alternative Synthesis of Nitrogen and Carbon Co-doped TiO₂ for Removing Fluoroquinolone Antibiotics in Water under Visible Light. *Catal. Today* **2019**. [[CrossRef](#)]
297. Zhang, J.; Xing, Z.; Cui, J.; Li, Z.; Tan, S.; Yin, J.; Zou, J.; Zhu, Q.; Zhou, W. C,N Co-doped Porous TiO₂ hollow Sphere Visible Light Photocatalysts for Efficient Removal of Highly Toxic Phenolic Pollutants. *Dalton Trans.* **2018**, *47*, 4877–4884. [[CrossRef](#)] [[PubMed](#)]
298. Boscaro, P.; Cacciaguerra, T.; Cot, D.; Fajula, F.; Hulea, V.; Galarneau, A. C,N-doped TiO₂ Monoliths with Hierarchical Macro-/Mesoporosity for Water Treatment under Visible Light. *Microporous Mesoporous Mater.* **2019**, *280*, 37–45. [[CrossRef](#)]
299. Ji, L.; Zhou, S.; Liu, X.; Gong, M.; Xu, T. Synthesis of Carbon- and Nitrogen-Doped TiO₂/Carbon Composite Fibers by a Surface-Hydrolyzed PAN Fiber and Their Photocatalytic Property. *J. Mater. Sci.* **2019**, *55*, 2471–2481. [[CrossRef](#)]
300. Abdullah, A.M.; Al-Thani, N.J.; Tawbi, K.; Al-Kandari, H. Carbon/Nitrogen-Doped TiO₂: New Synthesis Route, Characterization and Application for Phenol Degradation. *Arab. J. Chem.* **2016**, *9*, 229–237. [[CrossRef](#)]
301. Wang, M.; Han, J.; Hu, Y.; Guo, R. Mesoporous C, N-codoped TiO₂ Hybrid Shells with Enhanced Visible Light Photocatalytic Performance. *RSC Adv.* **2017**, *7*, 15513–15520. [[CrossRef](#)]
302. Liu, X.; Chen, Y.; Cao, C.; Xu, J.; Qian, Q.; Luo, Y.; Xue, H.; Xiao, L.; Chen, Y.; Chen, Q. Electrospun Nitrogen and Carbon Co-doped Porous TiO₂ Nanofibers with High Visible Light Photocatalytic Activity. *New J. Chem.* **2015**, *39*, 6944–6950. [[CrossRef](#)]
303. Zhang, X.; Zhang, Y.; Zhou, L.; Li, X.; Guo, X. In Situ C,N-codoped Mesoporous TiO₂ Nanocrystallites with High Surface Areas and Worm-like Structure for Efficient Photocatalysis. *J. Porous Mater.* **2017**, *25*, 571–579. [[CrossRef](#)]
304. Chen, D.; Jiang, Z.; Geng, J.; Wang, Q.; Yang, D. Carbon and Nitrogen Co-Doped TiO₂ with Enhanced Visible-Light Photocatalytic Activity. *Ind. Eng. Chem. Res.* **2007**, *46*, 2741–2746. [[CrossRef](#)]
305. Zhang, X.; Cai, M.; Cui, N.; Chen, G.; Zou, G.; Zhou, L. One-Step Synthesis of b-N-TiO₂/C Nanocomposites with High Visible Light Photocatalytic Activity to Degrade Microcystis Aeruginosa. *Catalysts* **2020**, *10*, 579. [[CrossRef](#)]

306. Chen, H.; Chen, K.-F.; Lai, S.-W.; Dang, Z.; Peng, Y.-P. Photoelectrochemical Oxidation of Azo Dye and Generation of Hydrogen via CN Co-doped TiO₂ Nanotube Arrays. *Sep. Purif. Technol.* **2015**, *146*, 143–153. [[CrossRef](#)]
307. Wu, T.; Niu, P.; Yang, Y.; Yin, L.; Tan, J.; Zhu, H.; Irvine, J.T.S.; Wang, L.; Liu, G.; Cheng, H. Homogeneous Doping of Substitutional Nitrogen/Carbon in TiO₂ Plates for Visible Light Photocatalytic Water Oxidation. *Adv. Funct. Mater.* **2019**, *29*, 1901943. [[CrossRef](#)]
308. Zhang, D.; Ma, X.; Zhang, H.; Liao, Y.; Xiang, Q. Enhanced Photocatalytic Hydrogen Evolution Activity of Carbon and Nitrogen Self-Doped TiO₂ Hollow Sphere with the Creation of Oxygen Vacancy and Ti³⁺. *Mater. Today Energy* **2018**, *10*, 132–140. [[CrossRef](#)]
309. Chaudhary, J.P.; Mahto, A.; Vadodariya, N.; Kholiya, F.; Maiti, S.; Nataraj, S.K.; Meena, R. Fabrication of Carbon and Sulphur-Doped Nanocomposites with Seaweed Polymer Carrageenan as an Efficient Catalyst for Rapid Degradation of Dye Pollutants Using a Solar Concentrator. *RSC Adv.* **2016**, *6*, 61716–61724. [[CrossRef](#)]
310. Romanovska, N.I.; Manoryk, P.A.; Selyshchev, O.V.; Ermokhina, N.I.; Yaremov, P.S.; Grebennikov, V.M.; Shcherbakov, S.M.; Zahn, D.R.T. Effect of the Modification of TiO₂ with Thiourea on Its Photocatalytic Activity in Doxycycline Degradation. *Theor. Exp. Chem.* **2020**, *56*, 183–191. [[CrossRef](#)]
311. Mansingh, S.; Das, K.K.; Behera, A.; Subudhi, S.; Sultana, S.; Parida, K. Bandgap Engineering via Boron and Sulphur Doped Carbon Modified Anatase TiO₂: A Visible Light Stimulated Photocatalyst for Photo-Fixation of N₂ and TCH Degradation. *Nanoscale Adv.* **2020**, *2*, 2004–2017. [[CrossRef](#)]
312. Sun, H.; Bai, Y.; Cheng, Y.; Jin, W.; Xu, N. Preparation and Characterization of Visible-Light-Driven Carbon–Sulfur-Codoped TiO₂ Photocatalysts. *Ind. Eng. Chem. Res.* **2006**, *45*, 4971–4976. [[CrossRef](#)]
313. Hohol, M.; Sanytsky, M.; Kropyvnytska, T.; Barylyak, A.; Bobitski, Y. The Effect of Sulfur- and Carbon-Codoped TiO₂ Nanocomposite on the Photocatalytic and Mechanical Properties of Cement Mortars. *EEJET* **2020**, *4*, 6–14. [[CrossRef](#)]
314. Chung, J.; Chung, J.W.; Kwak, S.-Y. Adsorption-Assisted Photocatalytic Activity of Nitrogen and Sulfur Codoped TiO₂ under Visible Light Irradiation. *Phys. Chem. Chem. Phys.* **2015**, *17*, 17279–17287. [[CrossRef](#)]
315. Akan, P.; Birben, N.C.; Bekbolet, M. Adsorption of Molecular Size Fractions of Humic Acid onto Anion-Doped TiO₂ specimens. *Desalin. Water Treat.* **2015**, *57*, 2455–2465. [[CrossRef](#)]
316. Bakar, S.A.; Ribeiro, C. Prospective Aspects of Preferential {001} Facets of N,S-co-doped TiO₂ Photocatalysts for Visible-Light-Responsive Photocatalytic Activity. *RSC Adv.* **2016**, *6*, 89274–89287. [[CrossRef](#)]
317. Ju, J.; Chen, X.; Shi, Y.; Miao, J.; Wu, D. Hydrothermal Preparation and Photocatalytic Performance of N, S-Doped Nanometer TiO₂ under Sunshine Irradiation. *Powder Technol.* **2013**, *237*, 616–622. [[CrossRef](#)]
318. Zhang, Y.; Wu, H.; Liu, P. Enhanced Transformation of Atrazine by High Efficient Visible Light-Driven N, S-Codoped TiO₂ Nanowires Photocatalysts. *Int. J. Photoenergy* **2014**, 1–8. [[CrossRef](#)]
319. Rengifo-Herrera, J.A.; Mielczarski, E.; Mielczarski, J.; Castillo, N.C.; Kiwi, J.; Pulgarin, C. Escherichia Coli Inactivation by N, S Co-Doped Commercial TiO₂ Powders under UV and Visible Light. *Appl. Catal. B-Environ.* **2008**, *84*, 448–456. [[CrossRef](#)]
320. Gao, H.; Liu, Y.; Ding, C.; Dai, D.; Liu, G. Synthesis, Characterization, and Theoretical Study of N, S-Codoped Nano-TiO₂ with Photocatalytic Activities. *Int. J. Miner. Metall. Mater.* **2011**, *18*, 606–614. [[CrossRef](#)]
321. Antonopoulou, M.; Giannakas, A.; Bairamis, F.; Papadaki, M.; Konstantinou, I. Degradation of Organophosphorus Flame Retardant Tris (1-Chloro-2-Propyl) Phosphate (TCPP) by Visible Light N,S-codoped TiO₂ Photocatalysts. *Chem. Eng. J.* **2017**, *318*, 231–239. [[CrossRef](#)]
322. Chen, J.; Zhong, J.; Li, J.; Dou, L. Enhanced Sunlight Photocatalytic Performance of N,S-codoped TiO₂ Prepared by Sol-Gel Method Using Ammonium Thiocyanate. *Synth. Synth. React. Inorg. Met. Chem.* **2016**, *46*, 1596–1604. [[CrossRef](#)]
323. Eslami, A.; Amini, M.M.; Yazdanbakhsh, A.R.; Mohseni-Bandpei, A.; Safari, A.A.; Asadi, A. N,S Co-doped TiO₂ nanoparticles and Nanosheets in Simulated Solar Light for Photocatalytic Degradation of Non-Steroidal Anti-Inflammatory Drugs in Water: A Comparative Study. *J. Chem. Technol. Biotechnol.* **2016**, *91*, 2693–2704. [[CrossRef](#)]
324. Yan, J.; Zhao, J.; Hao, L.; Hu, Y.; Liu, T.; Guan, S.; Zhao, Q.; Zhu, Z.; Lu, Y. Low-Temperature S-Doping on N-doped TiO₂ Films and Remarkable Enhancement on Visible-Light Performance. *Mater. Res. Bull.* **2019**, *120*, 110594. [[CrossRef](#)]
325. Farhadian, N.; Akbarzadeh, R.; Pirsaeed, M.; Jen, T.-C.; Fakhri, Y.; Asadi, A. Chitosan Modified N, S-doped TiO₂ and N, S-Doped ZnO for Visible Light Photocatalytic Degradation of Tetracycline. *Int. J. Biol. Macromol.* **2019**, *132*, 360–373. [[CrossRef](#)]
326. Khalilian, H.; Behpour, M.; Atouf, V.; Hosseini, S.N. Immobilization of S, N-codoped TiO₂ Nanoparticles on Glass Beads for Photocatalytic Degradation of Methyl Orange by Fixed Bed Photoreactor under Visible and Sunlight Irradiation. *Sol. Energy* **2015**, *112*, 239–245. [[CrossRef](#)]
327. Koltsakidou, A.; Antonopoulou, M.; Evgenidou, E.; Konstantinou, I.; Giannakas, A.E.; Papadaki, M.; Bikiaris, D.; Lambropoulou, D.A. Photocatalytical Removal of Fluorouracil Using TiO₂-P25 and N/S Doped TiO₂ Catalysts: A Kinetic and Mechanistic Study. *Sci. Total Environ.* **2017**, *578*, 257–267. [[CrossRef](#)]
328. Jiao, W.; Li, N.; Wang, L.; Wen, L.; Li, F.; Liu, G.; Cheng, H.-M. High-Rate Lithium Storage of Anatase TiO₂ Crystals Doped with Both Nitrogen and Sulfur. *Chem. Commun.* **2013**, *49*, 3461. [[CrossRef](#)]
329. Malini, B.; Allen Gnana Raj, G. C,N and S-doped TiO₂—Characterization and Photocatalytic Performance for Rose Bengal Dye Degradation under Day Light. *J. Environ. Chem. Eng.* **2018**, *6*, 5763–5770. [[CrossRef](#)]
330. Wang, F.; Ma, Z.; Ban, P.; Xu, X. C, N and S Codoped Rutile TiO₂ Nanorods for Enhanced Visible-Light Photocatalytic Activity. *Mater. Lett.* **2017**, *195*, 143–146. [[CrossRef](#)]

331. Lei, X.F.; Xue, X.X.; Yang, H.; Chen, C.; Li, X.; Niu, M.C.; Gao, X.Y.; Yang, Y.T. Effect of Calcination Temperature on the Structure and Visible-Light Photocatalytic Activities of (N, S and C) Co-doped TiO₂ Nano-Materials. *Appl. Surf. Sci.* **2015**, *332*, 172–180. [[CrossRef](#)]
332. Chun, H.-H.; Jo, W.-K. Heterogeneous Decomposition of Volatile Organic Compounds by Visible-Light Activated N, C, S-embedded Titania. *J. Nanosci. Nanotechnol.* **2016**, *16*, 4544–4553. [[CrossRef](#)]
333. Amreetha, S.; Dhanuskodi, S.; Nithya, A.; Jothivenkatachalam, K. Photocatalytic Degradation of Rhodamine B by C-N-S Tridoped TiO₂ nanoparticles. In *Oxide-Based Materials and Devices VI*; Teherani, F.H., Look, D.C., Rogers, D.J., Eds.; SPIE: Bellingham, WA, USA, 2015. [[CrossRef](#)]
334. Amreetha, S.; Dhanuskodi, S.; Nithya, A.; Jothivenkatachalam, K. Three Way Electron Transfer of a C–N–S Tri Doped Two-Phase Junction of TiO₂ Nanoparticles for Efficient Visible Light Photocatalytic Dye Degradation. *RSC Adv.* **2016**, *6*, 7854–7863. [[CrossRef](#)]
335. Yan, X.; Xing, Z.; Cao, Y.; Hu, M.; Li, Z.; Wu, X.; Zhu, Q.; Yang, S.; Zhou, W. In-Situ C-N-S-Tridoped Single Crystal Black TiO₂ Nanosheets with Exposed {001} Facets as Efficient Visible-Light-Driven Photocatalysts. *Appl. Catal. B Environ.* **2017**, *219*, 572–579. [[CrossRef](#)]
336. Li, D.; Xing, Z.; Yu, X.; Cheng, X. One-Step Hydrothermal Synthesis of C-N-S-Tridoped TiO₂-based Nanosheets Photoelectrode for Enhanced Photoelectrocatalytic Performance and Mechanism. *Electrochim. Acta* **2015**, *170*, 182–190. [[CrossRef](#)]
337. Guo, Y.; Guo, T.; Chen, J.; Wei, J.; Bai, L.; Ye, X.; Ding, Z.; Xu, W.; Zhou, Z. Synthesis of C–N–S Co-doped TiO₂ Mischcrystal with an Isobandgap Characteristic and Its Photocatalytic Activity under Visible Light. *Catal. Sci. Technol.* **2018**, *8*, 4108–4121. [[CrossRef](#)]
338. Wang, P.; Yap, P.-S.; Lim, T.-T. C–N–S Tridoped TiO₂ for Photocatalytic Degradation of Tetracycline under Visible-Light Irradiation. *Appl. Catal. A Gen.* **2011**, *399*, 252–261. [[CrossRef](#)]
339. Folli, A.; Jakobsen, U.H.; Guerrini, G.L.; Macphee, D.E. Rhodamine B Discolouration on TiO₂ in the Cement Environment: A Look at Fundamental Aspects of the Self-Cleaning Effect in Concretes. *J. Adv. Oxid. Technol.* **2009**, *12*. [[CrossRef](#)]
340. Eun, S.-R.; Mavengere, S.; Cho, B.; Kim, J.-S. Photocatalytic Reactivity of Carbon–Nitrogen–Sulfur-Doped TiO₂ Upconversion Phosphor Composites. *Catalysts* **2020**, *10*, 1188. [[CrossRef](#)]
341. Dong, F.; Zhao, W.; Wu, Z. Characterization and Photocatalytic Activities of C, N and S Co-Doped TiO₂ with 1D Nanostructure Prepared by the Nano-Confinement Effect. *Nanotechnology* **2008**, *19*, 365607. [[CrossRef](#)]
342. Wang, Y.; Huang, Y.; Ho, W.; Zhang, L.; Zou, Z.; Lee, S. Biomolecule-Controlled Hydrothermal Synthesis of C–N–S-Tridoped TiO₂ Nanocrystalline Photocatalysts for NO Removal under Simulated Solar Light Irradiation. *J. Hazard. Mater.* **2009**, *169*, 77–87. [[CrossRef](#)] [[PubMed](#)]
343. Lan, N.T.; Anh, V.H.; An, H.D.; Hung, N.P.; Nhiem, D.N.; Van Thang, B.; Lieu, P.K.; Khieu, D.Q. Synthesis of C-N-S-Tridoped TiO₂ from Vietnam Ilmenite Ore and Its Visible Light-Driven-Photocatalytic Activity for Tetracycline Degradation. *J. Nanomater.* **2020**, 1–14. [[CrossRef](#)]